J. Fluid Mech. (2006), *vol.* 559, *pp.* 151–203.
doi:10.1017/S0022112006000255 Printed in the United Kingdom

Trajectory analysis for non-Brownian inertial suspensions in simple shear flow

By G. SUBRAMANIAN AND J. F. BRADY

Division of Chemistry and Chemical Engineering, California Institute of Technology, Pasadena, CA 91125, USA

(Received 26 August 2003 and in revised form 18 November 2005)

We analyse pair trajectories of equal-sized spherical particles in simple shear flow for small but finite Stokes numbers. The Stokes number, $St = \dot{\gamma}\tau_p$, is a dimensionless measure of particle inertia; here, τ_p is the inertial relaxation time of an individual particle and $\dot{\gamma}$ is the shear rate. In the limit of weak particle inertia, a regular small-St expansion of the particle velocity is used in the equations of motion to obtain trajectory equations to the desired order in St. The equations for relative trajectories are then solved, to $O(St)$, in the dilute limit, including only pairwise interactions. Particle inertia is found to destroy the fore–aft symmetry of the zero-Stokes trajectories, and finite-St open trajectories suffer net transverse displacements in the velocity gradient and vorticity directions. The vorticity displacement remains $O(St)$, while the scaling of the gradient displacement increases from $O(St)$ for far-field open trajectories, to $O(St^{1/2})$ for open trajectories with $O(St^{1/2})$ upstream gradient offsets. The gradient displacement also changes sign, being negative close to the plane of the reference sphere (the shearing plane) on account of dominant lubrication interactions, and then becoming positive at larger off-plane separations. The transverse displacements accompanying successive pair interactions lead to a diffusive behaviour for long times. The shear-induced diffusivity in the vorticity direction is $O(St^2\phi\dot{\gamma}a^2)$, while that in the gradient direction scales as $O(St^2 \ln St\, \phi\dot{\gamma}a^2)$ and $O(St^2\phi \ln(1/\phi)\dot{\gamma}a^2)$ in the limits $\phi \ll St^{1/3}$ and $St^{1/3} \ll \phi \ll 1$, respectively. Further, the region of zero-Stokes closed trajectories is destroyed, and there exists a new attracting limit cycle whose location in the shearing plane is, at leading order, independent of St. The extension of the present analysis to include a generic linear flow, and the implications of the finite-St trajectory modifications for coagulating systems are discussed.

1. Introduction

Inertial effects are important in many natural and industrial flow situations including fluidized beds, drilling fluids, landslides, etc. Understanding the role of inertia in fluid–particle flows is thus critical both to the successful design and scale-up of industrial processes and to the modelling of naturally occurring phenomena. From a fundamental viewpoint, it is of interest to investigate the separate roles of particle and fluid inertia in such flows. In simple shear flow of dilute suspensions, the magnitude of particle inertia is determined by the Stokes number $St = \dot{\gamma}\tau_p$, which is the ratio of the inertial relaxation time of an isolated particle $\tau_p = m/(6\pi\eta a)$ to the flow time scale $\dot{\gamma}^{-1}$, $\dot{\gamma}$ being the shear rate. Here, m is the mass of the particle, a is its radius and η is the viscosity of the suspending fluid. Fluid inertial effects are characterized by the Reynolds number defined in this case as $Re = \rho_f \dot{\gamma} a^2/\eta$,

where ρ_f is the density of the suspending fluid. We examine suspensions of massive particles, $\rho_p/\rho_f \gg 1$, ρ_p being the particle density, for which the Stokes number is finite, but the Reynolds number of the flow is small enough for convective inertial forces in the fluid to be neglected. In the limit of zero Re, if one also neglects the unsteady term in the Navier–Stokes equations, an assumption that is reasonable except in cases of rapidly accelerating flows, the motion of the fluid satisfies the quasi-steady Stokes equations and is uniquely determined by the current velocities and configuration of the particles (and positions and velocities of the boundaries, if any). The hydrodynamic interactions between particles in this limit are completely characterized by configuration-dependent resistance tensors whose expressions for the case of pairwise interactions are well-known and have been tabulated in detail (see Kim & Karrila 1991). For finite St, however, the particles do not instantaneously relax to the local fluid velocity and the momentum of the particle enters as an independent variable in the kinetic equation for the probability density – the Louiville equation, which governs the evolution of the phase-space probability density of a system of non-Brownian particles for finite St (see Mcquarrie 1976). Gas–solid suspensions fall in this parameter regime; for instance, considering 10 micron particles in air ($\eta \approx 10^{-5}$ Pa s, $\rho_p/\rho_f \approx 1000$) and a typical shear rate $\approx 10\,\mathrm{s}^{-1}$, one has $St = 0.1$ and $Re = 10^{-4}$. In contrast, for particles suspended in a liquid, $St \approx Re$, and particle and fluid inertia are of comparable importance.

Inertialess flows of suspensions have been studied extensively and are fairly well understood (Happel & Brenner 1965; Brady & Bossis 1988; Kim & Karrila 1991). Work for cases where inertial effects exert a significant influence is fairly recent, however. Here too, there has been relatively limited work accounting for inertia of the suspending fluid – the sole theoretical efforts aimed at characterizing the rheology of a dilute suspension at finite Re remain those of Lin, Peery & Schowalter (1970) and Ryskin (1980). The former examined, via singular perturbation techniques, the modification of the flow field around a single force-free particle in an ambient simple shear flow for $Re \ll 1$, and thence determined the stress tensor to $O(\phi Re^{3/2})$, ϕ being the volume fraction. In contrast to the inertialess limit where the particulate phase, at $O(\phi)$, only enhances the Newtonian viscosity (see Leal 1992), inertial effects led to a shear-dependent viscosity and normal stress differences.

The effect of pair interactions on suspension rheology, again for zero inertia, was first determined by Batchelor & Green (1972*b*) who found the microstructure, at the pair level, to be determined by the nature of the ambient flow; simple shear flow, in particular, led to an indeterminate microstructure owing to the existence of closed pair trajectories in the absence of non-hydrodynamic forces and Brownian motion. As observed by Koch & Hill (2001), a rigorous treatment of pair hydrodynamic interactions, and their role in finite-Re suspension rheology, presents a formidable challenge owing to the nonlinearity and unsteady nature of the governing equations; the latter, for instance, leads to the inertial interaction between two particles at any instant of time being, in principle, dependent on the entire time history leading up to the current configuration.

Thus, on one hand, efforts aimed at understanding fluid inertial effects have focused on characterizing the dynamics of a single particle in more complex ambient flows (see Bagchi & Balachandar 2002*a*, *b*, 2003), while on the other simulations of interacting systems of particles at finite Re have, for the most part, been restricted to a pre-determined microstructure: for example, Koch & Ladd (1997) and Hill, Koch & Ladd (2001) have considered flow in porous media at moderate Re using lattice-Boltzmann simulations; earlier, Kim, Elghobashi & Sirigano (1993) had examined,

over a range of Re, the forces that arise on a pair of fixed spheres oriented transversely with respect to an ambient uniform flow. Wylie, Koch & Ladd (2003) have recently examined suspension rheology at high St and moderate Re using a combination of kinetic theory and lattice-Boltzmann simulations. However, the restriction to periodic boundary conditions in the latter protocol makes it rather difficult to isolate the dynamics of pair interactions from such simulations. Owing to the computational expense involved, dynamical simulations based on finite element techniques that consider the motion of a finite number of interacting particles at non-zero Re have so far been restricted to sedimentation, and largely to two dimensions, as evidenced in the works of Hu, Joseph & Crochet (1992) and Feng, Hu & Joseph (1994).

Treating the effects of particulate-phase inertia is easier and the early efforts of Savage & Jeffrey (1981) and Lun *et al.* (1984) initiated a flurry of activity aimed at deriving equations governing the macroscopic flow behaviour of granular systems under conditions of rapid flow. The methods of analysis are based on those originally used in the kinetic theory for treating molecular gases (Chapman & Cowling 1970). The statistics of the grains are thus governed by a Boltzmann equation that accounts for momentum transfer via instantaneous inelastic binary collisions. Much of the granular flow literature, however, either neglects the interstitial fluid phase, so St as defined previously is effectively infinite, or treats it in an *ad-hoc* fashion by including a viscous drag.

The effects of the suspending fluid have been analysed in a rigorous manner by Koch and coworkers (Koch 1990; Kumaran & Koch 1993*a*, *b*; Tsao & Koch 1995; Sangani *et al.* 1996) who, in a series of papers, studied the flow behaviour of non-Brownian suspensions in the limit $Re = 0,\ St > O(1)$. Fluid inertia is again negligible, and the hydrodynamic interactions between the inertial particles were found to be similar to those in a fixed bed. The macroscopic behaviour of dilute suspensions in this limit is found to depend on the relative magnitudes of the inertial relaxation time τ_p and the collision time $\tau_c = af(\phi)/T^{1/2}$, where $af(\phi)$ is the mean free path with $f(\phi) \to \phi^{-1}$ as $\phi \to 0$, and $T = \langle \boldsymbol{U}' \cdot \boldsymbol{U}' \rangle$ is a measure of the magnitude of particle velocity fluctuations. A pronounced non-Newtonian rheology results at $O(1)$ Stokes numbers, characterized by the presence of normal stress differences.

Herein, we study the simple shear flow of dilute non-Brownian suspensions of spherical particles at the other end of the inertial spectrum, that is, in the limit $Re = 0,\ St \ll 1$, via a trajectory analysis. This then serves to complement the aforementioned granular flow studies, and helps describe suspension flow characteristics as a function of St for zero Re. Pair trajectories for neutrally buoyant spheres in the limit $Re = St = 0$, and in the absence of non-hydrodynamic forces, were originally determined by Batchelor & Green (1972*a*, *b*). We investigate, in depth, the deviation from this limit for small but finite particle inertia, and discuss the implications with regard to hydrodynamic diffusion in dilute inertial suspensions. For small St, lubrication forces between particles during close approach will always be strong enough to prevent solid-body contacts (see § 2 and Appendix A), and the subset of initial configurations for which particle pairs come close enough for their separation to become comparable to molecular length scales, for instance the mean free path in a gas–solid suspension, is expected to be negligible. We therefore assume the continuum approximation for the suspending fluid to remain valid for all possible particle configurations, and solid-body collisions are not considered as a source of momentum transfer.

One of the principal results of our analysis is that particle inertia destroys the fore–aft symmetry of zero-Stokes pair trajectories; this, of course, stems from the

reversibility both of the Stokes equations and the inertialess particles' equations of motion. Finite-St open trajectories suffer net transverse displacements in both the gradient and vorticity directions. As discussed in more detail in § 3, the vorticity displacements scale regularly, being $O(St)$ for $St \ll 1$, while the scaling of the gradient displacements depends on the initial upstream offset of the open trajectory. The gradient displacements increase with decreasing upstream gradient offset from being $O(St)$ for far-field open trajectories, to $O(St^{1/2})$ for open trajectories with $O(St^{1/2})$ upstream offsets in the gradient direction lying close to the finite-St separatrix envelope; the latter acts to partition the finite-St trajectory space into open and spiralling trajectories. The trajectory analysis serves to highlight the sensitivity of the zero-Stokes-number trajectory configuration to the inclusion of even a tiny amount of inertia. In particular, the structurally unstable ensemble of inertialess closed pair trajectories is destroyed, and for small but finite St, there exist trajectories, arriving from infinity, that converge onto a limit cycle in the plane of the reference sphere leading to the formation of a bound pair. The attracting limit cycle with a non-trivial basin of attraction implies that the resulting configuration of finite-St trajectories is structurally stable, and is therefore expected to remain qualitatively unaltered in a finite range of St, provided only that $St < O(1)$.

The aforementioned increase in the gradient displacement scaling also leads to shear-induced diffusivities in the gradient direction that are larger than the $O(St^2\phi\dot{\gamma}a^2)$ magnitude anticipated for a particle suffering $O(St\,a)$ displacements at a frequency of $O(\dot{\gamma})$ due to pair interactions. When $\phi \ll St^{1/3}$, the suspension is sufficiently dilute that the transition from an $O(St)$ to an $O(St^{1/2})$ scaling for the gradient displacement of a test particle, due solely to pair interactions at small gradient offsets, persists. This then leads to an enhancement of the gradient component of the diffusivity by $O(\ln St)$. However, it would be difficult to observe this $O(St^2 \ln St\,\phi\dot{\gamma}a^2)$ diffusivity in practice, since for $\phi \ll St^{1/3}$, most particles eventually end up as bound pairs. On the other hand, when $St^{1/3} \ll \phi \ll 1$, the pair interactions are cut off at offsets greater than $O(St^{1/2})$ by a third particle, leading to diffusivities in the gradient direction that now scale as $O(St^2 \ln(1/\phi)\phi\dot{\gamma}a^2)$ in the steady state. Particle inertia therefore provides a mechanism for diffusive behaviour with pairwise interactions even in the absence of short-range interparticle forces or surface roughness (Leighton & Acrivos 1987*a*, *b*; daCunha & Hinch 1996; Davis 1996).

The paper is organized as follows. In § 2, we derive the equations governing the trajectories of a pair of neutrally buoyant spherical particles in simple shear flow in the limit $St \ll 1$, including the first inertial corrections. Thereafter, in § 3, we present a detailed qualitative discussion of the main results of the trajectory analysis. Herein, we employ arguments that exploit the known structure of pair-particle trajectories in the limit of zero inertia and the generic behaviour of a finite mass particle when moving along a curvilinear path, in order to anticipate the structure of the finite-St trajectory space. The discussion is first carried out in the simpler context of inertial trajectories in the plane of the reference sphere (§ 3.1), and later for 'off-plane' inertial trajectories (§ 3.2). While some inferences, and the scalings of relevant quantities, certainly emerge only from the details of the analysis carried out subsequently, we believe that it is important, at the very outset, to have a qualitative view of the finite-St trajectory configuration in relation to its inertialess counterpart. It is hoped then that the overall picture delineated in §§ 3.1 and 3.2 will serve as a valuable guide for the reader when delving into the mathematical framework presented in § 4. The latter comprises §§ 4.1 and 4.2 where we write down the governing trajectory equations and the perturbation expansions, § 4.3 where we derive the gradient and

vorticity displacements for trajectories with gradient offsets that are much greater than $O(St^{1/2})$, §4.4 where we examine finite-St trajectories with $O(St^{1/2})$ upstream gradient offsets, and §4.5 where we obtain an equation governing the location of the in-plane attracting limit cycle. Results for the transverse displacements obtained from a numerical integration of the $O(St)$ trajectory equations are presented in §§4.3 and 4.4 to support the conclusions of the analysis *vis-a-vis* open trajectories; the numerical results also confirm the location of the in-plane limit cycle and show that it is independent of St.

In §5, we show typical plots of both open and spiralling finite-St trajectories, again generated numerically, that serve to verify the general predictions of §3. In §6, we use earlier analytical results to derive the scaling for the shear-induced diffusivities, and then discuss the implications of the trajectory analysis for diffusive behaviour in a dilute suspension of inertial particles. In §7 we numerically integrate the small-St equations of relative motion for the particles in their primitive form to independently confirm the results obtained for the finite-St trajectory space in previous sections. Finally, in §8, along with a summary of the findings, we discuss the generalization of the present trajectory analysis to the case of a general linear flow, and the relevance of the anticipated findings to the problem of aerosol coagulation in complex flows.

2. Equations for particle trajectories

It is shown below that a straightforward power series expansion in St for the particle velocity when used in the exact equation of motion yields the required inertial corrections to the leading-order hydrodynamic velocity field at successive orders in St. From the linearity of the Stokes equations for the fluid motion, the equation of motion for a spherical particle can be written as:

$$St\, \boldsymbol{m} \cdot \frac{\mathrm{d}\boldsymbol{U}}{\mathrm{d}t} = -\boldsymbol{R}^{FU} \cdot \left(\boldsymbol{U} - \boldsymbol{R}^{FU^{-1}} \cdot \hat{\boldsymbol{F}}^{o}\right). \tag{2.1}$$

The force $\hat{\boldsymbol{F}}^{o}$ for a linear flow field is given by

$$\hat{\boldsymbol{F}}^{o} = \boldsymbol{R}^{FU} \cdot \boldsymbol{U}^{\infty} + \boldsymbol{R}^{FE} : \boldsymbol{E}^{\infty}, \tag{2.2}$$

where $\boldsymbol{U}^{\infty}$ is the ambient velocity at the location of the particle, $\boldsymbol{E}^{\infty}$ is the rate of strain tensor, $\boldsymbol{R}^{FU}$ and $\boldsymbol{R}^{FE}$ are elements of the hydrodynamic resistance tensor, the nature of the coupling indicated by the corresponding superscripts (see Brady & Bossis 1988), while

$$\boldsymbol{m} = \begin{pmatrix} \boldsymbol{I} & 0 \\ 0 & \frac{2}{5}\boldsymbol{I} \end{pmatrix}$$

is the inertia tensor for solid spheres. It must be noted, as is also evident from the expression for $\boldsymbol{m}$, that $\boldsymbol{U}$ and the resistance tensors include both translational and rotational degrees of freedom. In (2.1) and all subsequent equations, we have used the following scalings: $t \sim \dot{\gamma}^{-1}$, $U \sim \dot{\gamma} a$, $R^{FU} \sim \eta a$, R^{LU}, $R^{F\Omega}$, $R^{FE} \sim \eta a^2$, $R^{L\Omega} \sim \eta a^3$, $\hat{F}^{o} \sim 6\pi\eta\dot{\gamma}a^2$ etc., in order to render the various quantities non-dimensional.

One recognizes that the acceleration on the left-hand side of (2.1) involves the Lagrangian derivative of the particle velocity; since $\boldsymbol{U}(t) \equiv \boldsymbol{U}(\boldsymbol{x}(t))$, one can rewrite (2.1) as

$$St\, \boldsymbol{m} \cdot [\boldsymbol{U} \cdot \nabla_{\boldsymbol{x}} \boldsymbol{U}] = -\boldsymbol{R}^{FU} \cdot (\boldsymbol{U} - \boldsymbol{R}^{FU^{-1}} \cdot \hat{\boldsymbol{F}}^{o}). \tag{2.3}$$

Equation (2.3) is, of course, still equivalent to (2.1); however, in expanding the relative velocity $\boldsymbol{U}$ as $\boldsymbol{U}_0 + St\, \boldsymbol{U}_1 + \ldots$ for small St, one eliminates the need for an initial

condition, thereby restricting the validity of the resulting solution to times much greater than the initial period of momentum relaxation of $O(\tau_p)$; one obtains

$$O(1): \qquad -\boldsymbol{R}^{FU}\cdot(\boldsymbol{U}^{(0)}-\boldsymbol{R}^{FU^{-1}}\cdot\hat{\boldsymbol{F}}^{o})=0, \tag{2.4}$$

$$O(St^{i}): \qquad \boldsymbol{m}\cdot\sum_{k=0}^{i-1}\boldsymbol{U}^{(k)}\cdot\nabla_{\boldsymbol{x}}\boldsymbol{U}^{(i-k-1)}=-\boldsymbol{R}^{FU}\cdot\boldsymbol{U}^{(i)} \qquad (i\geqslant 1), \tag{2.5}$$

whence, solving successively,

$$\left.\begin{aligned}
\boldsymbol{U}^{(0)}&=\boldsymbol{R}^{FU^{-1}}\cdot\hat{\boldsymbol{F}}^{o},\\
\boldsymbol{U}^{(1)}&=-(\boldsymbol{R}^{FU^{-1}}\cdot\hat{\boldsymbol{F}}^{o})\cdot\nabla_{\boldsymbol{x}}(\boldsymbol{R}^{FU^{-1}}\cdot\hat{\boldsymbol{F}}^{o})\cdot\boldsymbol{m},\\
\boldsymbol{U}^{(2)}&=(\boldsymbol{R}^{FU^{-1}}\cdot\hat{\boldsymbol{F}}^{o})\cdot\nabla_{\boldsymbol{x}}\left[(\boldsymbol{R}^{FU^{-1}}\cdot\hat{\boldsymbol{F}}^{o})\cdot\nabla_{\boldsymbol{x}}(\boldsymbol{R}^{FU^{-1}}\cdot\hat{\boldsymbol{F}}^{o})\cdot\boldsymbol{m}\right]\\
&\quad+\left[(\boldsymbol{R}^{FU^{-1}}\cdot\hat{\boldsymbol{F}}^{o})\cdot\nabla_{\boldsymbol{x}}(\boldsymbol{R}^{FU^{-1}}\cdot\hat{\boldsymbol{F}}^{o})\cdot\boldsymbol{m}\right]\cdot\nabla_{\boldsymbol{x}}(\boldsymbol{R}^{FU^{-1}}\cdot\hat{\boldsymbol{F}}^{o}),
\end{aligned}\right\} \tag{2.6}$$

and so forth.

In a statistically homogeneous suspension, only the relative positions of the centres of mass are relevant. An additional restriction on pair interactions implies that the only relevant spatial coordinate is the relative vector separation of the two spheres $\boldsymbol{r}=\boldsymbol{x}_2-\boldsymbol{x}_1$; the equations for the relative particle trajectories, to $O(St)$, are then given by

$$\frac{\mathrm{d}\boldsymbol{r}}{\mathrm{d}t}=\boldsymbol{V}^{(0)}(\boldsymbol{r})+St\;\boldsymbol{V}^{(1)}(\boldsymbol{r}), \tag{2.7}$$

where

$$\boldsymbol{V}^{(0)}=\left(\boldsymbol{U}_2^{\infty}-\boldsymbol{U}_1^{\infty}\right)-2\left(\boldsymbol{M}_{UF}^{11}-\boldsymbol{M}_{UF}^{12}\right)\cdot\left(\boldsymbol{R}_{FE}^{11}+\boldsymbol{R}_{FE}^{12}\right):\boldsymbol{E}^{\infty}$$
$$-2\left(\boldsymbol{M}_{UL}^{11}+\boldsymbol{M}_{UL}^{12}\right)\cdot\left(\boldsymbol{R}_{LE}^{11}+\boldsymbol{R}_{LE}^{12}\right):\boldsymbol{E}^{\infty}, \tag{2.8}$$

$$\boldsymbol{V}^{(1)}=-\left(\boldsymbol{M}_{UF}^{11}-\boldsymbol{M}_{UF}^{12}\right)\cdot\left\{\boldsymbol{V}^{(0)}\cdot\nabla_{\boldsymbol{r}}\boldsymbol{V}^{(0)}\right\}+\frac{2}{5}\left(\boldsymbol{M}_{UL}^{11}+\boldsymbol{M}_{UL}^{12}\right)\cdot\left\{\boldsymbol{V}^{(0)}\cdot\nabla_{\boldsymbol{r}}\left[\left(2(\boldsymbol{M}_{\Omega F}^{11}-\boldsymbol{M}_{\Omega F}^{12}\right)\right.\right.$$
$$\left.\left.\cdot\left(\boldsymbol{R}_{FE}^{11}+\boldsymbol{R}_{FE}^{12}\right):\boldsymbol{E}^{\infty}+2\left(\boldsymbol{M}_{\Omega L}^{11}+\boldsymbol{M}_{\Omega L}^{12}\right)\cdot\left(\boldsymbol{R}_{LE}^{11}+\boldsymbol{R}_{LE}^{12}\right):\boldsymbol{E}^{\infty}\right]\right\}. \tag{2.9}$$

Here we have used $\boldsymbol{V}$ to denote the relative translational velocity, and the resistance and mobility tensors are as defined in Kim & Karrila (1991). The $O(St)$ inertial correction $\boldsymbol{V}^{(1)}$ is of the general form $\boldsymbol{V}\cdot\nabla_{\boldsymbol{r}}\boldsymbol{V}$ (see (2.3)), symptomatic of translational inertia; the second term in $\boldsymbol{V}^{(1)}$, of the form $\boldsymbol{V}\cdot\nabla_{\boldsymbol{r}}\boldsymbol{\Omega}$, arises due to the coupling of the translational and rotational degrees of freedom in the presence of hydrodynamic interactions.

The velocity field on the right-hand side of (2.7) is a known function of $\boldsymbol{r}$, and a particle at $\boldsymbol{r}$ can only move with this velocity. Therefore the particle momenta are no longer allowed to vary in an independent manner. One may imagine endowing the dilute system of non-Brownian particles with an arbitrary set of initial velocities. Upon allowing the system to evolve, the particles rapidly relax in a time of $O(\tau_p)$ to the value given by the field $\boldsymbol{V}^{(0)}+St\;\boldsymbol{V}^{(1)}$ at their current locations; for all later times, the trajectories for pair interactions are accurately described, to $O(St)$, by (2.7).†

† The above argument is not restricted to dilute suspensions; equation (2.7) is, in fact, valid for a suspension of arbitrary volume fraction provided the hydrodynamic resistance tensors are modified accordingly, and the variable $\boldsymbol{r}$ is extended to include all configurational degrees of freedom; the inertial relaxation time τ_p is in general a decreasing function of volume fraction.

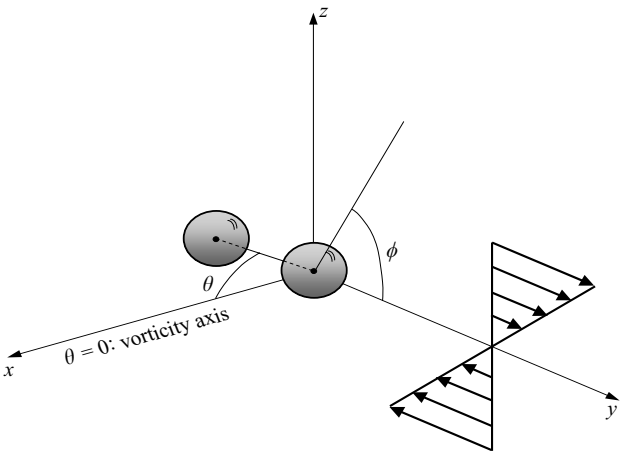

FIGURE 1. The coordinate system used to describe the zero- and finite-St trajectory configurations in simple shear flow.

3. General features of the finite-*St* trajectory space

We attempt here to motivate, based on physical arguments, the nature of pair trajectories that must arise owing to hydrodynamic interactions at small but finite St. The resulting qualitative picture then serves as a guide for the ensuing analysis in § 4. As will be seen, the predictions of this section are borne out by the results of the detailed analysis.

The trajectories are described in a frame of reference that translates with one of the spheres. It is then easily seen from symmetry arguments that pair trajectories lying in the plane of the reference sphere (the shearing plane) for $St = 0$ – the 'in-plane' trajectories – will continue to do so even for finite St. The elimination of one degree of freedom, that of motion in the vorticity direction, makes this a convenient point to begin a discussion of the finite-St modifications. It must, however, be noted that the shearing plane, although an invariant manifold in the above sense, may still be stable or unstable depending on the long-time behaviour of finite-St trajectories originating close to it. In the inertialess limit, reversibility and the resulting fore–aft symmetry imply that the shearing plane is neutrally stable; a trajectory that starts upstream at a finite value of the vorticity coordinate, remains a finite distance away from the shearing plane for all subsequent times. In § 3.2 it is shown that there exist regions in the shearing plane that are asymptotically stable for non-zero St. A second, trivially invariant, manifold is the vorticity axis, since a pair of spheres separated in the vorticity direction exhibit no relative motion. Again, the vorticity axis, which is neutrally stable in the inertialess limit, becomes unstable for finite St.

3.1. *Finite-St trajectories in the flow–gradient plane*

At zero St, trajectories in the shearing plane ($\theta = \pi/2$ – see figures 1, 2 and 3) may be divided into two classes:

(*a*) 'Open' trajectories that start from a finite upstream offset in the gradient direction, and tend to an identical downstream offset as $t \to \infty$ as shown in figure 2, thereby being consistent with the fore–aft symmetry in the absence of inertia.

(*b*) fore–aft symmetric 'closed' trajectories that represent bound orbits of the two spheres (see figure 3).

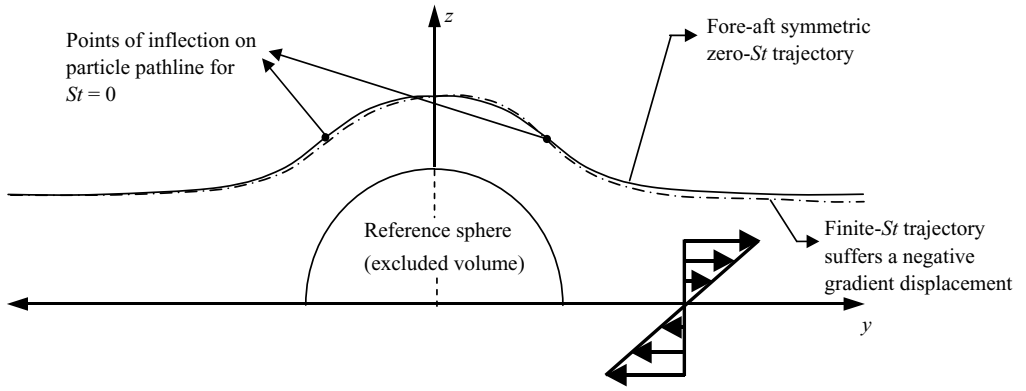

FIGURE 2. A typical zero-Stokes open trajectory (solid line) when viewed along the vorticity axis (x); the pair of inflection points, separating regions of opposite curvature, are shown. The finite-St trajectory, depicted by a dot-dashed line, is shown to suffer a negative gradient displacement.

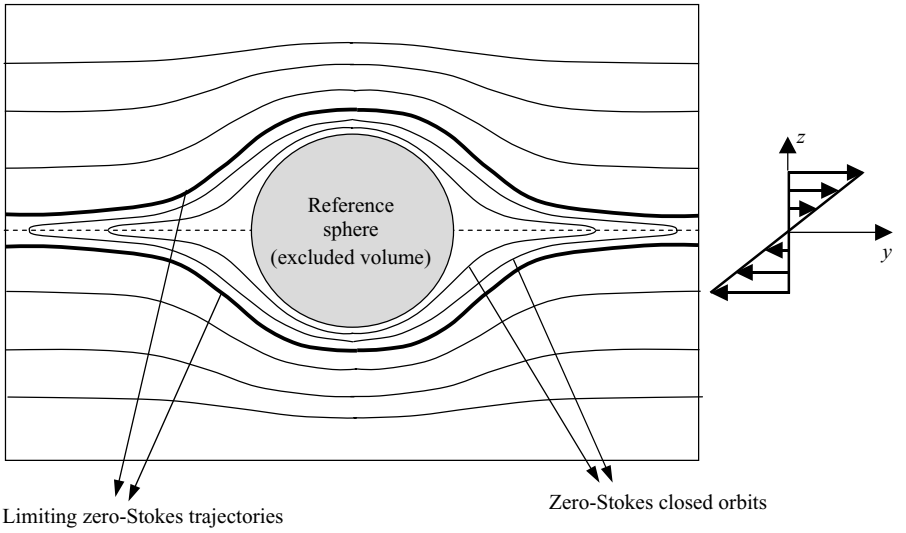

FIGURE 3. Phase plane of trajectories for $St = 0$ in simple shear flow.

The limiting zero-Stokes open trajectory, or the separatrix, separates these two classes and tends to a zero gradient offset both upstream and downstream (figure 3).

Since the effect of inertia in the particle equation of motion (2.3) is represented by $St(\boldsymbol{V}\cdot\nabla_{\boldsymbol{r}}\boldsymbol{V})$, the $O(St)$ inertial modifications of the zero-Stokes phase plane may be understood by considering this term with $\boldsymbol{V}$ now taken as the relative velocity $\boldsymbol{V}^{(0)}(\boldsymbol{r})$ along a zero-Stokes trajectory.† The term $\boldsymbol{V}\cdot\nabla_{\boldsymbol{r}}\boldsymbol{V}$ is then related to the change in the velocity vector along the zero-Stokes pathline, and thence to its curvature. From figure 2, it is evident that any open zero-Stokes trajectory in the plane of shear has a pair of inflection points that serve to separate regions of positive curvature

† As seen from (2.9), there is also an inertial term of the form $(\boldsymbol{V}\cdot\nabla_{\boldsymbol{r}}\boldsymbol{\Omega})$ associated with the translation–rotation coupling that arises in the presence of hydrodynamic interactions. This effect is relatively small, however, and is restricted to a quantitative modification of the phase plane (see Subramanian 2002).

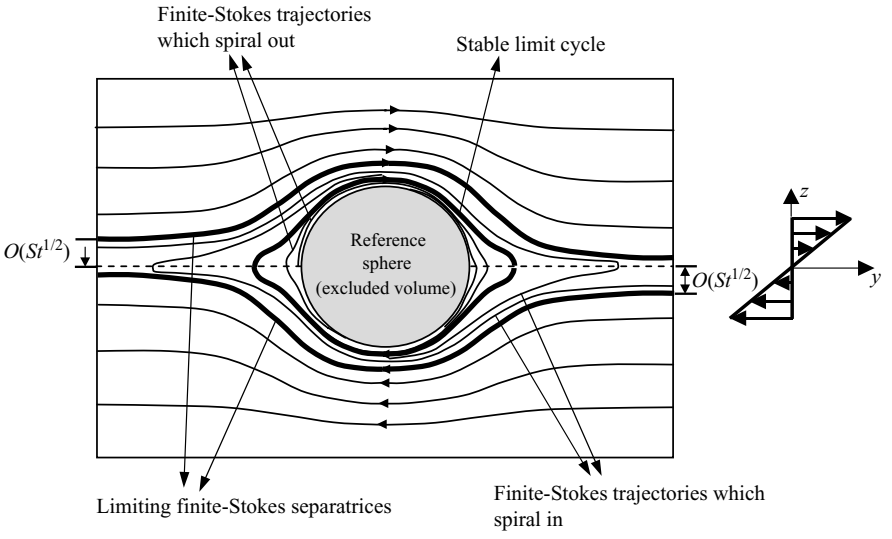

FIGURE 4. Phase plane of trajectories for finite St in simple shear flow.

(concave upward with respect to the y-axis) lying outside from the region of negative curvature (concave downward) in between. Starting from far upstream, a spherical particle with finite inertia is unable to faithfully follow the (upwardly) concave portion of the zero-Stokes trajectory, and thus comes closer to the reference sphere than a similar inertialess particle. The intermediate region of negative curvature then pushes the particle outward, causing it to cross the z-axis ($\phi = \pi/2$) with a positive radial velocity; the region of positive curvature in the downstream portion of the trajectory again pushes the particle down, leading to a net displacement in the velocity gradient direction (Δz) that is negative for z positive. The magnitude of the net displacement Δz evidently depends on the inertia of the particle, and is found to be $O(St)$ for open trajectories with $O(1)$ upstream offsets ($z^{-\infty}$) in the gradient direction. Particle inertia thus destroys the fore–aft symmetry of the zero-Stokes open trajectories in the shearing plane by inducing a non-zero gradient displacement.

With decreasing upstream offsets $z^{-\infty}$, Δz becomes increasingly negative. For small enough offsets, the finite-St trajectory passes very close to the reference sphere in the region where it is concave downward and lubrication forces reduce the effective inertia of the particle, which in turn suppresses its outward radial motion. At the same time, the regions of positive curvature are enhanced since the trajectory has to now pass around the excluded volume of the reference sphere. In fact, the magnitude of Δz will be shown to increase from $O(St)$ for far-field open trajectories to $O(St^{1/2})$ for open trajectories with $z^{-\infty} \sim O(St^{1/2})$. Finally, the net displacement Δz becomes equal to the upstream offset for the finite-St in-plane separatrix. The latter demarcates the open from the spiralling trajectories (see below) for finite St, and unlike its zero-Stokes analogue, is asymmetric, starting from a finite $O(St^{1/2})$ gradient offset upstream and tending to a zero offset far downstream (see figure 4).

Inertial modifications with regard to the in-plane zero-Stokes closed trajectories may also be deduced from arguments similar to those above. Closed trajectories that lie just beneath the zero-Stokes separatrix (see figure 2) resemble, for the most part, open trajectories lying just above. Thus, the equivalent of a negative gradient displacement for these trajectories would be an asymmetry between their points of intersection with the flow axis: the downstream point of intersection now lies closer to

the origin relative to the preceding upstream one, leading to a spiralling-in behaviour for finite St. Indeed, all inertial trajectories with upstream gradient offsets smaller than that corresponding to the in-plane finite-St separatrix, spiral in towards the reference sphere. The difference between the coordinates of successive points of intersection with the flow axis need not be $O(St)$, however. This is due to the non-uniformity arising from squeezing the entire family of zero-Stokes closed orbits spanning the y-axis into an extremely small interval of $O(10^{-5}a)$ on the z-axis, a being the radius of the sphere (see Arp & Mason 1977); the resulting inward spiralling, especially at large distances from the reference sphere, is then very rapid even for $St \ll 1$.† On the other hand, zero-Stokes closed trajectories very near the reference sphere are almost circular, and must therefore give rise to finite-St trajectories that spiral out with the addition of the centrifugal force; the 'effective viscosity' in this near-field region is very high on account of lubrication, and the resulting centrifugal velocities weak, leading to very tight outward spirals. The change in the sense of spiralling implies the existence of a limit cycle, very close to the surface of the reference sphere, that acts as a local attractor for small but finite St. In addition, since the forces causing both inward and outward spiralling scale as $O(St)$, a balance between them, at leading order, must be independent of St. In other words, the location of the attracting limit cycle in the shearing plane, to $O(St)$, is fixed regardless of St!

The zero- and finite-St trajectories in the plane of shear depicted in figures 3 and 4, respectively, have not been drawn to scale; the near-field portions of the trajectory plane, for instance, have been intentionally magnified in order to clearly depict the finite-St modifications. It is seen that the inertial alteration of the phase plane is consistent with the antisymmetry of the ambient simple shear flow.

3.2. *Finite-St off-plane trajectories*

The above in-plane inertial modifications and the underlying physical mechanisms serve as valuable aids in understanding the off-plane trajectory behaviour for finite St. Off-plane inertial modifications are described below in §§ 3.2.1 and 3.2.2 for a single quadrant ($x > 0, z > 0$) of the whole trajectory space. The arguments easily extend to the entire space using the antisymmetry of simple shear and symmetry across the plane of shear.

3.2.1. *Off-plane open trajectories*

We begin by looking at zero-Stokes open trajectories outside the shearing plane and the effect of inertia on their fore–aft symmetry when viewed in the flow–vorticity (x, y) plane. Off-plane zero-Stokes trajectories, unlike those in the shearing plane, are not confined to the velocity–velocity gradient (yz)-plane. As shown by dotted lines in figure 5, their projections onto the xy-plane are not straight lines but qualitatively resemble the in-plane open trajectories in that they too include a pair of inflection points. Following arguments in the previous section, one again considers the direction of the inertial force over regions of positive and negative curvature in the xy-projection. The net vorticity displacement (Δx), similar to the in-plane gradient

† A measure of the rate of spiralling may be obtained using the following argument – the in-plane zero-Stokes separatrix, at large distances, is given by $z^2 \approx (16/9y^3)$ (Batchelor & Green 1972*a*). Thus, the inertialess separatrix would cross the flow axis at a point where the magnitude of the induced gradient displacement equals the above approximate form for its ordinate. Since the gradient displacement is $O(St^{1/2})$, we have $St \sim 1/y^3$, so $y \sim O(St^{-1/3})$. The ensemble of inertial trajectories with upstream offsets less than the in-plane finite-St separatrix would therefore cross the downstream portion of the flow axis in the interval $(O(St^{-1/3}), \infty)$.

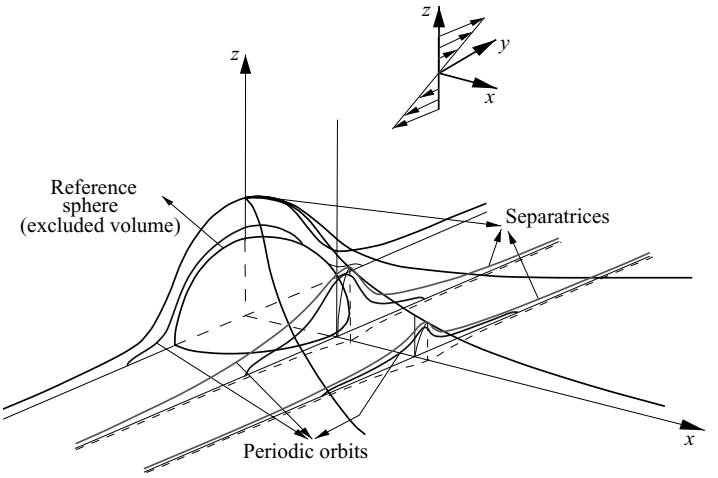

FIGURE 5. Axisymmetric separatrix envelope enclosing closed orbits at $St = 0$.

displacement, will then be $O(St)$ and negative for finite-St off-plane trajectories, at least those with $O(1)$ upstream offsets ($x^{-\infty}$) in the vorticity direction; by a negative Δx, here, we mean that the open trajectory ends up closer to the shearing plane far enough downstream. For $x^{-\infty} \to 0$ the off-plane trajectories become increasingly planar since they approach their counterparts in the plane of shear, and their xy-projections do not have to pass around the projection of the reference sphere onto the xy-plane. In fact, in contrast to the in-plane trajectories in figure 2, regions of positive and negative curvature in the xy-projections, rather than becoming more pronounced, approach straight lines as $x^{-\infty} \to 0$. Therefore, notwithstanding their flattening out into straight lines, the xy-projections are expected to remain qualitatively similar for all values of $x^{-\infty}$, implying that Δx is always negative and goes to zero as we approach the shearing plane. This also shows that one should not expect an analogue of the singular $O(St^{1/2})$ region for Δx at small $x^{-\infty}$, as was the case for the in-plane gradient displacement,

We next examine Δz for finite-St off-plane open trajectories, the physical reasoning again being based on the curvature of the corresponding zero-Stokes trajectories. Since the yz-projection of the zero-Stokes trajectory in figure 5 evidently has two inflection points, the argument employed in the previous paragraphs implies that Δz will again be $O(St)$ and negative for $z^{-\infty} \sim O(1)$. For small values of $x^{-\infty}$ the off-plane trajectories still resemble those in the plane of shear in that they pass very close to the surface of the reference sphere for small $z^{-\infty}$. Lubrication interactions therefore dominate in the near-field portions (with negative curvature as seen in the yz-plane) of these trajectories, again leading to an increasingly negative Δz as $z^{-\infty} \to 0$. Albeit smaller in magnitude than the in-plane gradient displacement for the same $z^{-\infty}$, Δz should still exhibit the same qualitative behaviour for small $x^{-\infty}$. Thus, there must exist a singular region in $z^{-\infty}$ of $O(St^{1/2})$, where (Δz) becomes $O(St^{1/2})$, and thence the same order of magnitude as $z^{-\infty}$. Accordingly, for small $x^{-\infty}$ there is an off-plane limiting trajectory for each $x^{-\infty}$ – the separatrix curve – that starts from a finite gradient offset of $O(St^{1/2})$ upstream and goes to zero far downstream (i.e. $z^{+\infty} = 0$ as $y \to \infty$), still suffering only an $O(St)$ vorticity displacement. As for the in-plane case, trajectories starting from smaller gradient offsets for these values of $x^{-\infty}$ will cross the y-axis at a finite distance downstream, resulting in a spiralling behaviour that is discussed in the next section.

The above arguments with regard to Δz, however, remain valid only for off-plane trajectories with a negative gradient displacement. For fixed $z^{-\infty}$ and for

$x^{-\infty}$ increasing, the trajectories move further away from the reference sphere, thereby diminishing the importance of the near-field lubrication interactions. For large enough $x^{-\infty}$, the magnitude of inertial forces acting between the two inflection points of the in-plane projection becomes sufficient to reverse the sign of Δz for small $z^{-\infty}$. This then implies the existence of an intermediate finite-St limiting trajectory – the 'neutral trajectory' – corresponding to a critical value of the off-plane coordinate, $x_c^{-\infty}$, for which $z^{\pm\infty} \to 0$, i.e. $\Delta z = 0$ (see figure 8 below); later, in § 5, $x_c^{-\infty}$ is found to be approximately 0.9. The finite-St separatrices for smaller values of $x^{-\infty}$ are as described above. For $x^{-\infty} \geqslant x_c^{-\infty}$, the limiting trajectories start instead from $z^{-\infty} = 0$ and suffer a positive gradient displacement, the scaling again being $St^{1/2}$ for St small enough. These trajectories are limiting in that they still separate the open and spiralling trajectories in this region. However, as will be seen in the next section, the nature of the spiralling trajectories in this region differs from that in $x < x_c^{-\infty}$. Despite the absence of a gradient displacement, the neutral trajectory is not fore–aft symmetric since it still suffers an $O(St)$ displacement in the vorticity direction; even its in-plane projection would be antisymmetric. We also observe that, while the magnitude of the negative Δz for $x^{-\infty} < x_c^{-\infty}$ is smaller for smaller St, the inertial forces effecting its sign reversal with increasing $x^{-\infty}$ are also correspondingly smaller. Therefore, the location $x_c^{-\infty}$ of the neutral trajectory, similar to the in-plane limit cycle in § 3.1, must be independent of St at leading order.

Now considering a fixed $x^{-\infty} (> x_c^{-\infty})$ and varying $z^{-\infty}$, the aforementioned arguments imply that open trajectories with $z^{-\infty} \sim O(1)$ or greater have a negative Δz, while those with $z^{-\infty}$ sufficiently small have a positive Δz. Thus, Δz must change sign across $z^{-\infty} = z_c^{-\infty}$ (say). As mentioned earlier, this occurs because for trajectories sufficiently far away from the reference sphere there is no lubrication mechanism to suppress the effects of inertial forces acting along the regions of negative curvature. Since both regions of positive and negative curvature become more pronounced for small $z^{-\infty}$, as manifested in a bigger hump in the yz-projection,† it is plausible that the two contributions to the gradient displacement will balance out at a certain critical value of the gradient offset denoted above by $z_c^{-\infty}$. Again, since the underlying inertial mechanisms leading to both positive and negative gradient displacements scale as $O(St)$, one expects that, similar to $x_c^{-\infty}$, the value of $z_c^{-\infty}$ for fixed $x^{-\infty}$ will be independent of St. For the neutral trajectory at $x_{-\infty} = x_c^{-\infty}$, $z_c^{-\infty}$ is, of course, equal to zero.

We therefore see that, while open off-plane trajectories with gradient offsets $O(1)$ or greater are altered for finite St, along lines consistent with our intuition based on the investigations of in-plane trajectories in § 3.1, those with smaller gradient offsets behave quite differently. The neutral off-plane trajectory at $x_c^{-\infty}$ acts to compartmentalize the finite-St trajectory space in a sense that dictates the nature of the spiralling trajectories discussed next. This compartmentalization is independent of St for St small, and has consequences for suspension microstructure and macroscopic properties. The structure of the zero- and finite-St separatrix envelopes are illustrated in figures 6 and 7.

3.2.2. *Off-plane spiralling trajectories*

Finally, we consider the inertial modifications of the off-plane zero-Stokes closed orbits, i.e. of the ensemble of trajectories lying inside the axisymmetric

† This occurs for off-plane zero-Stokes trajectories with small offsets because, for $z^{-\infty}$ small enough, they have to conform to the excluded volume of the axisymmetric separatrix envelope (see figures 5 and 6).

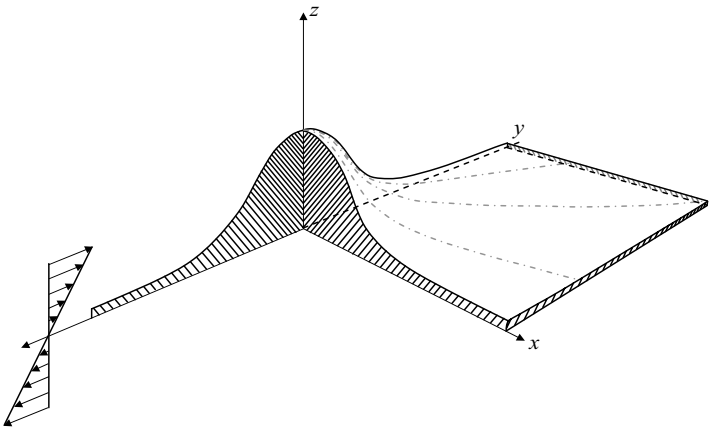

FIGURE 6. The structure of the axisymmetric separatrix envelopes at $St = 0$, that separates open and closed inertialess pair trajectories; the other half of the envelope may be constructed by symmetry about the flow–vorticity plane.

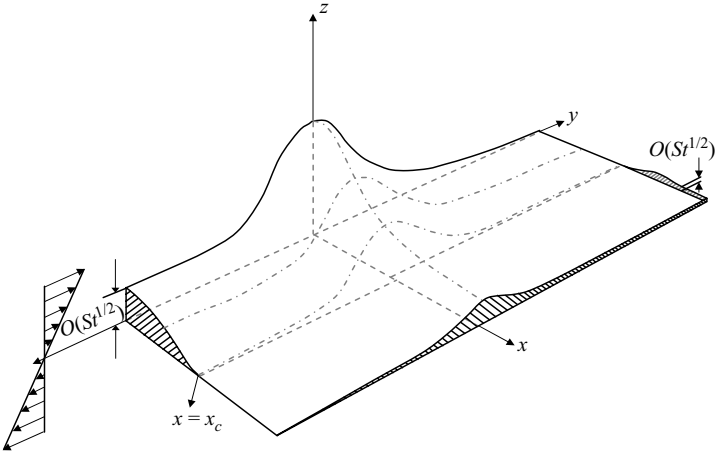

FIGURE 7. The separatix envelope for small but finite St. The envelope separates open and spiralling inertial pair trajectories and is symmetric about the plane of shear; the entire envelope may be constructed by (antisymmetric) reflection about the vorticity axis, and by symmetry about the shearing plane.

zero-Stokes separatrix envelope in figure 5. As for the in-plane case, the inertialess closed trajectories for any fixed (non-zero) value of the off-plane coordinate are similar in shape to open trajectories lying just outside the separatrix surface, except in regions asymptotically close to their points of intersection with the xy-plane where the curvature (of the yz-projection) changes sign as the trajectory crosses the xy-plane. Therefore one expects the qualitative effects of inertial forces, at least with regard to the vorticity displacement Δx, to remain the same even when acting on these closed orbits. Thus, the equivalent of the non-zero Δx in § 3.2.1 for a zero-Stokes closed trajectory would be an $O(St)$ difference between the x-coordinates of the points of intersection with the flow–vorticity (xy) plane. The resulting finite-St trajectory is no longer closed; if one begins at $x = x_1$ and $\phi = \pi$ (say), the next point of intersection at $\phi = 0$ (moving in a clockwise manner when viewed down the positive x-axis) will correspond

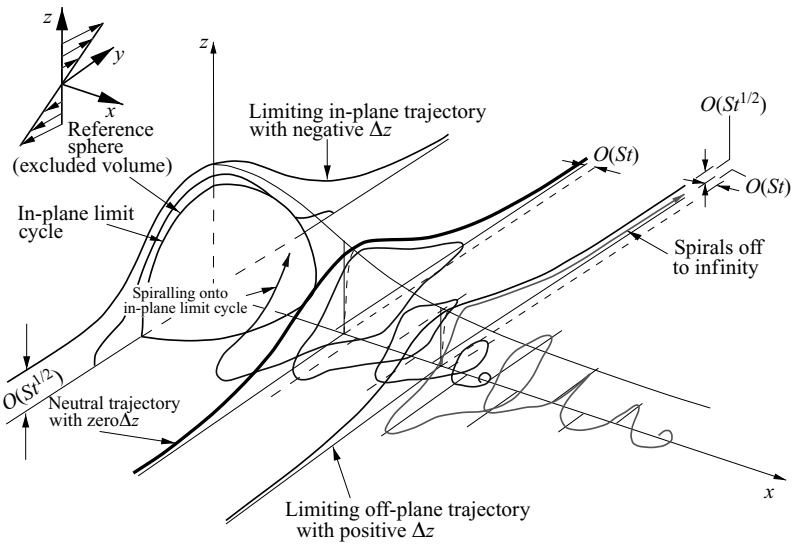

FIGURE 8. Finite-St spiralling trajectories within the modified separatrix envelope.

to $x_2 = x_1 + St(\Delta x)_1$ with $x_2 < x_1$ since Δx is negative. From the antisymmetry of the simple shear flow, it immediately follows that this pattern repeats itself, i.e. the inertial trajectory will again intersect the xy plane at a third point ($\phi = \pi$) corresponding to $x_3 = x_2 + St\,(\Delta x)_2$ with $x_3 < x_2$, and so on. The inertial trajectory, in effect, spirals towards the plane of shear, advancing by a distance of $O(St)$ in each cycle (see figure 8).

The yz-projection of the above spiralling trajectories is now examined. Unlike the in-plane case, however, the terms spiralling 'inward' and 'outward' used below need further qualification; specifically, we base our description of spiralling on the y-coordinates of the points of intersection with the xy-plane of the inertial trajectory, i.e. if successive points of intersection have coordinates y_1, y_2, such that $y_2 > y_1$, then the trajectory is said to spiral outward, and vice versa. This becomes necessary because an off-plane trajectory might spiral outward in z (applying the above definition to points of intersection of the trajectory with the xz-plane), but inward in y; in fact, the former is the case for virtually all off-plane spiralling trajectories since the z extent of the finite-St separatrix envelope diminishes as one moves away from the plane of shear; such trajectories are then still referred to as spiralling inward. In addition, it must be kept in mind that the spiralling trajectories always lie within the envelope formed by the finite-St separatrices discussed in the previous section. Thus, the phrase 'spiralling off to infinity', also used below, will refer to a spiralling trajectory that goes off to infinity while remaining within this envelope.

With the above terminology in mind, the nature of the spiralling trajectories, as seen in the yz-plane, may again be deduced from the sign of Δz for open trajectories in their vicinity. The equivalent of a non-zero Δz for a zero-Stokes closed trajectory, similar to the case of a non-zero Δx, is an asymmetry with respect to the y-coordinates of the points of intersection with the xy-plane of the resulting finite-St trajectory. Again, similar to the in-plane case, the difference between the y-coordinates of successive intersections need not be $O(St)$. This is because, for any fixed value of the off-plane coordinate, the entire family of zero-Stokes closed orbits covering the y-axis is still squeezed into an interval of $O(d)$ or smaller on the z-axis, d being the ordinate of the separatrix envelope at $\phi = \pi/2$. This squeezing occurs regardless of

the proximity to the reference sphere, the distance from this sphere only deciding the relative magnitudes of the lubricating and inertial forces. The former, as seen earlier in § 3.1, shrinks the interval on the z-axis bounded by the separatrix envelope to $O(10^{-5}a)$ close to the plane of shear. Thus, the inward or outward spiralling for off-plane trajectories at large distances from the vorticity axis will again be very rapid even with St small.

The finite-St spiralling trajectories may be divided into the following three categories:

(a) Finite-St trajectories just below the separatrix envelope (i.e. whose points of intersection with the xy-plane are at large distances from the vorticity axis) in the region $x < x_c^{-\infty}$ will spiral inward owing to the negative Δz for open trajectories immediately above; they eventually spiral onto the limit cycle in the plane of shear. Their behaviour resembles, and indeed asymptotes to, that of the spiralling in-plane trajectories of § 3.1 which lie outside the limit cycle but below the limiting in-plane trajectory.

(b) Finite-St trajectories will spiral outward for $x > x_c^{-\infty}$ owing to the reversal in the sign of Δz across $x = x_c^{-\infty}$. There is also an outward spiralling when $x < x_c^{-\infty}$ for trajectories that lie close to the reference sphere, since they have to conform to the sphere's excluded volume as they approach the plane of shear. These trajectories are still consistent with the negative Δz (for open trajectories) in $x < x_c^{-\infty}$, however, since though the points of intersection with the xy-plane move away from the vorticity axis, the trajectory still moves closer to the surface of the sphere.

(c) A subset of the finite-St trajectories that spiral out will approach the limit cycle in the shearing plane from 'within'. The long-time behaviour of these trajectories asymptotes to that of the in-plane trajectories in § 3.1 which spiral out onto the limit cycle in the shearing plane.

It must be emphasized that the above regimes need not necessarily correspond to distinct trajectories. Indeed, the first two cases may describe different stages of the same finite-St trajectory as it approaches the plane of shear. We do not consider the third case further, since in any event trajectories belonging to this class form a vanishingly small portion of the whole trajectory space.

The precise transition for a given finite-St trajectory from a diverging to a converging spiral may be seen as follows. At zero Stokes number, the trajectory space contains at least two neutrally stable invariant manifolds, the shearing plane and the vorticity axis. For finite-St the two manifolds remain invariant, and the modifications of trajectories in the plane of shear was described in § 3.1. An off-plane finite-St spiralling trajectory originates from (say) some point very near the vorticity axis ($t \to -\infty$), and to begin with, spirals outwards from it. During its motion towards the plane of shear in $O(St)$ increments, the trajectory if it comes closer than $x_c^{-\infty}$ will eventually begin spiralling inward and approach the in-plane limit cycle as $t \to \infty$ (see figure 9). On the other hand, if the outward spiralling is fast enough relative to the rate of approach, the trajectory will spiral off to infinity before crossing the neutral plane at $x_c^{-\infty}$. The possibility of escape does not exist for $x < x_c^{-\infty}$ since the outlet to infinity is now cut off by the envelope of limiting trajectories that tends to a zero offset downstream for $x < x_c^{-\infty}$ (see figures 7 and 9).† Even having considered all open trajectories in the previous section, there were still regions of space, infinite in extent,

† To be precise, the neutral plane should correspond to the downstream off-plane coordinate of the neutral trajectory, namely $x_c^{-\infty} - St(\Delta x)_c$, since it is beyond this value that the finite-St limiting envelope cuts off the escape to $y = \infty$.

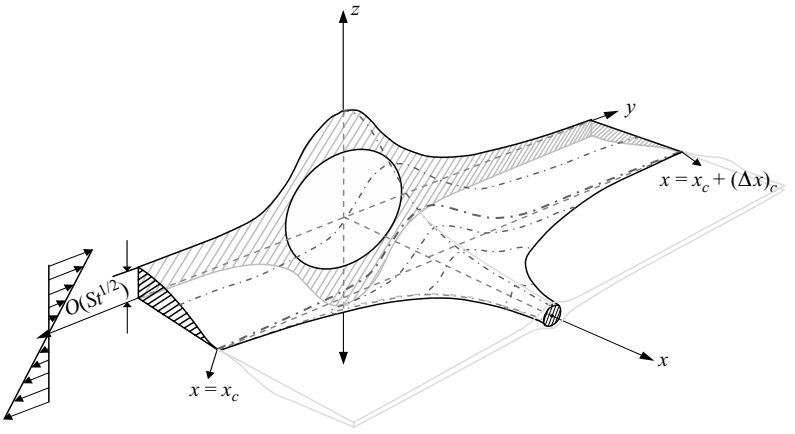

FIGURE 9. A schematic of the envelope of finite-St trajectories that spiral onto the limit cycle in the plane of shear; the projection of the sphere is depicted by a circle in the shearing plane. This envelope is identical to the finite-St separatrix envelope for $x < x_c^{-\infty}$. For $x > x_c^{-\infty}$, the original separatrix envelope is shown as grey lines, in order to emphasize the decrease in extent of the spiralling envelope in both the gradient and flow directions.

left unaccounted for: for example, in the quadrant $x, z > 0$, the region $y > 0, x > x_c^{-\infty}$, with z(of $O(St^{1/2})$), bounded by the family of limiting finite-St open trajectories, and similar symmetrically placed regions in other quadrants. It is precisely these regions that will be filled by trajectories spiralling off to infinity.

The correspondence between the nature of spiralling close to the separatrix envelope and the sign of Δz for the corresponding limiting open trajectory will not be exact due to 'end effects', that is to say, the transition from outward to inward spiralling for such trajectories will not occur exactly at $x = x_c^{-\infty}$ where Δz for the limiting off-plane trajectories changes sign. This discrepancy should be expected not only because of the small but finite distance of the spiralling trajectories from the separatrix envelope, but more importantly on account of inertial forces acting to push the spiralling trajectories further outwards (the equivalent of a positive Δz) in the regions close to $\phi = 0, \pi$ where the curvature changes sign.

The above finite-St modifications of the closed orbits is confirmed by numerical integration of the finite-St trajectory equations later in § 5. As for the in-plane case, the inertial modifications of the off-plane inertialess closed orbits are still consistent with the antisymmetry of the ambient simple shear flow, since the same arguments could be carried out for the quadrant $x > 0, z < 0$ with only the sign of y being reversed. Every finite-St spiralling trajectory for $x > 0$ therefore has a mirror image, obtained by reflection across the vorticity axis, and this pair of trajectories can, simplistically speaking, be likened to a pair of helices separated by half a pitch and winding around a cylindrical surface. This topology will then be invariant to a rotation through π as is required by the antisymmetry of simple shear.

In passing, it is worth mentioning that the above transition from a region of zero-Stokes closed trajectories to a region of finite-Stokes spiralling trajectories, bounded by the respective separatrix envelopes, may be viewed from a dynamical systems perspective (see Guckenheimer & Holmes 1983). The region enclosed by the axisymmetric zero-Stokes separatrix envelope in figure 5 may be regarded as a (degenerate) centre manifold embedded in three dimensions; the vorticity axis lying within this envelope comprises a continuum of elliptic fixed points (or 'centres'), and

the zero-Stokes closed trajectories may then be regarded as neutrally stable orbits around the centres. Such a configuration is structurally unstable, and even the smallest amount of 'hyperbolicity' can qualitatively alter the trajectory configuration. In our case, particle inertia is the source of this hyperbolicity. A similar situation occurs in the (geometrically) simpler context of inertialess rotation of an axisymmetric body in a Newtonian fluid, where the structurally unstable centre manifold is now the unit sphere of orientations with the pair of elliptic fixed points being given by the intersections of the vorticity axis with the unit sphere; the Jeffery trajectories are neutrally stable orbits around these centres (Jeffery 1922). It is known that a tiny amount of inertia (Subramanian & Koch 2005), or a slightly non-Newtonian fluid rheology (Leal 1975), qualitatively alters the trajectory configuration, and thence the orientation behaviour of the particle. In all cases, the modified trajectory configurations are stable to small perturbations.

As will be discussed in § 8, the non-trivial modification of pair-particle trajectories, on account of particle inertia, is not specific to simple shear flow alone. This is important since simple shear is an exceptional member in the family of linear flows, wherein extension and vorticity balance exactly, leading to rectilinear streamlines. The streamline configuration is thus susceptible to the addition of an arbitrarily small amount of extension or vorticity. For a generic linear flow, for instance planar linear flows with a ratio of extension to vorticity that differs from unity, the streamlines of the ambient flow form a structurally stable configuration. However, with the inclusion of hydrodynamic interactions, the resulting configuration of pair-particle pathlines, for flow with a sufficient amount of ambient vorticity, turns out to be structurally unstable, and there exists the possibility of a finite-St bifurcation.

4. Relative trajectories of two spheres in simple shear flow: perturbation analysis

4.1. *Analysis of singular points*

It helps to first compare the relative magnitudes of the velocities $\boldsymbol{V}^{(0)}$ and $St\,\boldsymbol{V}^{(1)}$ in equation (2.7) as functions of $\boldsymbol{r}$ in order to ascertain the existence of regions of non-uniformity where the perturbation expansion may be singular, knowledge of which would then help solve (2.7) for the particle-pair trajectories. Using explicit expressions for the resistance and mobility tensors for a general linear flow we find

$$V_i^{(0)} = \Gamma_{ij}^{\infty} r_j - \left[A \frac{r_i r_j}{r^2} + B \left(\delta_{ij} - \frac{r_i r_j}{r^2} \right) \right] E_{jk}^{\infty} r_k, \tag{4.1}$$

where A and B are functions of the scalar separation r and $\boldsymbol{\Gamma}^{\infty}$ is the velocity gradient tensor. Explicit expressions for A and B may be obtained in terms of the resistance and mobility functions defined in Jeffrey & Onishi (1984) and Kim & Mifflin (1985); for instance, $A = x_{11}^{g} - x_{12}^{g}$. For $St \ll 1$, the inertial velocity $St\,\boldsymbol{V}^{(1)}$ remains asymptotically small compared to $\boldsymbol{V}^{(0)}$ for large r because $\boldsymbol{V}^{(1)}_{(r \gg 1)} \approx \boldsymbol{V}^{(0)} \cdot \nabla_{\boldsymbol{r}} \boldsymbol{V}^{(0)} \approx (\boldsymbol{\Gamma}^{\infty} \cdot \boldsymbol{\Gamma}^{\infty}) \cdot \boldsymbol{r}$, and therefore grows in the same manner as the leading-order velocity. In fact, the inertial corrections at all higher orders are at most $O(r)$ for $r \gg 1$, in particular $\boldsymbol{V}^{(i)} \propto (\boldsymbol{\Gamma}^{\infty})^i \cdot \boldsymbol{r}$. For simple shear flow, $(\boldsymbol{\Gamma}^{\infty})^i = 0$ $(i \geqslant 2)$, and the inertial corrections therefore decay for large r.† This then precludes the existence of a radial boundary layer at infinity.

† Here, $(\boldsymbol{\Gamma}^{\infty})^i = \boldsymbol{\Gamma}^{\infty} \cdot \boldsymbol{\Gamma}^{\infty} \cdot \cdots \cdot \boldsymbol{\Gamma}^{\infty} i$ times.

In order to examine the possible presence of a radial boundary layer at contact, we consider the radial component of $\boldsymbol{V}^{(0)}$ for very small separations:

$$\lim_{r\to 2} V_r^{(0)} = \lim_{r\to 2}(1-A)E_{ij}^{\infty}\frac{r_i r_j}{r},$$
$$= 4.077(r-2)\left(2E_{ij}^{\infty}n_i n_j\right),$$

where we have used the near-field behaviour of A; $\boldsymbol{n}$ is the unit normal directed along the line of centres from particle 1 to 2. Thus, the radial component of $\boldsymbol{V}^{(0)}$ goes to zero linearly with decreasing interparticle separation. The tangential components of $\boldsymbol{V}^{(0)}$, however, remain finite at contact. The near-field behaviour of the inertial corrections $\boldsymbol{V}^{(i)}$ for $i \geqslant 1$ can be deduced by examining a simplified form of the exact equation of motion in one dimension (see Appendix A). It is thereby shown that for small enough separations, the relative approach velocity always decreases linearly with separation, the point of transition to this asymptotic regime being a strong function of St, however. (This may be seen from (A 4) by looking at the fictitious separation corresponding to a zero approach velocity which has an exponential dependence on St.) Thus, the radial components of the inertial corrections $\boldsymbol{V}^{(i)}$ $(i \geqslant 1)$ at all orders, similar to that of $\boldsymbol{V}^{(0)}$, vanish in a linear manner for small enough separations. The tangential components of $\boldsymbol{V}^{(i)}$ also tend to zero, albeit not always linearly. This then precludes the possibility of a radial boundary layer at contact.

The above asymptotic linear variation also implies that two approaching particles do not come into contact in a finite time. Indeed, it has already been pointed out by Sundararajakumar & Koch (1996) that interparticle contact, and hence solid-body collisions, need to be taken into account only for $St > O(1)$ when the gap thickness reduces to levels where the continuum approximation breaks down. For $St \ll 1$, lubrication forces still dominate the near-field behaviour and the situation is identical to that for inertialess particles. The absence of radial boundary layers still does not imply a regular perturbation expansion. Indeed, there are points of symmetry in the leading-order linear flow where $V_r^{(0)}$ is identically zero, and which give rise to angular boundary layers since the $O(St)$ correction has a non-zero radial component at these locations. As seen below, the fore–aft symmetric trajectory space in simple shear flow gives rise to singular points at $\phi = 90^\circ$ and 270°, corresponding to the gradient–vorticity plane. The perturbation analysis for finite-St in-plane trajectories in the next section takes these into account.

4.2. *Governing trajectory equations for* $St \ll 1$

Batchelor & Green (1972*a*) derived equations for the zero-Stokes pathlines of a pair of equal-sized spheres in simple shear flow; each relative trajectory was characterized by functions $\phi(r)$ and $\theta(r)$, (r, θ, ϕ) being the spherical polar coordinates with the origin at the centre of one sphere (see figure 1); $\theta = 0$ corresponds to the direction of the ambient vorticity (x-axis), and $\theta = \pi/2$ represents the plane of shear (the yz-plane, y being the direction of flow). We too formulate equation (2.7) for the $O(St)$ corrected particle trajectories in spherical coordinates, thereby exploiting the availability of an explicit expression for the leading-order solution.

Taking the ratios of the radial velocity to the angular velocities in the azimuthal (θ) and polar (ϕ) directions, one obtains the trajectory equations, to $O(St)$, as

$$\frac{\mathrm{d}\phi}{\mathrm{d}r} = \frac{-\{\sin^2\phi + (B/2)(\cos^2\phi - \sin^2\phi)\} + St\ f_1(r,\theta,\phi)/\sin\theta}{r(1-A)\sin^2\theta\sin\phi\cos\phi + St\ f_2(r,\theta,\phi)}, \tag{4.2}$$

$$\frac{\mathrm{d}\theta}{\mathrm{d}r} = \frac{(1-B)\sin\theta\cos\theta\sin\phi\cos\phi + St\ f_3(r,\theta,\phi)}{r(1-A)\sin^2\theta\sin\phi\cos\phi + St\ f_2(r,\theta,\phi)}, \tag{4.3}$$

where

$$f_1(r,\theta,\phi) = -H\sin^2\theta\sin\phi\cos\phi\left[\left\{2B(A-B)-r(1-A)\frac{\mathrm{d}B}{\mathrm{d}r}\right\}\sin\theta\frac{(\cos^2\phi-\sin^2\phi)}{2}\right.$$
$$\left.+2(A-B)\sin\theta\sin^2\phi\right]-\frac{6E}{5r}\sin\theta\sin\phi\cos\phi\left[\sin^2\theta\frac{(\cos^2\phi-\sin^2\phi)}{2}\right.$$
$$\left.\times\left\{r(1-A)\frac{\mathrm{d}C}{\mathrm{d}r}+2C(B-1)\right\}+\frac{C}{2}(1+\sin^2\theta)\right],$$
$$f_2(r,\theta,\phi) = -rG\left[\sin^4\theta\sin^2\phi\cos^2\phi\left\{(A-B)^2-r(1-A)\frac{\mathrm{d}A}{\mathrm{d}r}\right\}\right.$$
$$\left.+\frac{(B-2A)}{2}\sin^2\phi\sin^2\theta-\frac{B}{2}\cos^2\phi\sin^2\theta-\frac{B(B-2A)}{4}\sin^2\theta\right],$$
$$f_3(r,\theta,\phi) = -H\sin\theta\cos\theta\left[\frac{B(B-2)}{4}+\sin^2\theta\sin^2\phi\cos^2\phi\ \{2(B-1)(A-B)\right.$$
$$\left.-r(1-A)\frac{\mathrm{d}B}{\mathrm{d}r}\right\}\Big]-\frac{6E}{5r}\sin\theta\cos\theta\left[\sin^2\theta\sin^2\phi\cos^2\phi\right.$$
$$\left.\times\left\{r(1-A)\frac{\mathrm{d}C}{\mathrm{d}r}+2C(B-1)\right\}+\frac{C}{4}(2\sin^2\phi-B)\right],$$

Here, rf_3 and $(r\sin\theta f_1)$, respectively, denote the $O(St)$ corrections to the polar and azimuthal components of the inertialess angular velocity, while f_2 is the $O(St)$ correction to the radial component. The functions A and B, as before, characterize the relative translational velocity of two inertialess spheres, while C denotes the corresponding angular velocity correction on account of hydrodynamic interactions; the function E represents the translation–rotation coupling. Explicit expressions for A, B, C, E, G and H may again be obtained from Jeffrey & Onishi (1984) and Kim & Mifflin (1985); for instance, $G = x^a_{11} - x^a_{12}$, $H = y^a_{11} - y^a_{12}$, $E = y^b_{11} - y^b_{12}$, etc. Although we have retained the $O(St)$ denominator term on the right-hand sides of (4.2) and (4.3), the resulting solution is meaningful only to $O(St)$. We first note that (4.2) and (4.3), with only the leading-order terms, remain unchanged on replacing ϕ by $\pi \pm \phi$, indicating the fore–aft symmetry of the zero-Stokes trajectory space. With the $O(St)$ terms included, the system remains unchanged only on replacing ϕ by $\pi + \phi$, as is required by the antisymmetry of simple shear. Further, on account of symmetry across the plane of shear ($\theta \leftrightarrow \pi - \theta$), it suffices to consider the quadrant $0 \leqslant \theta \leqslant \pi/2$, $0 \leqslant \phi \leqslant \pi$ of the entire trajectory space.

As indicated in the previous section, a regular small-St expansion provides a uniform approximation with respect to r, but not with respect to ϕ. In particular, at $\phi = \pi/2$, the $O(1)$ terms in the denominator of the right-hand side in (4.2), and in both the numerator and denominator in (4.3), equal zero, since the zero-Stokes trajectory is perpendicular to the gradient–vorticity plane. On the other hand, $f_2(c/\sin\theta_t, \theta_t, \pi/2)$ and $f_3(c/\sin\theta_t, \pi/2)$ (where c is the zero-Stokes coordinate along the gradient (z) axis and θ_t is the value of θ, both at $\phi = \pi/2$) do not equal zero owing to the radial and (polar) angular velocities induced at $O(St)$, that also destroy the fore–aft symmetry. The perturbation is therefore singular in nature, necessitating care in the analysis when ϕ is close to $\pi/2$. The analysis in the following subsections will yield a picture of the entire (r, θ, ϕ) phase space. In what follows, it will be necessary to treat ϕ and θ as dependent variables and not r, since the solution of the trajectory equation

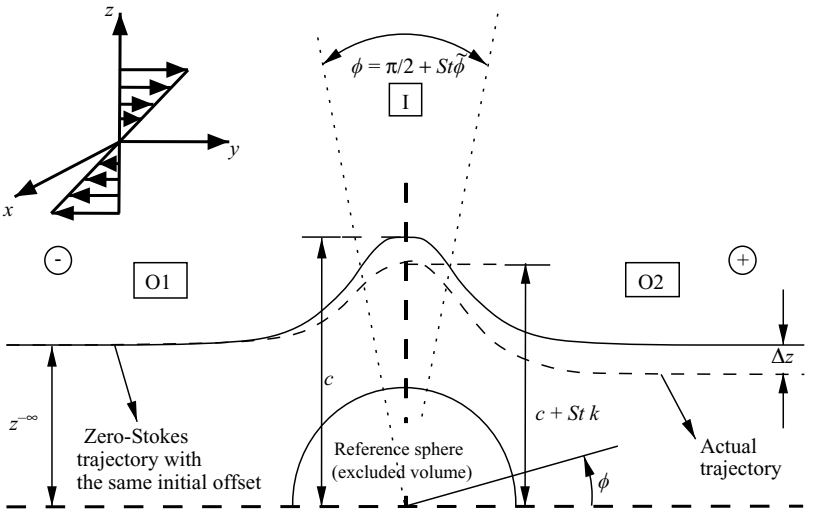

FIGURE 10. A finite-St (dashed line) and a zero-Stokes (solid line) open trajectory with identical upstream gradient offsets ($z^{-\infty}$), when viewed along the vorticity direction (x-axis). Note that the inertialess trajectory is fore–aft symmetric, while the inertial trajectory undergoes a net transverse displacement in the gradient direction. The two dotted rays emanating from the centre of the reference sphere demarcate the three regions of space, in which the perturbation expansions differ in form: the outer upstream layer O1, the inner layer I, and the outer downstream layer O2.

at the zeroth order yields ϕ and θ as explicit functions of r and not the other way around (Batchelor & Green 1972*a*).† Also, (4.2) and (4.3) are first-order differential equations, needing only a single boundary condition each. The corresponding zero-Stokes trajectories may be characterized by prescribing their offsets, both gradient and vorticity, far upstream or downstream (the 'outer' layers), or those at $\phi = \pi/2$ (the 'inner' layer) – see figure 10. Depending on where this boundary condition is imposed, the solutions in the particular layer are determined to all orders in St. These then determine the solutions in the other layers via the matching procedure. In this sense, the method of analysis here differs from the situation normally encountered in the method of matched asymptotic expansions, applied to second- or higher-order differential equations, wherein none of the solutions in any layer satisfy all boundary conditions; of course, the undetermined constants in each solution are again determined from matching, at successive orders, in the regions of overlap. We shall impose the boundary condition in the outer layers by requiring that both the actual and zero-Stokes trajectories start from the same upstream offsets; upstream in the polar coordinate system adopted here refers to the region $\phi \to \pi, r \to \infty$ for $z > 0$, so the solution in the outer layer denoted O1 below is determined to all orders independent of other layers. In what follows, we present a rather succinct description of the perturbation analysis while omitting a few aspects, for instance the matching of the asymptotic expansions in different regions; interested readers may refer to Subramanian (2002) for details.

† Even otherwise, treating r as the independent variable turns out to be convenient since the finite-St asymmetry is characterized by the net displacements transverse to the flow direction; their evaluation requires the limiting value of the difference between the upstream and downstream transverse coordinates over an infinite stretch of the trajectory.

4.3. *Open trajectories with upstream gradient offsets much greater than* $O(St^{1/2})$

In this section we develop a perturbation scheme for finite-St open trajectories with $O(1)$ upstream gradient offsets (see figure 10). It will be seen later that the method, in fact, remains valid for trajectories with gradient offsets greater than $O(St^{1/2})$. Owing to the singularity identified in the neighborhood of $\phi = \pi/2$, it will be necessary to use separate expansions in the following three portions of a typical finite-St open trajectory:

$$\text{Outer (upstream) layer O1}: \phi \in \left(\frac{\pi}{2} + O(1), \pi\right), \theta \in \left(\theta_t + O(1), \frac{\pi}{2}\right), r > \frac{c}{\sin\theta_t} + O(1),$$

$$\text{Inner layer I}: \phi = \frac{\pi}{2} + St\,\tilde{\phi}, \theta = \theta_t + St\,\hat{\theta}_f + St^2\tilde{\theta}, r = \frac{c}{\sin\theta_t} + St\,k + St^2\tilde{r},$$

$$\text{Outer (downstream) layer O2}: \phi \in \left(0, \frac{\pi}{2} - O(1)\right), \theta \in \left(\theta_t + O(1), \frac{\pi}{2}\right), r > \frac{c}{\sin\theta_t} + O(1).$$

The respective regions are depicted in figure 10.

4.3.1. *Outer layer* $O1$

In this layer we use the regular expansions:

$$\theta = \theta_0 + St\,\theta_1 + \cdots, \tag{4.4}$$

$$\phi = \phi_0 + St\,\phi_1 + \cdots. \tag{4.5}$$

Substituting these in (4.2) and (4.3), one obtains

$$O(1): \frac{\mathrm{d}\theta_0}{\mathrm{d}r} = \frac{(1-B)}{r(1-A)}\frac{\cos\theta_0}{\sin\theta_0}, \tag{4.6}$$

$$O(St): \frac{\mathrm{d}\theta_1}{\mathrm{d}r} = -\frac{(1-B)}{r(1-A)\sin^2\theta_0}\theta_1 + \left\{\frac{f_3(r,\theta_0,\phi_0)}{r(1-A)\sin^2\theta_0\cos\phi_0\sin\phi_0} - \frac{(1-B)f_2(r,\theta_0,\phi_0)\cos\theta_0}{r^2(1-A)^2\sin^3\theta_0\cos\phi_0\sin\phi_0}\right\}, \tag{4.7}$$

and

$$O(1): \frac{\mathrm{d}\phi_0}{\mathrm{d}r} = -\frac{\sin^2\phi_0 + \frac{1}{2}B(\cos^2\phi_0 - \sin^2\phi_0)}{r(1-A)\sin^2\theta_0\sin\phi_0\cos\phi_0}, \tag{4.8}$$

$$O(St): \frac{\mathrm{d}\phi_1}{\mathrm{d}r} = \left\{\frac{\frac{1}{2}B - \sin^2\phi_0}{r(1-A)\sin^2\phi_0\,\cos^2\phi_0\,\sin^2\theta_0}\right\}\phi_1 + \left\{\frac{2\cos\theta_0\left\{\sin^2\phi_0(1-B) + \frac{1}{2}B\right\}}{r(1-A)\sin^3\theta_0\cos\phi_0\sin\phi_0}\right\}\theta_1 \times \left\{\frac{f_1(r,\theta_0,\phi_0)}{r(1-A)\sin^3\theta_0\sin\phi_0\,\cos\phi_0} + \frac{\left\{(1-B)\,\sin^2\phi_0 + \frac{1}{2}B\right\}f_2(r,\theta_0,\phi_0)}{r^2(1-A)^2\sin^4\theta_0\sin^2\phi_0\,\cos^2\phi_0}\right\}, \tag{4.9}$$

at successive orders. Since the equations for θ_0 and θ_1 do not depend on ϕ_0 and ϕ_1, respectively, it is convenient to first solve for θ at each order.

The upstream boundary conditions are

$$r\cos\theta \to x^{-\infty}, \tag{4.10}$$

$$r\sin\theta\sin\phi \to z^{-\infty}, \tag{4.11}$$

that, at successive orders in St, may be written as

$$O(1) : r\cos\theta_0 \to x^{-\infty} \quad \text{as} \quad r \to \infty,$$
$$O(St) : r\,\theta_1^- \to 0 \quad \text{as} \quad r \to \infty\,(\phi_0 \to \pi),$$

$$O(1) : r\sin\theta_0\sin\phi_0 \to z^{-\infty} \quad \text{as} \quad r \to \infty,$$
$$O(St) : r\phi_1^- \to 0 \quad \text{as} \quad r \to \infty\,(\phi_0 \to \pi),$$

where the branches of ϕ_1 and θ_1 in the interval $\phi_0 \in (\pi/2, \pi)$ are denoted by the superscript '$-$'; the corresponding branches in $\phi_0 \in (0, \pi/2)$ will be denoted by '$+$'. The asymmetry of the finite-St open trajectories will be characterized by their net displacements in the gradient and vorticity directions.

The displacement in the gradient and vorticity directions are given by

$$(\Delta x) = r\cos\theta\,|_{\phi\to\pi}^{\phi\to 0} = -\,St\,\lim_{r\to\infty} r\,\theta_1^+, \tag{4.12}$$

$$\Delta z = r\sin\theta\sin\phi\,|_{\phi\to\pi}^{\phi\to 0} = St\,\lim_{r\to\infty} r\phi_1^+, \tag{4.13}$$

where we have used the fore–aft symmetry of the zero-Stokes trajectory.

Using the boundary conditions at $O(1)$, we obtain the Batchelor–Green expressions for ϕ_0 and θ_0:

$$O(1)\colon \cos\theta_0 = \frac{x^{-\infty}}{r}\exp\left[\int_r^\infty \frac{q(r')}{2}\,\mathrm{d}r'\right], \tag{4.14}$$

$$r^2\sin^2\phi_0 = \frac{(z^{-\infty})^2}{\sin^2\theta_0}\exp\left[\int_r^\infty q(r')\,\mathrm{d}r'\right] + \frac{1}{\sin^2\theta_0}\int_r^\infty \exp\left[-\int_{r'}^r q(r'')\,\mathrm{d}r''\right]\frac{B'r'}{(1-A')}\,\mathrm{d}r', \tag{4.15}$$

where

$$q(r) = \frac{2(A-B)}{(1-A)r},$$

and the prime on A, B, etc. implies evaluation at r'.

Keeping in mind the expressions (4.12) and (4.13) for the transverse displacements, the solutions, at $O(St)$, are given in terms of $r\,\theta_1$ and $r\phi_1$:

$$O(St)\colon r\,\theta_1^- = -\frac{1}{\sin\theta_0}\int_r^\infty \exp\left[-\int_{r'}^r \frac{q(r'')}{2}\mathrm{d}r''\right]\left\{\frac{f_3(r',\theta_0',\phi_0')}{(1-A')\sin\theta_0'\cos\phi_0'\sin\phi_0'}\right.$$
$$\left. -\frac{(1-B')f_2(r',\theta_0',\phi_0')\cos\theta_0'}{r'(1-A')^2\sin^2\theta_0'\cos\phi_0'\sin\phi_0'}\right\}\mathrm{d}r', \tag{4.16}$$

$$r\phi_1^- = -\frac{1}{r\cos\phi_0\sin\phi_0\sin^2\theta_0}\int_r^\infty \exp\left[-\int_{r'}^r q(r'')\,\mathrm{d}r''\right]$$
$$\times\left\{\frac{2r'\cos\theta_0'\{(1-B')\sin^2\phi_0' + \frac{1}{2}B'\}}{(1-A')\sin\theta_0'}\,\theta_1^- + \frac{r'f_1(r',\theta_0',\phi_0')}{(1-A')\sin\theta_0'}\right.$$
$$\left. + \frac{\{(1-B')\sin^2\phi_0' + \frac{1}{2}B'\}f_2(r',\theta_0',\phi_0')}{(1-A')^2\sin^2\theta_0'\sin\phi_0'\cos\phi_0'}\right\}\mathrm{d}r'. \tag{4.17}$$

We note that, for given values of $x^{-\infty}$ and $z^{-\infty}$, the solution for ϕ_0 in (4.15) is real valued only for $r \geqslant c/\sin\theta_t$, where

$$c^2 = (z^{-\infty})^2 \exp\left[-\int_{\frac{c}{\sin\theta_t}}^{\infty} q(r')\,\mathrm{d}r'\right] + \int_{\frac{c}{\sin\theta_t}}^{\infty} \exp\left[-\int_{r'}^{\frac{c}{\sin\theta_t}} q(r'')\,\mathrm{d}r''\right] \frac{B'r'}{(1-A')}\,\mathrm{d}r'. \quad (4.18)$$

Here, $r = c/\sin\theta_t$ is the distance of nearest approach of the zero-Stokes trajectory with upstream offsets $(x^{-\infty}, z^{-\infty})$, and c, as before, is the ordinate of its point of intersection with the gradient–vorticity plane. The breakdown of the outer expansion is evident from (4.17) for ϕ_1^-, where $\cos\phi_0$ tends to zero as $(r, \theta, \phi) \to (c/\sin\theta_t, \theta_t, \pi/2)$. For ϕ_0 close to $\pi/2$, $\cos\phi_0 \propto (r - c/\sin\theta_t)^{1/2}$, so $St\,\phi_1^-$ eventually becomes comparable with ϕ_0 for regions of the trajectory sufficiently near the gradient–vorticity plane. This necessitates a re-scaling to account for inertial corrections that become important, at leading order, in a narrow interval across the gradient–vorticity plane.

4.3.2. *Inner layer I*

Herein, the radial component of the $O(St)$ inertial velocity is important at leading order in the equation for ϕ. Since ϕ is close to $\pi/2$, and r close to $c/\sin\theta_t$, the leading-order balance suggests rescaled coordinates $\tilde{\phi}$ and $\tilde{r}$ of the form

$$\phi^I = \frac{\pi}{2} + St\,\tilde{\phi}, \quad r = \frac{c}{\sin\theta_t} + Stk + St^2\tilde{r}, \quad \theta = \theta_t + O(St),$$

where the constant k will be found from matching the inner and outer expansions in their domain of overlap, and will turn out to be negative since the in-plane inertial trajectory, starting from the same upstream offset, ends up closer to the reference particle at $\phi = \pi/2$ than the corresponding zero-Stokes trajectory. In addition, since θ_0, unlike ϕ_0, remains real valued even for values of r less than the zero-Stokes minimum $(c/\sin\theta_t)$, for purposes of determining the transverse displacements Δx and Δz, it suffices to directly match the limiting expressions in the outer upstream and downstream layers $O1$ and $O2$. We therefore restrict ourselves to considering the inner layer for ϕ alone.

In terms of the rescaled coordinates, (4.3), at leading order, becomes

$$\frac{\mathrm{d}\tilde{\phi}}{\mathrm{d}\tilde{r}} = \frac{\left(1 - \frac{1}{2}B_0\right)}{c\sin\theta_t\,(1-A_0)\tilde{\phi} - f_2\left(c/\sin\theta_t, \theta_t, \frac{1}{2}\pi\right)}, \quad (4.19)$$

where the subscript '0' used for the hydrodynamic functions here and in all subsequent expressions denotes the value of the function at $r = c/\sin\theta_t$ unless stated otherwise.

The solution to (4.19) is given by

$$\tilde{\phi}^{\mp} = \frac{G_0(2-B_0)(2A_0-B_0)}{4(1-A_0)}\left[1 \pm \left\{1 + \frac{16(\tilde{r} - I_i)(1-A_0)}{c\,G_0^2(2-B_0)(2A_0-B_0)^2\sin\theta_t}\right\}^{1/2}\right], \quad (4.20)$$

where I_i is an integration constant. The two distinct values of $\tilde{\phi}$ for each value of $\tilde{r}$ indicate the $O(St)$ asymmetry of the inertial trajectory. As will be seen, the value of I_i does not affect the matching to $O(St)$, and a qualitative picture of the inner solution may therefore be obtained by setting $I_i = 0$ in (4.20). It is then seen that the minimum value of r occurs when

$$\tilde{r}_{min} = -\frac{c\,G_0^2(2-B_0)(2A_0-B_0)^2}{16(1-A_0)\sin\theta_t},$$

where the two branches $\tilde{\phi}^+$ and $\tilde{\phi}^-$ coincide, i.e.

$$\tilde{\phi}^+ = \tilde{\phi}^- = \tilde{\phi}_{min} = \frac{G_0(2-B_0)(2A_0-B_0)}{4(1-A_0)}.$$

The value of $\tilde{\phi}_{min}$ being positive, $\phi \in (\pi/2, \pi)$, and the smallest radial separation occurs in the upstream quadrant.

4.3.3. *Outer layer O2*

Since the zero-Stokes trajectory is fore–aft symmetric, the leading-order solution remains the same as in O1. The $O(St)$ solutions in this layer is given by

$$r\theta_1^+ = \frac{I_{\theta_1^+}}{\sin\theta_0}\exp\left[\int_r^\infty \frac{q(r')}{2}\,\mathrm{d}r'\right] - \frac{1}{\sin\theta_0}\int_r^\infty \exp\left[-\int_{r'}^r \frac{q(r'')}{2}\,\mathrm{d}r''\right] \times \left\{\frac{f_3(r',\theta_0',\phi_0')}{(1-A')\sin\theta_0'\cos\phi_0'\sin\phi_0'} - \frac{(1-B')f_2(r',\theta_0',\phi_0')\cos\theta_0'}{r'(1-A')^2\sin^2\theta_0'\cos\phi_0'\sin\phi_0'}\right\}\mathrm{d}r', \tag{4.21}$$

$$\begin{aligned} r\phi_1^+ = {} & \frac{z^{-\infty} I_{\phi_1^+}}{r\cos\phi_0\sin\phi_0\sin^2\theta_0}\exp\left[\int_r^\infty q(r')\,\mathrm{d}r'\right] \\ & - \frac{1}{r\cos\phi_0\sin\phi_0\sin^2\theta_0}\int_r^\infty \exp\left[-\int_{r'}^r q(r'')\,\mathrm{d}r''\right]\left\{\frac{2r'\cos\theta_0'\left\{(1-B')\sin^2\phi_0' + \frac{1}{2}B'\right\}}{(1-A')\sin\theta_0'}\theta_{1m}^- \right. \\ & \left. + \frac{r' f_1(r',\theta_0',\phi_0')}{(1-A')\sin\theta_0'} + \frac{\left\{(1-B')\sin^2\phi_0' + \frac{1}{2}B'\right\} f_2(r',\theta_0',\phi_0')}{(1-A')^2\sin^2\theta_0'\sin\phi_0'\cos\phi_0'}\right\}\mathrm{d}r' \\ & - \frac{I_{\theta_1^+} x^{-\infty}\sin\phi_0}{r\sin^2\theta_0\cos\phi_0}\exp\left[\int_r^\infty q(r')\,\mathrm{d}r'\right]. \end{aligned} \tag{4.22}$$

where θ_{1m}^- is given by (4.16) with $\phi_0' \in (0, \pi/2)$; the integration constants, $I_{\theta_1^+}$ and $I_{\phi_1}^+$, are determined from matching considerations.

4.3.4. *Gradient and vorticity displacements*

The limiting forms of the inner and outer solutions tabulated above can be matched by rewriting them in appropriate intermediate variables, whence it is found that

$$\begin{aligned} k = {} & 2\sin\theta_t\frac{(1-A_0)}{c(2-B_0)}\int_{\frac{c}{\sin\theta_t}}^\infty \exp\left[-\int_{r'}^{\frac{c}{\sin\theta_t}} q(r'')\,\mathrm{d}r''\right]\left\{\frac{2r'\cos\theta_0'\left\{(1-B')\sin^2\phi_0' + \frac{1}{2}B'\right\}}{(1-A')\sin\theta_0'}\theta_{1m}^- \right. \\ & \left. + \frac{r' f_1(r',\theta_0',\phi_0')}{(1-A')\sin\theta_0'} + \frac{\left\{(1-B')\sin^2\phi_0' + \frac{1}{2}B'\right\} f_2(r',\theta_0',\phi_0')}{(1-A')^2\sin^2\theta_0'\sin\phi_0'\cos\phi_0'}\right\}\mathrm{d}r' \end{aligned} \tag{4.23}$$

and the expressions for the vorticity and gradient displacements are

$$\begin{aligned} \Delta x = {} & -2St\int_{\frac{c}{\sin\theta_t}}^\infty \exp\left[-\int_{r'}^\infty \frac{q(r'')}{2}\,\mathrm{d}r''\right]\left\{\frac{f_3(r',\theta_0',\phi_0')}{(1-A')\sin\theta_0'\cos\phi_0'\sin\phi_0'} \right. \\ & \left. - \frac{(1-B')f_2(r',\theta_0',\phi_0')\cos\theta_0'}{r'(1-A')^2\sin^2\theta_0'\cos\phi_0'\sin\phi_0'}\right\}\mathrm{d}r', \end{aligned} \tag{4.24}$$

$$\begin{aligned} \Delta z = {} & \frac{St}{z^{-\infty}}\left(2\int_{\frac{c}{\sin\theta_t}}^\infty \exp\left[-\int_{r'}^\infty q(r'')\,\mathrm{d}r''\right]\left\{\frac{2r'\cos\theta_0'\left\{(1-B')\sin^2\phi_0' + \frac{1}{2}B'\right\}}{(1-A')\sin\theta_0'}\theta_{1m}^- \right. \right. \\ & \left. \left. + \frac{r' f_1(r',\theta_0',\phi_0')}{(1-A')\sin\theta_0'} + \frac{\left\{(1-B')\sin^2\phi_0' + \frac{1}{2}B'\right\} f_2(r',\theta_0',\phi_0')}{(1-A')^2\sin^2\theta_0'\sin\phi_0'\cos\phi_0'}\right\}\mathrm{d}r'\right) - (\Delta x)\frac{x^{-\infty}}{z^{-\infty}}. \end{aligned} \tag{4.25}$$

	(*a*)		(*b*)	
$z^{-\infty}$	$(\Delta x)_{traj}\,(St=0.1)$	$(\Delta x)_{traj}\,(St=0.01)$	$(\Delta x)_{traj}\,(St=0.1)$	$(\Delta x)_{traj}\,(St=0.01)$
5	-7.716×10^{-5}	-7.718×10^{-6}	-3.536×10^{-4}	-3.537×10^{-5}
2	-1.557×10^{-3}	-1.552×10^{-4}	-5.146×10^{-3}	-5.137×10^{-4}
1	-6.295×10^{-3}	-6.302×10^{-4}	-1.427×10^{-2}	-1.421×10^{-3}
0.5	-8.784×10^{-3}	-8.921×10^{-4}	-1.719×10^{-2}	-1.711×10^{-3}
0.2	-9.424×10^{-3}	-9.593×10^{-4}	-1.697×10^{-2}	-1.684×10^{-3}

TABLE 1. Δx values for (*a*) $x^{-\infty}=0.2$ and (*b*) $x^{-\infty}=1$, and $z^{-\infty}$ ranging from 5 to 0.1; $St=0.1, 0.01$.

We first observe that (4.24) for Δx remains $O(St)$ for all finite-St open trajectories. Moreover, since $f_3(r,\pi/2,\phi)=0$, Δx tends to zero as $\theta_t\to\pi/2$, that is, as $x^{-\infty}\to0$, regardless of the gradient offset $z^{-\infty}$, consistent with physical arguments presented in § 3.2. In tables 1(*a*) and 1(*b*) we tabulate values of the vorticity displacement for open trajectories, denoted here by $(\Delta x)_{traj}$ for $St=0.1$ and 0.01. These values were obtained from a numerical integration of the trajectory equations, (4.2) and (4.3), using an adaptive Runge–Kutta fourth-order method, and confirm the $O(St)$ scaling. The values of the hydrodynamic functions required for the numerical integration were obtained as follows. For separations less than 4 particle radii, the values of the hydrodynamic functions were obtained by interpolating between tabulated values obtained from the twin multipole expansions given in Jeffrey & Onishi (1984) and Jeffrey (1992); the number of terms included in the expansion was 300. For separations greater than 4 particle radii, the approximate far-field expressions given in the same references were used.

On the other hand, the expression (4.25) for Δz is singular for $z^{-\infty}\to0$ provided the factor multiplying $1/z^{-\infty}$ in (4.25) remains non-zero. When $z^{-\infty}\sim O(St^{1/2})$, the predicted gradient displacement is of the same order of magnitude as $z^{-\infty}$, and the inertial correction $St\,\phi_1$ becomes comparable to ϕ_0 far enough downstream. The postulated expansion is thus no longer valid for trajectories with these and smaller upstream offsets. An alternative expression for Δz valid for trajectories with $O(St^{1/2})$ gradient offsets, and its dependence on $x^{-\infty}$, is derived in the next section.

4.4. *Open trajectories with $O(St^{1/2})$ upstream gradient offsets*

Equation (4.25) for Δz remains valid only for trajectories with upstream gradient offsets greater than $O(St^{1/2})$. The breakdown of the perturbation scheme for trajectories with $O(St^{1/2})$ or smaller offsets could not have been anticipated based on the order of magnitudes of terms in the governing equations, since the non-uniformity is on account of integrated effects; indeed, the $O(St)$ terms in (4.2) decay more rapidly than the leading-order terms in the limit $r\gg1$. In order to obtain the transverse displacements for a trajectory with an $O(St^{1/2})$ gradient offset, we therefore adopt a different approach. The upstream and downstream branches of the inertial trajectory are now calculated independently, and then pieced together at the gradient–vorticity plane ($\phi=\pi/2$). On one hand, this characterizes the relation between the initial offsets, both gradient and vorticity, of the upstream and downstream portions, thus determining the transverse displacements for an open trajectory lying above the finite-St separatrix envelope; on the other, when the gradient offset of the downstream portion is zero, the procedure yields the limiting upstream gradient offset of the separatrix as a function of the coordinate along the vorticity axis. The method is illustrated below for an inertial trajectory in the plane of shear, the analysis in this

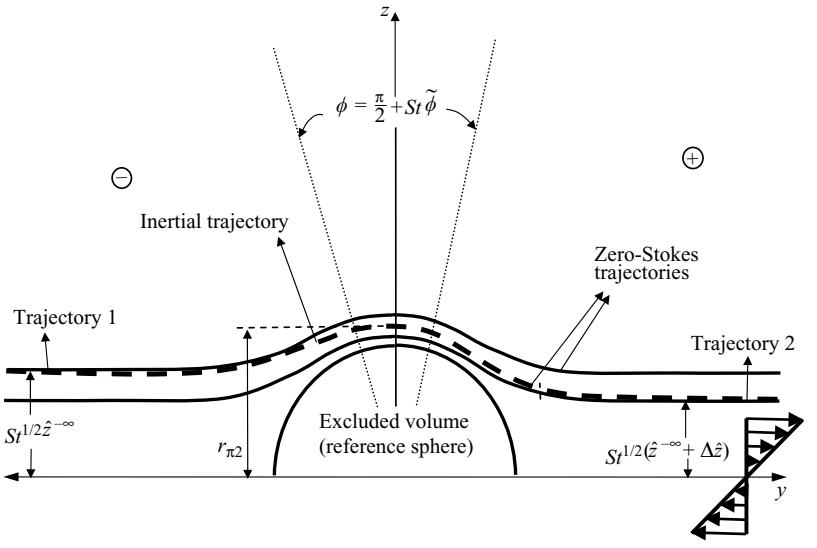

FIGURE 11. An in-plane finite-St trajectory (dashed line), with an upstream gradient offset of $O(St^{1/2})$, perturbed about two distinct zero-Stokes open trajectories (solid lines) labelled as trajectories 1 and 2. The inertial trajectory undergoes a gradient displacement of $St^{1/2}\Delta\hat{z}$. The two dotted rays emanating from the centre of the reference sphere demarcate the singular 'inner' layer spanning the gradient axis.

case being considerably simpler since the vorticity displacement is identically zero. The off-plane case, albeit more cumbersome, remains similar in concept, and we directly give the resulting expressions for both the gradient and vorticity displacements for off-plane trajectories with $O(St^{1/2})$ upstream gradient offsets.

As shown in figure 11, the '−' branch of the in-plane inertial trajectory ($\phi \in (\pi/2, \pi)$) is perturbed about a zero-Stokes trajectory, in the shearing plane, with the same upstream offset (trajectory 1), this being assumed equal to $\hat{z}^{-\infty} St^{1/2}$. Anticipating an in-plane gradient displacement of $O(St^{1/2})$, the '+' branch ($\phi \in (0, \pi/2)$) is perturbed about a second zero-Stokes trajectory (trajectory 2) with an initial offset equal to $(\hat{z}^{-\infty} + \Delta\hat{z})St^{1/2}$. From earlier qualitative arguments, one expects $\Delta\hat{z}$ to be negative. Using (4.18) for trajectories 1 and 2, and expanding for small St, we have

$$c = \left\{ \int_c^\infty \exp\left[-\int_{r'}^c q(r'')\,\mathrm{d}r'' \right] \frac{B'r'}{(1-A')}\,\mathrm{d}r' \right\}^{1/2} \times \left[1 + \frac{(\hat{z}^{-\infty})^2\,St}{2} \frac{\exp\left\{ \int_c^\infty q(r')\,\mathrm{d}r' \right\}}{\int_c^\infty \exp\left[-\int_{r'}^c q(r'')\,\mathrm{d}r'' \right] \frac{B'r'}{(1-A')}\,\mathrm{d}r'} \right], \tag{4.26}$$

$$c' = \left\{ \int_{c'}^\infty \exp\left[-\int_{r'}^{c'} q(r'')\,\mathrm{d}r'' \right] \frac{B'r'}{(1-A')}\,\mathrm{d}r' \right\}^{1/2} \times \left[1 + \frac{(\hat{z}^{-\infty} + \Delta\hat{z})^2\,St}{2} \frac{\exp\left\{ \int_{c'}^\infty q(r')\,\mathrm{d}r' \right\}}{\int_{c'}^\infty \exp\left[-\int_{r'}^{c'} q(r'')\,\mathrm{d}r'' \right] \frac{B'r'}{(1-A')}\,\mathrm{d}r'} \right], \tag{4.27}$$

where c and c' are the radial coordinates at $\phi = \pi/2$ of trajectories 1 and 2, respectively, in these cases also being the distances of nearest approach to the reference sphere. We note that an $O(St^{1/2})$ change in the upstream offset produces, at leading order, only an $O(St)$ alteration of the radial distance at $\phi = \pi/2$.

If d is the radial coordinate at $\phi = \pi/2$ of the in-plane zero-Stokes separatrix, this implies

$$d = \left\{ \int_d^\infty \exp\left[-\int_{r'}^d q(r'')\,\mathrm{d}r'' \right] \frac{B'r'}{(1-A')}\,\mathrm{d}r' \right\}^{1/2}. \tag{4.28}$$

Evidently, c and c' may be expressed in the forms $d + St\ p$ and $d + St\ p'$, respectively, whence one finds

$$p = \frac{(\hat{z}^{-\infty})^2}{d} \frac{(1-A_0)}{(2-B_0)} \exp\left[\int_d^\infty q(r')\,\mathrm{d}r' \right], \tag{4.29}$$

$$p' = \frac{(\hat{z}^{-\infty} + \Delta\hat{z})^2}{d} \frac{(1-A_0)}{(2-B_0)} \exp\left[\int_d^\infty q(r')\,\mathrm{d}r' \right], \tag{4.30}$$

where the subscript '0' now denotes evaluation of the particular hydrodynamic function at $r = d$. Both $O(St)$ corrections are proportional to $(1 - A_0)$, or since the value of d is very close to 2 and $(1 - A_0) \approx 4.077(d - 2)$ (see Kim & Karrila 1991), p and p' scale linearly with the interparticle separation. On account of lubrication, the effective inertia of the particle for near-field approach is thus characterized by a modified Stokes number $\hat{St} \propto St(r-2)$. Therefore, as seen in § 2, even for $St \sim O(1)$, there is always a separation at which $\hat{St} \ll 1$, and inertia of the particle is negligible.

Now, the perturbation scheme of the previous section may be applied to the upstream portion of the inertial trajectory. The radial coordinate at $\phi = \pi/2$, corresponding to the inner layer defined in § 4.3.2, is then given by

$$r^-_{\pi/2} = c + St\ k(c), \tag{4.31}$$

to $O(St)$, where the argument of k denotes its evaluation at c. The expression for k is again given by (4.23) with $\theta_t = \theta_0 = \pi/2$. An identical procedure is applied to the downstream portion (the '+' branch) of the finite-St trajectory; that is, this portion is perturbed about trajectory 2 by requiring that the two trajectories tend toward the same downstream offset. This then gives the radial distance at $\phi = \pi/2$ as

$$r^+_{\pi/2} = c' - St\ k(c'). \tag{4.32}$$

The difference in sign in this case compared to (4.31) is because we go from the choice of the negative to the positive square root for the inner solution $\tilde{\phi}$, but the corresponding matching contributions in the outer solutions, ϕ_1^- and ϕ_1^+, remain the same (see § 4.3).

The upstream and downstream portions being part of the same inertial trajectory, we have

$$\begin{aligned} & r^-_{\pi/2} = r^+_{\pi/2}, \\ \Rightarrow\ & c = c' - 2St\ k(d), \end{aligned} \tag{4.33}$$

to $O(St)$.

From (4.33), (4.29) and (4.30), one finally obtains a quadratic equation for $\Delta\hat{z}$,

$$(\Delta\hat{z})^2 + 2\hat{z}^{-\infty}(\Delta\hat{z}) - 2k(d)d\frac{(2-B_0)}{(1-A_0)} \exp\left[\int_{\mathrm{d}}^\infty q(r')\,\mathrm{d}r' \right] = 0. \tag{4.34}$$

Solving, the in-plane gradient displacement is given by

$$(\Delta z)_{inplane} = St^{1/2}\Delta\hat{z},$$
$$= \frac{1}{2}\left(-2\hat{z}^{-\infty} + \left[4(\hat{z}^{-\infty})^2 + 8k(d)d\frac{(2-B_0)}{(1-A_0)}\exp\left\{-\int_d^\infty \frac{2(A'-B')}{(1-A')r'}\,\mathrm{d}r'\right\}\right]^{1/2}\right), \tag{4.35}$$

with

$$k(d) = \frac{2}{d}\left(\frac{1-A_0}{2-B_0}\right)\int_c^\infty \exp\left[-\int_{r'}^c q(r'')\,\mathrm{d}r''\right] \times\left\{\frac{r' f_1(r',\phi_0')}{(1-A')} + \frac{\left\{(1-B')\,\sin^2\phi_0' + \frac{1}{2}B'\right\} f_2(r',\phi_0')}{(1-A')^2\sin\phi_0'\cos\phi_0'}\right\}\mathrm{d}r'. \tag{4.36}$$

The choice of the positive square root is so that (4.35), in the limit $\hat{z}^{-\infty} \gg 1$, matches to (4.25) with $\theta_0 = \theta_t = \pi/2$, the latter being the gradient displacement of in-plane trajectories with $O(1)$ upstream offsets.

Employing the above approach for off-plane trajectories with $O(St^{1/2})$ upstream gradient offsets, one similarly obtains for the gradient displacement,

$$\Delta z = \frac{St^{1/2}}{2}\left(-2\hat{z}^{-\infty} + \left\{4(\hat{z}^{-\infty})^2 + 4\left[\frac{2d}{\sin\theta_t^d}\frac{(2-B_0)}{(1-A_0)}k\left(d,\theta_t^d\right)\exp\left[-\int_{\frac{d}{\sin\theta_t^d}}^\infty q(r')\,\mathrm{d}r'\right] - 2(\Delta\bar{x})\,x^{-\infty}\right]\right\}^{1/2}\right). \tag{4.37}$$

where $z^{-\infty} = St^{1/2}\hat{z}^{\infty}$ is the upstream gradient offset and $k(d,\theta_t^d)$ is given by (4.23); the subscript '0' now denotes evaluation at $d/\sin\theta_t$, where (d,θ_t^d) correspond to the ordinate and the polar angle, at $\phi = \pi/2$, of the zero-Stokes separatix corresponding to the initial vorticity offset $x^{-\infty}$. The vorticity displacement, $\Delta x = St\,\Delta\bar{x}$, is still given by (4.24). It may again be seen that (4.37) reduces, at leading order, to (4.25) in the limit $\hat{z}^{-\infty} \gg 1$.

As defined in § 3.2.1, the neutral off-plane trajectory originates at $x = x_c^{-\infty}$ from a zero upstream gradient offset, and suffers no net displacement in the gradient direction. Using $\Delta z = 0$ for $z^{-\infty}(\hat{z}^{-\infty}) = 0$ in either (4.25), derived in the previous section, or in (4.37) above, this gives

$$2\int_{\frac{d^c}{\sin\theta_t^{d^c}}}^\infty \exp\left[-\int_{r'}^\infty q(r'')\,\mathrm{d}r''\right]\left\{\frac{2r'\cos\theta_0'\{(1-B')\sin^2\phi_0' + \frac{1}{2}B'\}}{(1-A')\sin\theta_0'}\theta_{1m}^- + \frac{r' f_1(r',\theta_0',\phi_0')}{(1-A')\sin\theta_0'} + \frac{\{(1-B')\sin^2\phi_0' + \frac{1}{2}B'\} f_2(r',\theta_0',\phi_0')}{(1-A')^2\sin^2\theta_0'\sin\phi_0'\cos\phi_0'}\right\}\mathrm{d}r' - \left\{(\Delta\bar{x})\,|_{x=x_c^{-\infty}}\right\}x_c^{-\infty} = 0, \tag{4.38}$$

for the location of the neutral trajectory, where d^c and $\theta_t^{d^c}$ may be obtained as functions of $x_c^{-\infty}$ from the zero-Stokes trajectory equations. In principle, the value of $x_c^{-\infty}$ is then given by the solution of (4.38); more importantly, the solution being independent of St, so is the location of this neutral trajectory, validating the physical arguments put forth in § 3.2.1. It is easier to locate the neutral trajectory via numerical integration of the trajectory equations, and this gives $x_c^{-\infty} \approx 0.9$; again, this value is found to be virtually independent of St for St ranging from 0.01 to 0.1.

St	$\hat{z}^{-\infty}_{sep\text{-}ip}St^{1/2}$ (numerical)	$\hat{z}^{-\infty}_{sep\text{-}ip}St^{1/2}$ (theoretical)
0.01	0.05	0.051
0.1	0.165	0.162
0.5	0.409	0.362
1	0.657	0.512

TABLE 2. Comparison of theoretical and numerical values of the critical offset in the shearing plane.

From (4.38), one observes that the second term in the argument of the square root in (4.37) changes sign across $x^{-\infty} = x_c^{-\infty}$. For $x^{-\infty} < x_c^{-\infty}$, this term is negative, so (4.37) ceases to be real-valued for $\hat{z}^{-\infty} < \hat{z}^{-\infty}_{sep}$ (say). The latter corresponds to the finite-St separatrix in the region $x^{-\infty} < x_c^{-\infty}$, that starts from a finite upstream gradient offset, $z^{-\infty}_{sep} = St^{1/2}\hat{z}^{-\infty}_{sep}$, and tends toward a zero downstream offset; one obtains

$$\hat{z}^{-\infty}_{sep} = \left(-\frac{2k(d,\theta_t^d)d}{\sin\theta_t^d}\frac{(2-B_0)}{(1-A_0)}\exp\left[-\int_{\frac{d}{\sin\theta_t^d}}^{\infty} q(r')\,\mathrm{d}r'\right] + 2(\Delta\bar{x})\,x^{-\infty}\right)^{1/2}. \tag{4.39}$$

For $x^{-\infty} > x_c^{-\infty}$, the aforementioned term is positive, so the limiting finite-St trajectory in this region is coincident with the corresponding zero-Stokes separatrix far upstream, and asymptotes to a downstream gradient offset of $O(St^{1/2})$. The expression for the resulting positive gradient displacement of this limiting trajectory is given by (4.37) with $\hat{z}^{-\infty} = 0$. This also confirms the anticipated change in sign of Δz for trajectories with small upstream gradient offsets.

Using (4.39), the upstream offset of the in-plane separatrix is given by $z^{-\infty}_{sep\text{-}ip} = St^{1/2}\hat{z}^{-\infty}_{sep\text{-}ip}$, where

$$\hat{z}^{-\infty}_{sep\text{-}ip} = \left(-\frac{2k(d)d}{\sin\theta_t^d}\frac{(2-B_0)}{(1-A_0)}\right)^{1/2}\exp\left[-\int_{\frac{d}{\sin\theta_t^d}}^{\infty}\frac{q(r')}{2}\,\mathrm{d}r'\right], \tag{4.40}$$

where k is now given by (4.36) In table 2 and figure 12, we compare the theoretical values obtained from evaluating (4.40) with that obtained from numerically integrating the trajectory equation (4.2) with $\theta = \pi/2$. The theoretical and numerical values agree well up to a Stokes number of about 0.5, and confirm the $St^{1/2}$ scaling of the critical offset. Even for a Stokes number of 1, the theoretical value is not far from agreement this is because for $St = 1$, the limiting finite-St trajectory still passes very close to the sphere ($r_{min} \sim 2.0001$), and as seen earlier, the inertia of the particle is suppressed by lubrication forces at these separations, which translates to an effective Stokes number for motion close to the sphere that is much less than 1.

In table 3, the numerical results also confirm the reversal in sign of the gradient displacement for small $z^{-\infty}$. Δz is found to change sign at $z^{-\infty} = 0.36$ and 0.24, respectively for the off-plane coordinates $x^{-\infty} = 1.5$ and 5; these values remain virtually unchanged for St ranging from 0.01 to 0.1.

4.5. *The in-plane limit cycle*

The zero-Stokes in-plane separatrix is fore–aft symmetric and asymptotes to a zero offset, with trajectories lying within forming closed orbits. For finite St, however small, this region of closed trajectories is destroyed and there exists an (locally) attracting

	$x^{-\infty} = 1.5$		$x^{-\infty} = 5$	
$z^{-\infty}$	$\Delta z\,(St = 0.1)$	$\Delta z\,(St = 0.01)$	$\Delta z\,(St = 0.1)$	$\Delta z\,(St = 0.01)$
5	-1.59×10^{-3}	-1.589×10^{-4}	-3.802×10^{-4}	-3.801×10^{-5}
2	-6.62×10^{-3}	-6.593×10^{-4}	-2.335×10^{-4}	-2.332×10^{-5}
1	-6.46×10^{-3}	-6.397×10^{-4}	-8.986×10^{-5}	-8.95×10^{-6}
0.5	-2.444×10^{-3}	-2.376×10^{-4}	-3.424×10^{-5}	-3.371×10^{-6}
0.2	5.502×10^{-3}	5.754×10^{-4}	1.331×10^{-5}	1.418×10^{-6}
0.1	1.516×10^{-2}	1.665×10^{-3}	1.007×10^{-4}	1.022×10^{-5}

TABLE 3. Values of Δz for $x^{-\infty} = 1.5$ and 5, $z^{-\infty}$ ranging from 5 to 0.1; $St = 0.1, 0.01$.

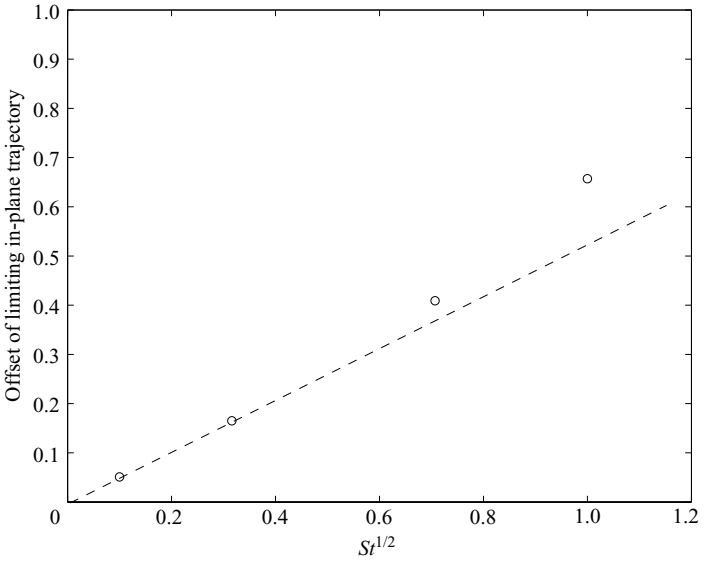

FIGURE 12. The in-plane critical offset $((\hat{z}^{-\infty}_{sep\text{-}ip})^c St^{1/2})$ values obtained from numerical integration of the trajectory equation, (4.2) with $\theta = \pi/2$, are plotted as a function of $St^{1/2}$; the dashed line represents the theoretical approximation (4.40).

limit cycle in the shearing plane. In § 3.1 we argued in physical terms for the existence of such a stable limit cycle; we now locate it in the shearing plane by applying the perturbation analysis developed in the previous section.

Owing to the antisymmetry of simple shear, the points of intersection of the limit cycle with the y- and z-axes must be symmetrically located with respect to the origin; the limit cycle itself will only be antisymmetric. Utilizing this symmetry one can analyse the limit cycle in a manner similar to the analysis of finite-St in-plane trajectories with $O(St^{1/2})$ upstream offsets. In particular, one perturbs portions of the limit cycle in $(0, \pi/2)$ and $(\pi/2, \pi)$ about the same zero-Stokes closed orbit (intersecting the y- and z-axes in $(\pm R_2^{lim}, 0)$ and $(0, \pm R_1^{lim})$, respectively), and then pieces the two portions together (see figure 13). Perturbing the $(\pi/2, \pi)$ branch gives us $r^-_{\pi/2} = R_1^{lim} + St\, k_{lim}$ for its radial distance at $\phi = \pi/2$, and perturbing the $(0, \pi/2)$ branch gives $r^+_{\pi/2} = R_1^{lim} - St\, k_{lim}$. The condition $r^+_{\pi/2} = r^-_{\pi/2}$ then reduces to

$$k_{lim} = 0, \tag{4.41}$$

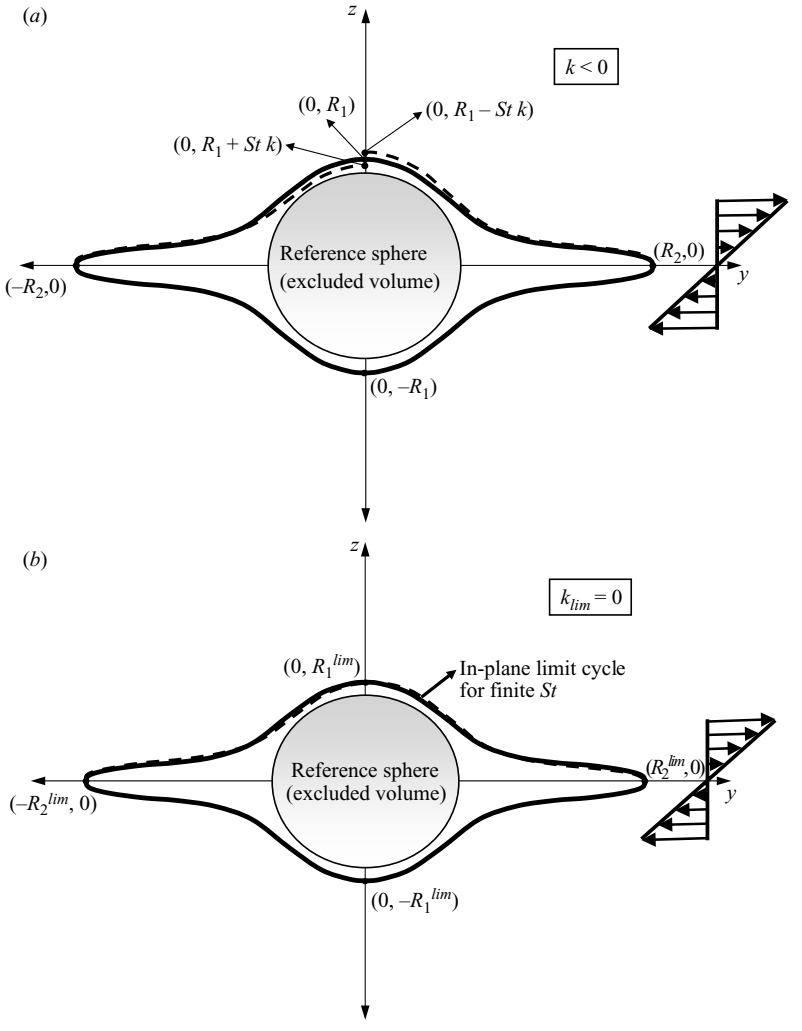

FIGURE 13. (*a*) A pair of spiralling-in trajectories that are perturbed about a zero-Stokes closed orbit. (*b*) The antisymmetric in-plane limit cycle, again perturbed about a zero-Stokes closed orbit that has the same points of intersection with the flow and gradient axes.

where $k_{lim} \equiv k(R_1^{lim}, R_2^{lim})$. The analysis that follows first determines the general expression for k, the inertial displacement at $\phi = \pi/2$, for a generic spiralling trajectory; equating it to zero would then yield the location of the limit cycle.

In order to find k, a finite-St spiralling trajectory is perturbed about a zero-Stokes closed orbit that has the same radial coordinate ($r = R_2$) at $\phi = 0$. The latter is imposed as a boundary condition in the inner layer around $\phi = 0$,† whence the $O(1)$ and $O(St)$

† The zero-Stokes closed orbits become purely tangential at the points $\phi = 0, \pi/2, 3\pi/2$ and π. Thus, besides those present for open trajectories, one has now to also account for angular boundary layers around $\phi = 0$ and π in the perturbation analysis.

solutions are given by

$$r^2 \sin^2\phi_0 = \int_r^{R_2} \exp\left[-\int_{r'}^{r} q(r'')\,\mathrm{d}r''\right] \frac{B'r'}{(1-A')}\,\mathrm{d}r',$$

$$r\phi_1 = \frac{1}{r\cos\phi_0 \sin\phi_0} \int_{R_2}^{r} \exp\left[-\int_{r'}^{r} q(r'')\,\mathrm{d}r''\right] \left\{ \frac{r' f_1(r', \phi_0')}{(1-A')} + \frac{\left\{(1-B')\,\sin^2\phi_0' + \frac{1}{2}B'\right\} f_2(r', \phi_0')}{(1-A')^2 \sin\phi_0'\,\cos\phi_0'} \right\} \mathrm{d}r',$$

and it may be verified that the $O(St)$ correction remains uniformly small for all r. On matching the solutions in the outer layer and in the inner layer around $\phi = \pi/2$, one obtains the radial distance of the finite-St spiralling trajectory at $\phi = \pi/2$ as $R_1 + St\,k$, where k is defined in terms of R_1 and R_2 as

$$k(R_1, R_2) = -\frac{2(1-A_0)}{c\,(2-B_0)} \int_{R_1}^{R_2} \exp\left[-\int_{r'}^{R_1} q(r'')\,\mathrm{d}r''\right] \left\{ \frac{r' f_1(r', \phi_0')}{(1-A')} + \frac{\left\{(1-B')\,\sin^2\phi_0' + \frac{1}{2}B'\right\} f_2(r', \phi_0')}{(1-A')^2 \sin\phi_0'\,\cos\phi_0'} \right\} \mathrm{d}r'. \quad (4.42)$$

Here, the subscript '0' indicates evaluation of the particular hydrodynamic function at $r = R_1$, R_1 being the radial coordinate of the zero-Stokes orbit at $\phi = \pi/2$. The above expression can be compared to the analogous expression obtained for open trajectories, namely (4.23) in § 4.3 with $\theta_t = \theta_0 = \pi/2$. For the closed trajectory, R_1 plays the role of c while R_2 replaces the infinity.

When $k < 0$, a finite-St spiralling trajectory starts from outside the zero-Stokes closed orbit at $\phi = \pi/2$ and intersects it at $\phi = 0$; a negative value of k would thus correspond to a trajectory that spirals in. Likewise, a positive value of k would imply a trajectory that spirals out. Using (4.41) and (4.42), one obtains

$$\int_{R_1^{lim}}^{R_2^{lim}} \exp\left[-\int_{r'}^{R_1^{lim}} q(r'')\,\mathrm{d}r''\right] \left\{ \frac{r' f_1(r', \phi_0')}{(1-A')} + \frac{\left\{(1-B')\,\sin^2\phi_0' + \frac{1}{2}B'\right\} f_2(r', \phi_0')}{(1-A')^2 \sin\phi_0'\,\cos\phi_0'} \right\} \mathrm{d}r' = 0, \quad (4.43)$$

for the limit cycle, where R_1^{lim} and R_2^{lim} are related by the zero-Stokes trajectory equation. Equation (4.43) serves as a nonlinear algebraic relation for the unknown R_1^{lim} (or R_2^{lim}) and determines, to $O(1)$, the coordinates of the limit cycle. Clearly, the solution of (4.43) is independent of St, asserting that the limit cycle is fixed regardless of the (small) magnitude of inertial effects. Numerical evaluation of the integral on the left-hand side of (4.43) shows a change sign at $R_2 \approx 2.05$, so the limit cycle intersects the y-axis at approximately $(\pm 2.05, 0)$.

In order to verify that this value is indeed independent of St, we numerically integrate the trajectory equation (4.2) with $\theta = \pi/2$ for two different values of St differing by an order of magnitude, namely 0.2 and 0.02, with the initial points being $(-2.1, 0)$ and $(-2.05, 0)$. Figures 14 and 15 depict trajectories for these cases; the figures show a magnified view of the finite-St spiralling trajectory in the region of its intersection with the negative y axis. One observes that while the spirals become tighter for the smaller value of St, the location of the limit cycle, as inferred from the nature of spiralling, remains virtually independent of St. Also, the much tighter outward spiralling in both instances shows that the limit cycle crosses the flow axis at symmetrically located points very close to ± 2.05.

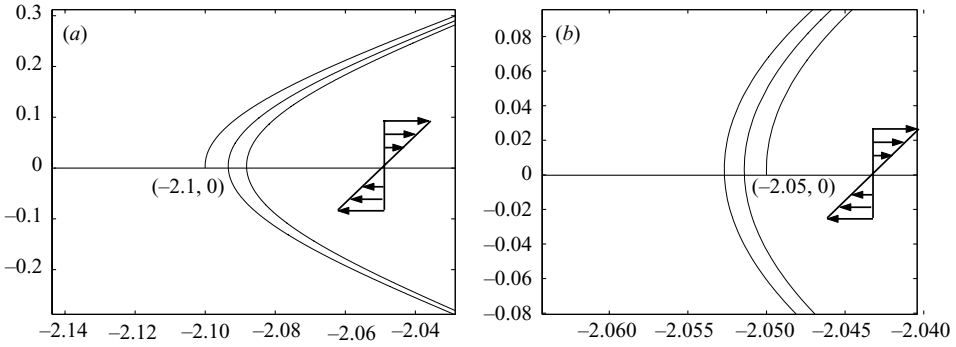

FIGURE 14. (*a*) An inertial trajectory spiralling in towards the limit cycle from $(y, z) \equiv (-2.1, 0)$ for $St = 0.2$; (*b*) a trajectory spiralling out onto the limit cycle from $(y, z) \equiv (-2.05, 0)$ for $St = 0.2$; note the reduced scale in the latter.

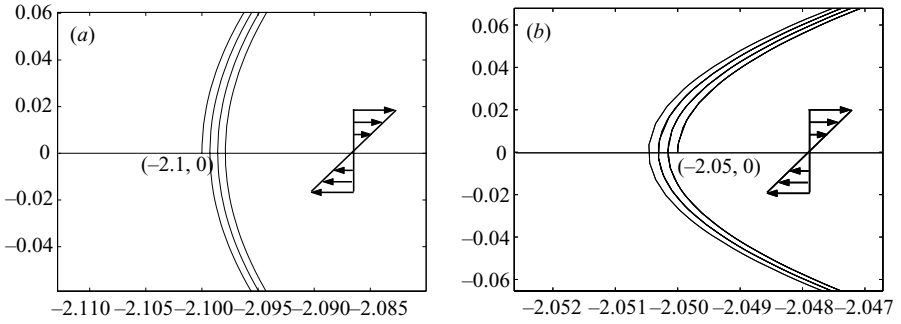

FIGURE 15. As figure 14 but for $St = 0.02$.

5. Finite-*St* trajectories from numerical integration of the $O(St)$ trajectory equations

So far, we have only presented numerical results in support of analytical predictions for the transverse displacements of finite-*St* off-plane open trajectories. In what follows, we show representative plots of both open and spiralling off-plane trajectories, again obtained numerically from integrating (4.2) and (4.3); these serve to reinforce the qualitative picture presented in § 3. The changes in the ensemble of inertial trajectories with *St* has been discussed in detail earlier, and all trajectories shown here are therefore restricted to $St = 0.1$.

In figures 16 and 17 the open trajectories correspond to $x^{-\infty} = 0.5$ and have upstream gradient offsets $z^{-\infty} = 0.5$ and 0.12, respectively; the Δz for these cases is negative, as is expected since $x^{-\infty} < x_c^{-\infty}$. The second trajectory is, in fact, very close to the limiting trajectory for this value of $x^{-\infty}$, and suffers a much larger displacement in the gradient direction in accordance with the theoretically predicted increase of Δz from $O(St)$ to $O(St^{1/2})$. Therefore $z^{+\infty} \to 0$ as $y \to \infty$ for this case; trajectories with smaller gradient offsets are no longer open. Note that since the figure only shows the portion of the trajectory between $y = -6$ and $y = 6$, that $z \to 0$ as $y \to \infty$ is not evident. However, this was verified by plotting the trajectory to a downstream y coordinate of 300.

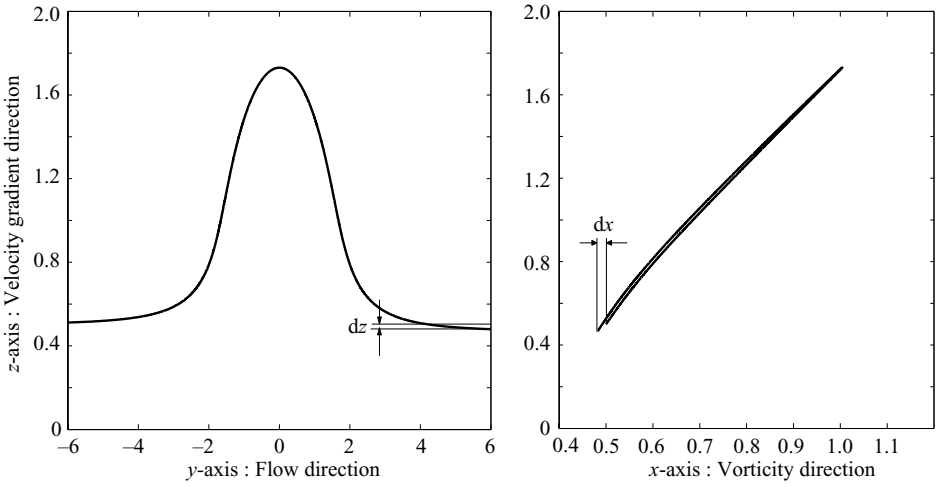

FIGURE 16. Off-plane open trajectory for $St = 0.1$ with $x^{-\infty} = 0.5$ and $z^{-\infty} = 0.5$: (*a*) yz- and (*b*) xz-projections.

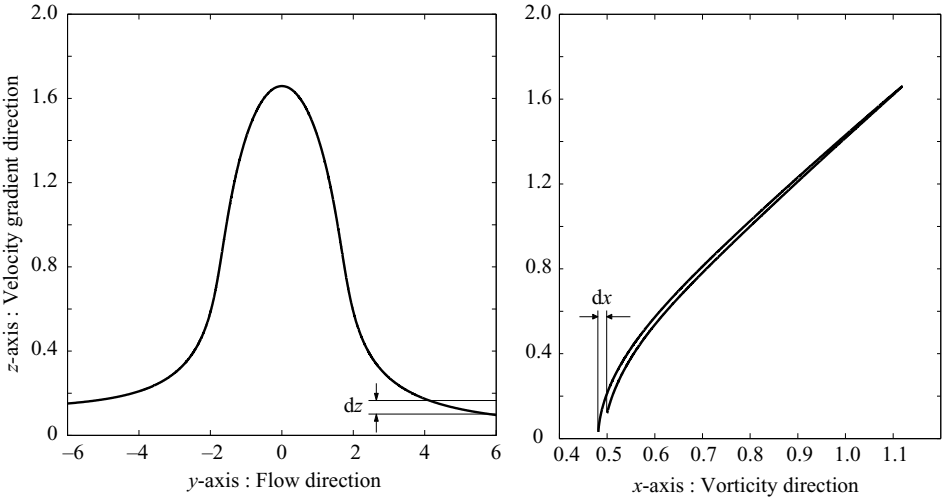

FIGURE 17. Limiting off-plane open trajectory for $St = 0.1$ with $x^{-\infty} = 0.5$ and $z^{-\infty} = 0.12$: (*a*) yz- and (*b*) xz-projections.

Figures 18, 19 and 20 show open trajectories for a larger value of the off-plane coordinate, $x^{-\infty} = 1.5$. The projections of the trajectories onto the yz- plane in these cases show relatively less-pronounced humps for the same gradient offsets, indicative of weakening hydrodynamic interactions. The trajectory starting from the largest gradient offset ($z^{-\infty} = 0.5$) still has a negative Δz similar to the in-plane trajectories. The trajectory with $z^{-\infty} = 0.15$ has a positive Δz, however. The limiting open trajectory in this case (figure 20) starts from $z^{-\infty} = 0$ far upstream and also has a positive Δz in sharp contrast to the corresponding limiting trajectory for $x^{-\infty} = 0.5$ (figure 17). For still larger values of $x^{-\infty}$, the qualitative behaviour of open trajectories remains similar except that the inertial effects grow progressively weaker.

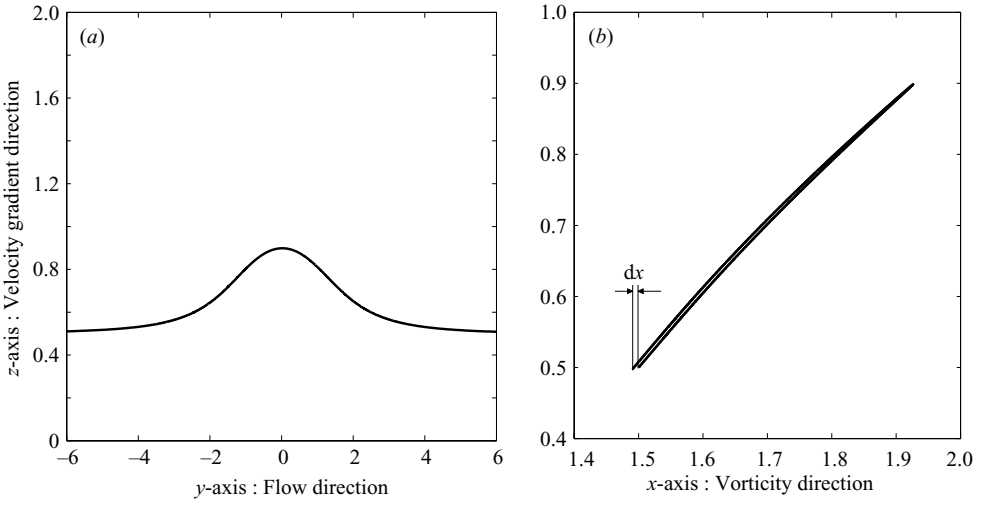

FIGURE 18. Off-plane open trajectory for $St = 0.1$ with $x^{-\infty} = 1.5$ and $z^{-\infty} = 0.5$: (*a*) yz- and (*b*) xz-projections.

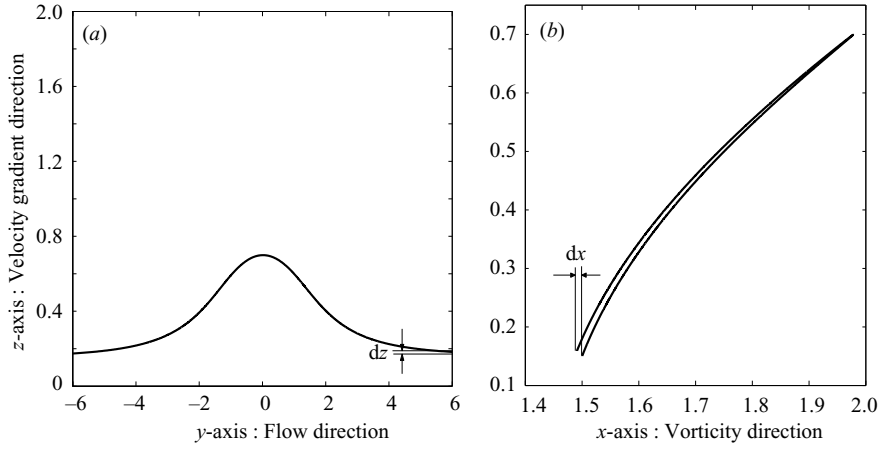

FIGURE 19. Off-plane open trajectory for $St = 0.1$ with $x^{-\infty} = 1.5$ and $z^{-\infty} = 0.15$: (*a*) yz- and (*b*) xz-projections.

An example of a trajectory that spirals in uniformly onto the in-plane limit cycle is shown in figure 21, where we also note the gradual approach, toward the plane of shear, in the xz-projection. Figures 22 and 23 show the other possible spiralling behaviours discussed in § 3.2.2. The trajectory in figure 22 spirals outward initially but eventually begins to spiral inward, again converging onto the in-plane limit cycle. The change in the nature of the spiralling can be seen as a retracing of its path in the yz-projection leading to the apparent crossing of trajectories in this view. On the other hand, the trajectory in figure 23 spirals out rapidly enough, finally going to infinity in the downstream direction. Although the scale in the figure stops at approximately $y = 11$, the trajectory is found to continue along this path till $y = 250$ with little change in z.

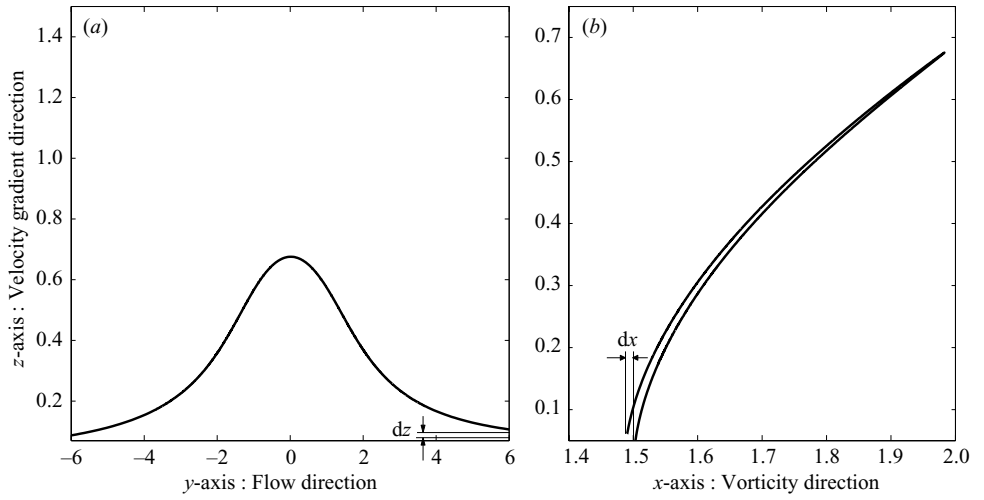

FIGURE 20. Limiting off-plane open trajectory for $St = 0.1$ with $x^{-\infty} = 1.5$ and $z^{-\infty} = 0$: (a) yz- and (b) xz-projections.

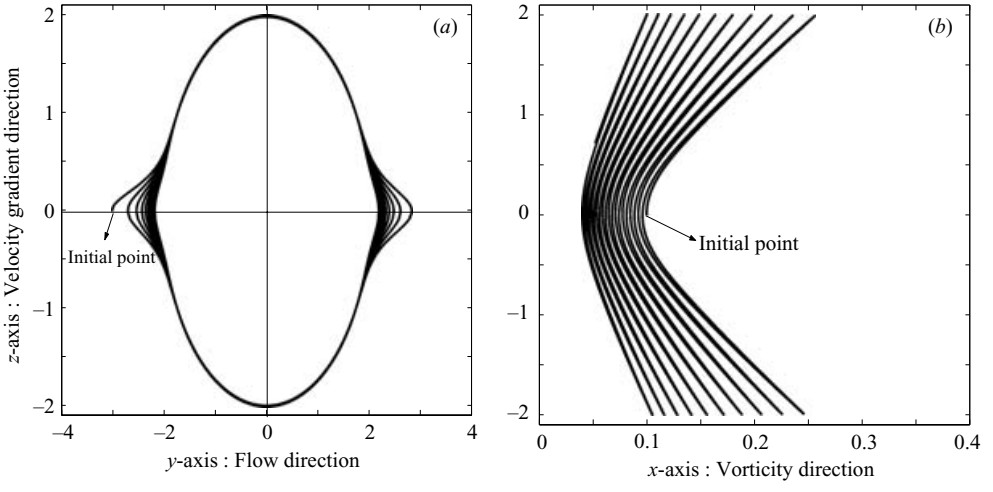

FIGURE 21. Inward spiralling off-plane trajectory starting from $(x, y, z) \equiv (0.1, -3, 0)$ for $St = 0.1$: (a) yz- and (b) xz-projections.

6. Self-diffusivities at finite St

A particle in a sheared non-Brownian suspension, for times long compared to $\dot{\gamma}^{-1}$, executes a random walk owing to hydrodynamic interactions with its neighbours, that may be characterized by a diffusivity (for instance, see Leighton & Acrivos 1987a,b; Eckstein, Bailey & Shapiro 1977). It is known that in the absence of non-hydrodynamic effects, inertialess pairwise interactions being fore–aft symmetric, diffusive behaviour arises from three-particle interactions and the resulting diffusivities are $O(\phi^2)$ for $\phi \to 0$. However, for cases where pairwise interactions are asymmetric on account of surface roughness, short-ranged repulsive forces or particle inertia (as in our case), the small-ϕ asymptotes of the diffusivities may be obtained by averaging the transverse displacements for successive uncorrelated pairwise interactions weighted

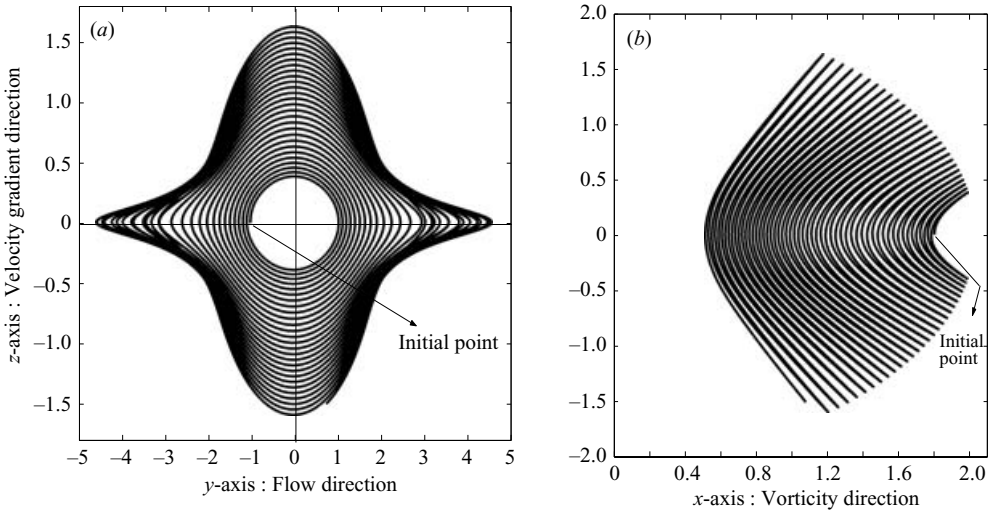

FIGURE 22. Spiralling off-plane trajectory starting from $(x, y, z) \equiv (1.8, -1, 0)$ for $St = 0.1$: (*a*) yz- and (*b*) xz-projections.

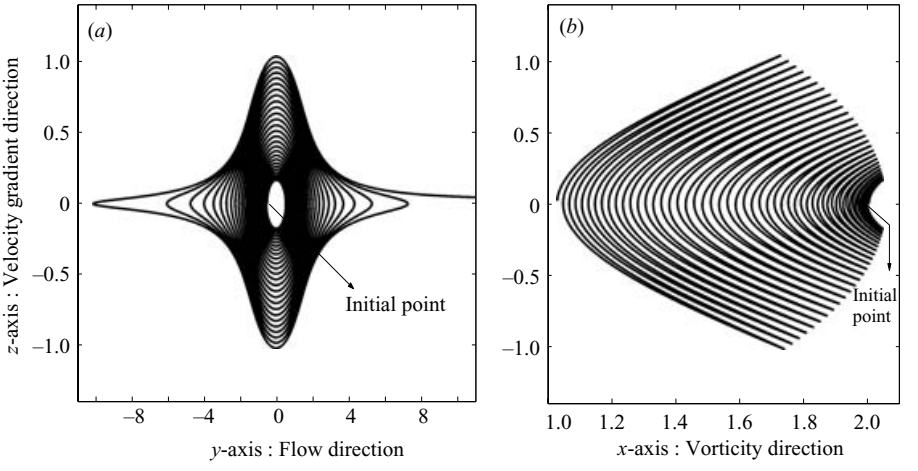

FIGURE 23. Off-plane trajectory starting from $(x, y, z) \equiv (2, -0.5, 0)$ for $St = 0.1$, and spiralling off to infinity: (*a*) yz- and (*b*) xz-projections.

by their frequency of occurrence. Here, we determine the scaling of the transverse components of the shear-induced self-diffusivity that arise due to asymmetric pairwise interactions at finite St, and are given by:

$$\hat{D}_{zz} = \frac{3}{8\pi} \int_{-\infty}^{\infty} \int_{-\infty}^{\infty} \mathrm{d}x^{-\infty}\, \mathrm{d}z^{-\infty} z^{-\infty} (\Delta z)^2, \tag{6.1}$$

$$\hat{D}_{xx} = \frac{3}{8\pi} \int_{-\infty}^{\infty} \int_{-\infty}^{\infty} \mathrm{d}x^{-\infty}\, \mathrm{d}z^{-\infty} z^{-\infty} (\Delta x)^2, \tag{6.2}$$

where $\hat{D}_{ii} = D_{ii}/\dot{\gamma} a^2 \phi$, and $z^{-\infty}$, a measure of the relative velocity of the particle pair, serves as the weighting factor for encounters in simple shear flow; the integrals for both components extend over the ensemble of open trajectories. From symmetry considerations $D_{xz} = D_{yz} = 0$, and further, it suffices to integrate over a quadrant

of the whole trajectory space when evaluating the non-zero components. The net transverse displacements here correspond to the laboratory reference frame, and equal half their respective values in relative coordinates, derived in § 4. The analysis in previous sections has shown that the gradient and vorticity displacements of finite-St trajectories behave very differently, in particular for small gradient offsets and close to the reference sphere when they no longer scale in the same manner with St. This then leads to an anisotropic inertial diffusivity tensor with $\hat{D}_{zz}$ and $\hat{D}_{xx}$ being $O(St^2 \ln St)$ and $O(St^2)$, respectively, in the pairwise limit. As shown below, the non-analytic scaling of the former arises since the singular layer comprising off-plane trajectories with $O(St^{1/2})$ gradient offsets and $O(St^{1/2})$ gradient displacements provides a cut-off to the logarithmically divergent diffusivity integral. Thus, the relative anisotropy characterized by $\hat{D}_{zz}/\hat{D}_{xx}$ is $O(\ln St)$ and increases as $St \to 0$.

Since the vorticity displacement remains $O(St)$ for all open trajectories, and the corresponding integrand in (6.2) may be shown to decay sufficiently rapidly to be integrable for large upstream offsets, it follows that $\hat{D}_{xx}$ will be $O(St^2)$. This naive argument does not, however, work for the gradient component $\hat{D}_{zz}$; (6.1) may be rewritten as

$$\hat{D}_{zz} = \frac{3St^2}{2\pi}\int_0^\infty \mathrm{d}x^{-\infty}\int_{z_{sep}^{-\infty}}^\infty \mathrm{d}z^{-\infty}(\Delta\bar{z})^2, \tag{6.3}$$

where $z_{sep}^{-\infty}$ is the upstream gradient offset of the finite-St separatrices. In the light of the structure of the inertial separatrix envelope discussed earlier, $z_{sep}^{-\infty} \sim O(St^{1/2})$ for $x < x_c^{-\infty}$, and $z_{sep}^{-\infty} = 0$ for $x \geqslant x_c^{-\infty}$. The integral with respect to $x^{-\infty}$ is convergent, since Δz, similar to Δx, decays rapidly for large $x^{-\infty}$. For purposes of scaling, it then suffices to consider the integral with respect to $z^{-\infty}$; here, we note that Δz, given by (4.25), is $O(St/z^{-\infty})$ for $St^{1/2} \ll z^{-\infty} \ll 1$, and is $O(St^{1/2})$ in the $O(St^{1/2})$ inner layer, being given by (4.37). Thus, the diffusivity integral is of the form

$$\hat{D}_{zz} \sim \int_0^\infty \mathrm{d}x^{-\infty}\int_{O(St^{1/2})}^\infty \mathrm{d}z^{-\infty} z^{-\infty}\left(\frac{St}{z^{-\infty}}\right)^2 \sim O(St^2 \ln St).$$

As a check on our analysis for the gradient component of the diffusivity, we compare the analytical and numerical values of its in-plane projection ($\theta = \pi/2$), defined as

$$\hat{D}_{zz}^{inplane} = \frac{3}{8\pi}\int_{-\infty}^\infty \mathrm{d}z^{-\infty} z^{-\infty}(\Delta z)_{inplane}^2. \tag{6.4}$$

Using appropriate expressions for $(\Delta z)_{inplane}$ for $z^{-\infty} \sim O(1)$ and $O(St^{1/2})$, it may then be shown that (see Subramanian 2002)

$$\frac{4\pi\hat{D}_{zz}^{ip}}{3} = 2(St)^2\left\{-\frac{(\hat{z}_{sep\text{-}ip}^{-\infty})^4}{8}\ln St + K' + K''\right\}, \tag{6.5}$$

where

$$K' = -\frac{(\hat{z}_{sep\text{-}ip}^{-\infty})^4}{16}\left\{1 + 4\ln\left(\frac{\hat{z}_{sep\text{-}ip}^{-\infty}}{2}\right)\right\}. \tag{6.6}$$

$$K'' = \int_0^\infty \mathrm{d}z^{-\infty}\left\{\frac{4}{z^{-\infty}}\left[\int_c^\infty \exp\left[-\int_{r'}^\infty q(r'')\,\mathrm{d}r''\right]\left\{\frac{r' f_1(r', \phi_0')}{(1-A')} + \frac{\{(1-B')\sin^2\phi_0' + \frac{1}{2}B'\}\, f_2(r', \phi_0')}{(1-A')^2 \sin\phi_0' \cos\phi_0'}\right\}\mathrm{d}r'\right]^2 - \frac{(\hat{z}_{sep\text{-}ip}^{-\infty})^4}{4z^{-\infty}}\mathrm{H}(1-\hat{z}^\infty)\right\}, \tag{6.7}$$

St	$\hat{D}^{ip}_{zz}$ (numerical)	$\hat{D}^{ip}_{zz}$ (analytical)
0.1	2.546×10^{-3}	2.643×10^{-3}
0.01	2.72×10^{-5}	2.841×10^{-5}
0.001	2.914×10^{-7}	3.039×10^{-7}

TABLE 4. Comparison of analytical and numerical values of the in-plane diffusivity for different Stokes numbers.

H(x) being the Heaviside function, and $\hat{z}^{-\infty}_{sep\text{-}ip}$, as before, is the scaled upstream offset of the in-plane inertial separatrix given by (4.40). In table 4 we compare the values of $\hat{D}^{ip}_{zz}$ given by (6.5) to those evaluated numerically. The latter were obtained by evaluating the diffusivity integral (6.4) numerically, the in-plane gradient displacement for each open trajectory being obtained from the numerical integration of the trajectory equation (4.2) with $\theta = \pi/2$.

The scaling derived above for the gradient and vorticity components of the self-diffusivity tensor in the limit $St \ll 1$ may be contrasted with that for corresponding elements in the limit of large St. For the latter case, the diffusive motion of a tagged particle in a dilute suspension, as shown by Tsao & Koch (1995), arises due to distinct mechanisms depending on the magnitude of the particle velocity variance or the 'temperature' T relative to $\dot{\gamma}^2 a^2$. In the so-called 'ignited state', $T \gg O(\dot{\gamma}^2 a^2)$, and the random motion of the particles dominates. The interparticle collisions are thus variance-driven, and a particle diffuses on account of successive uncorrelated (binary) solid-body collisions. The stress tensor is isotropic at leading order, and for dilute suspensions, the temperature $T \approx \langle u'^2 \rangle \sim (St/\phi)^2 \dot{\gamma}^2 a^2$. The diagonal components of the diffusivity tensor are then given by $D_{ii} \sim \langle u' \rangle^2 t_{corrln} \sim \dot{\gamma} a^2 St/\phi^2$, where the collisional time scale is the relevant correlation time and is defined as $\tau_c = a\phi^{-1}/T^{1/2}$; thus, $\hat{D}_{zz/xx} \sim St/\phi^3$. For higher concentrations, the scaling with St, at leading order, remains unchanged, the ϕ dependence now being modified by the contact value of the pair-distribution function (see equation (4.29) in Tsao & Koch 1995).† Of more relevance, however, is the scaling of the diffusivities in the 'quenched state' ($T \ll O(\dot{\gamma}^2 a^2)$), again defined in Tsao & Koch (1995), where the collisions and the resulting velocity fluctuations are shear-induced, similar to the hydrodynamic interactions for $St \ll 1$, both being dominated by uncorrelated pair events in the dilute limit. Since the particle now relaxes quickly in a time of $O(\tau_p)$, following a shear-induced collision, one obtains the scaling of the diffusivities from an estimate of an integral similar to (6.2). The transverse velocity due to a shear-induced collision is $O(\dot{\gamma} a)$, and the resulting displacements, in a time of $O(\tau_p)$, in both the gradient and vorticity directions are $O(St\, a)$. This then leads to diffusivities $D_{zz/xx} \sim \dot{\gamma} a^2 (St^2 \phi)$. The factor of $\ln St$ arising from the anisotropic nature of the hydrodynamic interactions along the gradient and vorticity axes for $St \ll 1$ is thus absent for large St, and the differing collision cross-sections in the two directions for the latter case result in only an $O(1)$ anisotropy.

† This is true only for perfectly elastic collisions for which the coefficient of restitution $e = 1$. When $0 < e < 1$, the resulting inelastic dissipation dominates the energy balance for St large enough; the temperature now scales as $O(\dot{\gamma} a)$ for $St \gg 1$, and the diffusivities, scaled by $\dot{\gamma} a^2$, are therefore independent of St in this limit (see Sangani *et al.* 1996).

The $O(\ln St)$ enhancement of the gradient component D_{zz}, at $O(\phi)$, depends critically on two factors: first, the smoothness of the interacting spheres that allows the existence of lubrication interactions; and second, that the trajectories of the interacting pair, for small relative offsets in the gradient direction, remain substantially unaffected even for relatively large separations, this second requirement being fulfilled only for very dilute suspensions. Assuming perfectly smooth particles, an estimate of the degree of diluteness required for the $O(\ln St)$ scaling to become evident can be made as follows. The $O(\ln St)$ scaling arises because, for trajectories with sufficiently small upstream gradient offsets $z^{-\infty}$, the gradient displacement Δz increases inversely with the upstream gradient offset for a range of offsets, eventually becoming comparable to it for offsets of $O(St^{1/2})$. We therefore consider a mechanism that disrupts the pair-inertial trajectory, breaking this divergent behaviour earlier than the $O(St^{1/2})$ offset at which it occurs in the limit of pairwise interactions; it involves a third particle-induced inertial displacement of the tagged sphere during the time that the pair (one of them being the tagged sphere) still interacts. Other more complicated scenarios considered by Acrivos *et al.* (1992) in their analysis of the longitudinal diffusivity (D_{xx}) are not relevant here, since unlike their case, we consider the gradient component of the diffusivity and inertial pair interactions for finite St are asymmetric.† In order that the divergent behaviour of Δz for small $z^{-\infty}$ be absent, the third particle must induce a displacement of the tagged sphere that is comparable to Δz during the time interval of pair interaction. This time interval, denoted by t_I below, is the same as that used in Acrivos *et al.* (1992) and is given by $t_I \sim O(\dot{\gamma}^{-1}(z^{-\infty})^{-5/3})$ for a pair initially separated by the gradient offset $z^{-\infty}$, because the finite-St open trajectories are asymptotically close to their inertialess counterparts at large interparticle separations.

Considering now a far-field third particle, say, at a (dimensionless) distance $L \gg 1$ from the test sphere, the corresponding induced inertial displacement will be $O(St/L^3)$, this being the far-field approximation for Δz (the transverse displacements are driven by hydrodynamic interactions that, for large pair-separations L, decay as L^{-3}, leading to the aforementioned approximation for Δz). Comparing this to the Δz for a pair interaction given by $O(St/z^{-\infty})$ for small z^{∞}, it is found that $N \sim O(L^3/z^{-\infty})$ particles need to interact with the test sphere during a time interval of $O(t_I)$. The rate of encounter of the test sphere with a third particle at a separation L is given by $\dot{\gamma} L^3 \phi$, so that the number of particles interacting within a time interval of $O(t_I)$ is given by $\dot{\gamma} L^3 \phi t_I = O(\phi L^3/(z^{-\infty})^{-5/3})$. Equating this to N, $\phi \sim O((z^{-\infty})^{2/3})$. In order for the divergent behaviour to be observed, the offset at which the above equality occurs must be less than its value of $O(St^{1/2})$ in the pair limit, that then leads to the diluteness condition $\phi \ll O(St^{1/3})$. Consideration of a third particle at $O(1)$ and $O(St^{1/2})$ offsets relative to the tagged sphere confirms the above estimate as being the most restrictive for the diluteness of ϕ. This condition should serve as a guide for a simulation effort aimed at analysing the diffusive behaviour in an inertial suspension. Verifying this condition may be difficult in practice, however, since determination of the St scaling of the gradient displacement requires considering different values of St, and the diluteness condition must be satisfied for the smallest among these.

It must be noted that open pair trajectories for zero St cover the entire range of non-zero initial offsets, while for finite St there exists, relative to the reference sphere,

† In Acrivos *et al.*'s analysis at zero St, a relatively distant third particle, for instance, would interact separately and almost reversibly with the particles constituting the pair, thereby leaving the pair-trajectory virtually unaltered; thence, the necessity to look at more complicated mechanisms that lead to pair-decorrelation in the flow direction.

an upstream window of extent $(\Delta z^{-\infty} \times \Delta x^{-\infty}) \approx (O(St^{1/2}) \times 2x_c^{-\infty})$ – the basin of attraction of the in-plane limit cycle – that serves as a trapping zone (see figure 9). Thus, in the above limit, namely $\phi \ll St^{1/3}$, the 'tagged' particle will eventually be captured by the limit cycle in the shearing plane of a second particle. Upon capture, the displacement of the tagged particle will asymptote to a periodic function of time. In an actual suspension, this trapping effect is not permanent, as the resulting bound pair will in general be broken by interaction with a third particle. The fraction of the total number of particles that exist as bound pairs may be estimated by equating the rates of formation and dissociation of a particle doublet. With $\phi \ll St^{1/3}$, the probability of encounter with a third particle when spiralling in onto the limit cycle is negligible, and almost every particle that enters the trapping window will go on to form a bound pair. The rate of formation may then be estimated as $O(\dot{\gamma} St \phi^2 x_c^{-\infty})$, or since $x_c^{-\infty}$ is $O(1)$, is simply given by $O(\dot{\gamma} St \phi^2)$. A bound pair, in the absence of mechanisms such as interparticle repulsive forces or Brownian motion, will only be broken due to interaction with a third particle. It may be shown that this can occur only due to a slow third particle at a relative gradient offset of $O(St^{1/2})$ (see Appendix B). The resulting fraction ϕ_d of particles forming bound pairs is thus found to be $O(\phi)$, and is therefore comparable with the total number of particles in the suspension when $\phi \ll St^{1/3}$. Since a bound pair is broken only due to interactions with slow third particles, the diluteness constraints for the relative dominance of bound pairs, and that for observing an $O(St^2 \ln St)$ gradient coefficient of the diffusivity, turn out to be identical; the $O(St^2 \ln St)$ scaling for gradient diffusion is therefore restricted to transient conditions.

When $St^{1/3} \ll \phi \ll 1$, slow pair interactions that occur for gradient offsets $z^{-\infty} \ll 1$ will be cut off first by a third-particle interaction even when $z^{-\infty} \sim \phi^{3/2} (\gg St^{1/2})$; the corresponding diffusivity in the gradient direction, at leading order, is then $O(St^2 \ln(1/\phi))$. Evidently, in this limit the process of formation of a bound pair will invariably be disrupted, so the diffusivities found apply to almost every particle in the dilute suspension at steady state. In fact, for $\phi \gg St^{1/3}$, the only bound pairs that result, and possibly persist, are related to the initial configuration of the particles in the suspension; in particular, these bound pairs may originate from the subset of initial particle pairs, that in § 3.2.2, comprised the third category. In any case, however, the volume occupied by the associated group of trajectories always constitutes an insignificant fraction of the finite-St trajectory space.

The only related experimental work on shear-induced diffusion appears to be the recent work by Madanshetty, Nadim & Stone (1996) who, using a method based on Taylor dispersion theory, determined the diffusion coefficients in the gradient direction for a concentrated suspension of neutrally buoyant particles sheared in a Couette device at $Re = St \sim 0.1$. Although the results indicate that inertial effects contribute to increased diffusivity values, there appear to be too many factors in play. These include, on one hand, the effects of fluid inertia, high concentration, etc. and on the other, the uncertainty in the measurements, particularly for dilute suspensions, and therefore do not allow us to relate the measurements, in any manner, to the mechanisms postulated here.

7. Comparison with direct numerical simulation

In this section we simulate pair-particle trajectories in simple shear flow with perturbative particle inertia by numerically integrating the exact equations of motion, (2.1), for small St. The values of the resulting transverse displacements are then

compared to those obtained from a numerical integration of the approximate trajectory equations, (4.2) and (4.3), derived in § 4.2.

The equations of relative translational and rotational motion, the appropriate dynamic variable being the sum of the individual angular velocities in the latter case, are again solved using an fourth-order adaptive-step Runge–Kutta routine, with the hydrodynamic functions required being obtained as described earlier for the trajectory calculations. The equations of relative motion are given by

$$\left.\begin{aligned} St\,\frac{\mathrm{d}\boldsymbol{V}}{\mathrm{d}t} &= -\left(\boldsymbol{R}^{11}_{FU}-\boldsymbol{R}^{12}_{FU}\right)\cdot\left(\boldsymbol{V}-\boldsymbol{\Gamma}\cdot\boldsymbol{r}\right)+\left(\boldsymbol{R}^{11}_{F\Omega}+\boldsymbol{R}^{12}_{F\Omega}\right)\cdot\left(\boldsymbol{\Omega}^{s}-2\boldsymbol{\Omega}^{\infty}\right)\\ &\quad -2\left(\boldsymbol{R}^{11}_{FE}+\boldsymbol{R}^{12}_{FE}\right):\boldsymbol{E}^{\infty},\\ \frac{2}{5}St\,\frac{\mathrm{d}\boldsymbol{\Omega}^{s}}{\mathrm{d}t} &= \left(\boldsymbol{R}^{11}_{F\Omega}+\boldsymbol{R}^{12}_{F\Omega}\right)^{\dagger}\cdot\left(\boldsymbol{V}-\boldsymbol{\Gamma}\cdot\boldsymbol{r}\right)-\left(\boldsymbol{R}^{11}_{L\Omega}+\boldsymbol{R}^{12}_{L\Omega}\right)\cdot\left(\boldsymbol{\Omega}^{s}-2\boldsymbol{\Omega}^{\infty}\right)\\ &\quad +2\left(\boldsymbol{R}^{11}_{LE}+\boldsymbol{R}^{12}_{LE}\right):\boldsymbol{E}^{\infty},\end{aligned}\right\} \tag{7.1}$$

where $\boldsymbol{\Omega}^{s}=\boldsymbol{\Omega}_1+\boldsymbol{\Omega}_2$. The system of equations, (7.1), is then solved in spherical coordinates together with the set of equations relating the spatial coordinates to the respective velocities, namely $\mathrm{d}\boldsymbol{x}/\mathrm{d}t=\boldsymbol{V}$. The integration is carried out starting from far upstream, the initial translational ($\boldsymbol{V}_{t=0}$) and angular velocities ($\boldsymbol{\Omega}^{s}_{t=0}$) being taken as that induced by the ambient simple shear flow at the initial position of the particle. It is important to note that for proper comparison with the results of trajectory calculations, one must look at the transverse displacement of a simulated trajectory starting from sufficiently far upstream. Starting the numerical integration of (7.1) from an intermediate interparticle separation, for instance, with the aforementioned initial conditions would introduce an initial period of inertial relaxation that is not accounted for in the $O(St)$ trajectory equations, thereby negating the comparison between the two.

In table 5, we compare the values of Δx and Δz from integrating (7.1) (denoted by $(\Delta x/\Delta z)_{dirnum}$) to those obtained from the trajectory equations (denoted by $(\Delta x/\Delta z)_{traj}$) for three different values of the off-plane coordinate, the gradient offset $z^{-\infty}$ being varied in each case from 5 down to 0.1; the Stokes number for all cases considered is 0.1. In general the values of Δx and Δz show good agreement. There is a relatively large discrepancy between the values of Δz near the point of zero-crossing ($z^{-\infty}=z_c^{-\infty}$) that is to be expected.

In addition, the simulations give the value of $x_c^{-\infty}$, the off-plane coordinate defining the neutral trajectory, as approximately 0.95, in close agreement with the earlier $O(St)$ trajectory calculations (see § 5, where $x_c^{-\infty}$ was found to be 0.9). This value is found to be virtually independent of St for St ranging from 0.01 to 0.1, confirming theoretical predictions.

An instance of how the small-St theory formulated in earlier sections can fail when $St\sim O(1)$ or greater is seen from plotting an in-plane spiralling trajectory obtained by integrating the equations of motion (7.1) with $St=2$; the trajectory in this case (see figure 24) shows crossing of paths. In contrast, the one obtained from integrating the $O(St)$ trajectory equation, (4.2) with $\theta=\pi/2$, shows the same qualitative character as those for $St\ll 1$ (for instance, see the (y, z)-projection in figure 21) and is found to finally spiral in to unrealistically small separations. The crossing of paths in figure 24 clearly suggests that for $St\sim O(1)$ one cannot reduce the full phase space to only the three positional degrees of freedom as in the $O(St)$ trajectory equations. This would then justify the apparent crossing of paths in figure 24, since it is always possible for the actual trajectories in the six-dimensional $(\boldsymbol{x}, \boldsymbol{V})$ phase space to intersect when projected onto subspaces of lower dimensions. The qualitative difference between the

	$z^{-\infty}$	$(\Delta x)_{dirnum}$	$(\Delta x)_{traj}$	$(\Delta z)_{dirnum}$	$(\Delta z)_{traj}$
(a)	5	0	0	-1.855×10^{-3}	-1.941×10^{-3}
	2	0	0	-1.565×10^{-2}	-1.587×10^{-2}
	1	0	0	-3.834×10^{-2}	-3.838×10^{-2}
	0.5	0	0	-4.802×10^{-2}	-4.806×10^{-2}
	0.2	0	0	-9.341×10^{-2}	-9.353×10^{-2}
	0.1	0	0	spirals	spirals
(b)	5	-1.798×10^{-4}	-1.892×10^{-4}	-1.813×10^{-3}	-1.897×10^{-3}
	2	-3.371×10^{-3}	-3.533×10^{-3}	-1.395×10^{-2}	-1.413×10^{-2}
	1	-1.244×10^{-2}	-1.309×10^{-2}	-3.008×10^{-2}	-2.991×10^{-2}
	0.5	-1.686×10^{-2}	-1.756×10^{-2}	-3.301×10^{-2}	-3.24×10^{-2}
	0.2	-1.831×10^{-2}	-1.779×10^{-2}	-4.694×10^{-2}	-4.496×10^{-2}
	0.1	spirals	spirals	spirals	spirals
(c)	5	-5.23×10^{-4}	-5.486×10^{-4}	-1.318×10^{-3}	-1.376×10^{-3}
	2	-3.801×10^{-3}	-3.954×10^{-3}	-3.942×10^{-3}	-4.003×10^{-3}
	1	-5.457×10^{-3}	-5.562×10^{-3}	-2.855×10^{-3}	-2.943×10^{-3}
	0.5	-5.043×10^{-3}	-4.896×10^{-3}	-9.471×10^{-4}	-7.601×10^{-4}
	0.2	-4.981×10^{-3}	-4.512×10^{-3}	2.699×10^{-3}	3.121×10^{-3}
	0.1	-5.276×10^{-3}	-4.707×10^{-3}	7.759×10^{-3}	8.541×10^{-3}

TABLE 5. Δx and Δz values for (*a*) $x^{-\infty} = 0$, (*b*) $x^{-\infty} = 0.5$, (*c*) $x^{-\infty} = 2$, and $z^{-\infty}$ ranging from 5 to 0.1; $St = 0.1$.

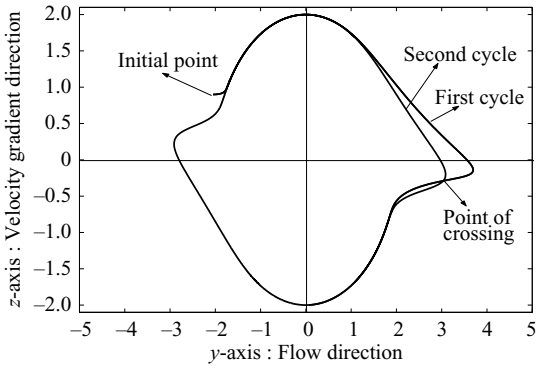

FIGURE 24. In-plane trajectory starting from $(x, y) \equiv (-2.03, 0.9)$ for $St = 2$.

two cases is not related to neglecting corrections of $o(St)$ in the trajectory equations. Indeed, incorporating any finite number of such corrections will still yield a single-valued inertial velocity field and thence non-intersecting paths. Interestingly, even for $St = 2$ there appears to exist an attracting limit cycle in the shearing plane.

8. Conclusions and discussion

In this paper we have analysed the hydrodynamic interactions of a pair of identical spheres in simple shear flow for small but finite St as a first step towards a complete understanding of the role of particle inertia in suspension microstructure and rheology. Particle inertia was found to fundamentally alter the nature of the resulting pair trajectories. The fore–aft symmetry of the zero-Stokes trajectory space is broken; the

resulting asymmetry leads to shear-induced diffusion, and is expected to give rise to normal stress differences. Inertialess closed trajectories give way to finite-St spiralling trajectories, a subset of which spiral onto a stable limit cycle close to the reference sphere; the location of the limit cycle in the shearing plane is, at leading order, independent of St. As shown in figure 9, the domain of attraction of the limit cycle, in the shearing plane, is bounded by the reference sphere on one hand, and the pair of separatrices with $O(St^{1/2})$ upstream gradient offsets on the other. Away from the plane of shear, the basin of attraction remains infinite in extent in the flow direction until an off-plane coordinate corresponding to the location of the neutral trajectory (with zero gradient displacement); the basin shrinks rapidly thereafter, approaching the vorticity axis, since the gradient displacement of the finite-St separatrices changes sign, thereby allowing a subset of spiralling trajectories to eventually separate in the flow direction.

As seen in § 3, there now exists a neutral trajectory off the plane of shear which acts to separate finite-St trajectories that spiral off to infinity from those that spiral onto an in-plane limit cycle. Since the location of this neutral trajectory is, to leading order, independent of St, so is its associated 'filtering' action. The region of spiralling trajectories has an infinite volume, and the effects described should therefore be observable even for the case of rough spheres. Indeed, even if the limit cycle or the neutral trajectory is destroyed on account of surface roughness, the far-field spiralling trajectories will persist. Although the time scale required to observe the inertial modifications, for instance, a gradual change in the separation of any bound pair, increases as $St \to 0$, the nature of pair-wise interactions between spherical particles for any non-zero St is nevertheless fundamentally altered.

The existence of inertial trajectories leading to the formation of bound pairs implies a net flux of pair probability from infinity into any volume that includes the limit-cycle associated with the reference sphere. Thus, there exists, in the limit of pairwise interactions, no steady solution to the equation governing the pair-distribution function for any finite St. A trajectory calculation (e.g. Zarraga & Leighton 2001) to characterize the microstructure and rheology of a finite-St suspension via pair-wise hydrodynamic interactions alone would therefore be an ill-posed problem unless one incorporates other mechanisms to obtain a finite pair-distribution function. This situation should be contrasted to that in the absence of inertia, where the ill-posedness of the pairwise limit arises from the absence of a unique steady state, the final form of the pair-distribution function in the region of closed pathlines being intimately related to the statistics of the initial pair-configuration (see Batchelor & Green 1972*b*).

Having summarized the first effects of particle inertia on pair trajectories in simple shear flow, it is worthwhile to briefly compare these with the modification of fluid streamlines around a single sphere in simple shear flow for small but finite Re. This helps highlight, in part, the differences between a concentrated (particle) and a distributed (fluid) source of inertia, and may be of relevance when considering pair interactions at both finite St and Re. In the inertialess limit, $Re = St = 0$, particle pathlines and fluid streamlines bear a close resemblance in ambient linear flows; for simple shear, both are fore–aft symmetric and include a region of closed trajectories spanning the flow–vorticity plane.† For finite Re, closed streamlines are again destroyed; however recirculating wakes appear close to the flow axis at

† The region of closed trajectories differs in its spatial extent for the two cases, being smaller in the former instance on account of near-field hydrodynamic interactions (Batchelor & Green 1972*a*); this is a detail, however.

distances of $O(Re^{-3/10})$; in addition, unlike the finite-St case, all streamlines within the finite-Re separatrix envelope spiral outward, and a limit cycle does not arise (see Subramanian & Koch 2006*a, b*; Robertson & Acrivos 1970). Even for trajectories that remain open, the $O(St)$ gradient displacement of a particle, sufficiently near the plane of shear, is negative, while an analysis of the inertially modified streamlines around a force-free sphere in simple shear (for instance, see Lin *et al.* 1970) shows that the $O(Re)$ correction induces a net positive gradient displacement in the plane of shear, at least in regions where viscous forces still dominate, i.e. for $r \ll aRe^{-1/2}$.† This change in sign in going from the particle to the fluid case makes sense if one recalls that the negative gradient displacement for particle pathlines close to the shearing plane, with small gradient offsets, arises from lubrication forces acting to suppress relative motion in a radially outward direction at small separations. This mechanism being absent for an infinitesmal fluid element, those close to the sphere must be displaced in the positive gradient direction on account of the streamline curvature. In addition, incompressibility dictates that the distant fluid elements conform to this near-field outward displacement, and the sign of the $O(Re)$ gradient displacement therefore remains positive. As noted in § 3.2, for off-plane pair trajectories where lubrication forces are no longer dominant, the gradient displacement is indeed positive for small enough gradient offsets. A more detailed comparison, for instance the far-field decay of the respective inertial displacements, is precluded, however, owing to the unavailability of detailed solutions to the linearized Navier–Stokes equations for simple shear flow.

It is of interest to note that the in-plane trajectory modifications found here are qualitatively similar to those found earlier by Van de Ven & Mason (1976), who considered the dependence of pair-particle interactions on the functional form of the interparticle potential when the particles were restricted to being in the plane of shear (referred to therein as 'equatorial encounters'). For a potential with an attractive far-field part, and that is repulsive for small pair separations, the authors found the existence of a stable closed orbit. In this case, the locus of the closed orbit is dependent on the relative magnitudes of the two parts of the interaction potential, and in addition, if the attractive force is strong enough, convergence to the limit cycle is possible in a finite time. This is unlike the present case where the spiralling trajectories do not converge onto the limit cycle in a finite time, and the latter's location the shearing plane is fixed regardless of St, since the 'attractive' and 'repulsive' inertial forces have a common physical origin.

One of the obvious implications of the finite-St trajectory analysis is with regard to stability of aerosols/colloids. In general, the stability of aerosols is influenced by several factors including Brownian motion, gravity, colloidal forces such as Van der Waals attraction or electrostatic double layer repulsion, and hydrodynamic shearing forces due to the ambient laminar or turbulent flow field. For sufficiently large particles (greater than about 5 microns) thermal effects are negligible, and the initial rate of (singlet) coagulation may be determined via a trajectory analysis, similar to ours, and now involving the relative motion of a pair of particles under both hydrodynamic and non-hydrodynamic forces. Such calculations, with the aim of

† It may be shown that the velocity field in the outer region ($r \gg Re^{-1/2}$) decays as $1/r^2$, so the net transverse displacement for any streamline is finite. This is not the case in two dimensions – the disturbance velocity field due to a torque free cylinder in an unbounded simple shear, at distances larger than the inertial screening length, is the $O(1/r)$ irrotational field due to a point vortex, and leads to unbounded displacements in the gradient direction.

characterizing aerosol stability as a function of flow type, have been carried out previously in the context of steady laminar flows (Zeichner & Schowalter 1977; Feke & Schowalter 1983), laminar chaotic flows (Bidkar & Khakhar 1990) and for a homogeneous stationary isotropic turbulence flow field (Brunk, Koch & Lion 1998). It has been found in these calculations that the neglect of hydrodynamic interactions usually leads to significant over-predictions of coagulation efficiency (Brunk *et al.* 1998). A comprehensive investigation of the effect of flow type on aerosol stability was carried out by Greene, Hammer & Olbricht (1994) for homogeneous laminar flows; they found, for purely attractive interparticle potentials, a narrow window of stability centred around simple shear flow. In all these studies, however, the effects of particle inertia on pair trajectories have been neglected, and pair hydrodynamic interactions in a linear flow are thence treated in accordance with that originally found by Batchelor & Green (1972*a*, *b*). Although our results would, in their present form, serve to predict the modified coagulation efficiency for simple shear flow of inertial particles, it is clearly of interest to extend the analysis to examine finite-St trajectory equations in a general linear flow. The immediate question that arises in this context is: do we expect the stability diagram of a colloid to look very different for non-zero St? This would, in part, be dependent on whether inertialess pair trajectories in a general linear flow are, similar to simple shear, non-trivially altered for small but finite-St.

To answer this question, we briefly compare pair-trajectory configurations, with and without inertia, in a two-dimensional linear flow with a ratio of extension to vorticity that differs from unity. We only include hydrodynamic forces and examine the more interesting case where the magnitude of extension exceeds vorticity, leading to a (hyperbolic) flow with open streamlines in the absence of interactions; in the opposite limit, inertialess pair trajectories are all closed, and inertial forces are again anticipated to destroy closed orbits.† Since simple shear is an exceptional member in the general family of linear flows, wherein extension and vorticity balance exactly to yield rectilinear streamlines, and since the streamlines in any other planar linear flow, either hyperbolic or elliptic, form structurally stable configurations, the initial expectation, at least for a steady linear flow, is that particle inertia would only lead to quantitative modifications. However, as shown originally by Kao, Cox & Mason (1977), closed particle pathlines exist even in a generic linear flow. The inhomogeneity introduced by the disturbance velocity fields of the particle pair implies that the ratio of the extension to vorticity is no longer a constant for the flow; the extensional contribution to the angular velocity of a hydrodynamically interacting pair lying, for instance, in the plane of the flow, is retarded by the factor $(1 - B(r))$, and decreases with decreasing separation. It thus becomes possible to add enough vorticity to the ambient flow so that there exists a compact region of closed pair trajectories. As shown in figure 25(*a*), the inertialess trajectory plane includes a centre (the reference sphere) and a pair of saddle points; the separatrix (shown in dashed lines) now consists of a pair of trajectories approaching or diverging from each of the saddle points, and extending to infinity, and a pair, finite in extent, connecting the two. The

† In general, interesting inertial modifications are expected to occur for linear flows in a window centered around simple shear. For a planar linear flow with vorticity far exceeding extension (thence, lying outside this window), inertialess pair trajectories are expected to form nearly convex closed curves; finite St should then lead to diverging spirals. For lower values of vorticity, still exceeding the extension, there exists, similar to the case of simple shear, the possibility of a non-trivial attracting limit cycle that results from a balance of inertial forces acting on regions of opposing curvature.

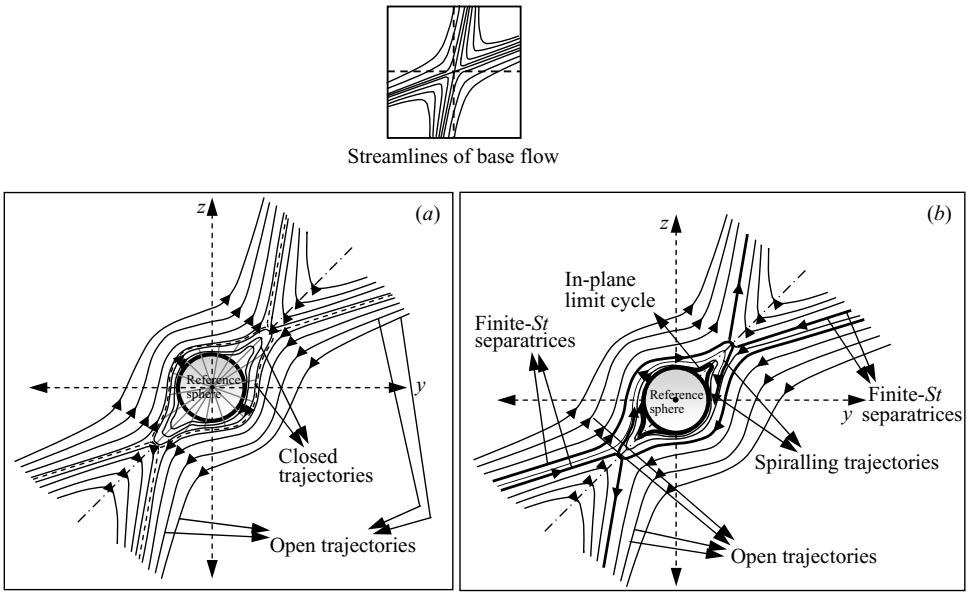

FIGURE 25. The anticipated configurations of (*a*) inertialess and (*b*) finite-*St* particle pathlines, in the plane of the reference sphere, for a generic two-dimensional linear flow.

second particle takes an infinite amount of time to approach any one saddle point, or go from one to the other, when moving along the separatrix. This is a structurally unstable configuration, because from the dynamical systems perspective, there exist heteroclinic connections between the pair of saddle points (see Ottino 1989). The anticipated changes for finite St, in the plane of the reference sphere, are shown in figure 25(*b*), where it is seen that the addition of vorticity may actually increase the collision efficiency, since it opens up channels, extending to infinity, where trajectories now approach the reference sphere. It should be noted that the inertialess region of closed trajectories is three-dimensional, and becomes smaller in extent away from the plane of the reference sphere with diminishing interactions, terminating at a pair of points on the vorticity axis symmetrically located about the shearing plane, and at a finite distance from it; thus, the inertial modifications are more involved, and we again expect the non-planar off-plane closed trajectories to yield finite-St spiralling trajectories that possibly converge towards the in-plane limit cycle (see figure 26). These consequences of inertia are in contrast to earlier observations regarding the inhibiting effect of vorticity in the inertialess limit due to rotation in closed orbits (Brunk *et al.* 1998). Similar, more interesting, modifications are anticipated for pair trajectories in a general three-dimensional linear flow. The inertial effects discussed above may be of particular importance with regard to hetero-coagulation, as the extent of the domain comprising closed trajectories increases in extent for dissimilar particles (see Kao *et al.* 1977).

The aforementioned modifications are also expected to be relevant in turbulent coagulation of monodisperse sub-Kolmogorov particles, since the turbulence, on the scale of the interparticle separation, may be represented as a linear flow with a stochastically varying velocity gradient tensor; the magnitude of particle inertia is now characterized by the product of τ_p and the Kolmogorov shear rate. Inertial effects in this context have been included in the recent work of Chun *et al.* (2006). However, the authors only account for the forces on a finite-St particle arising from the curvature of

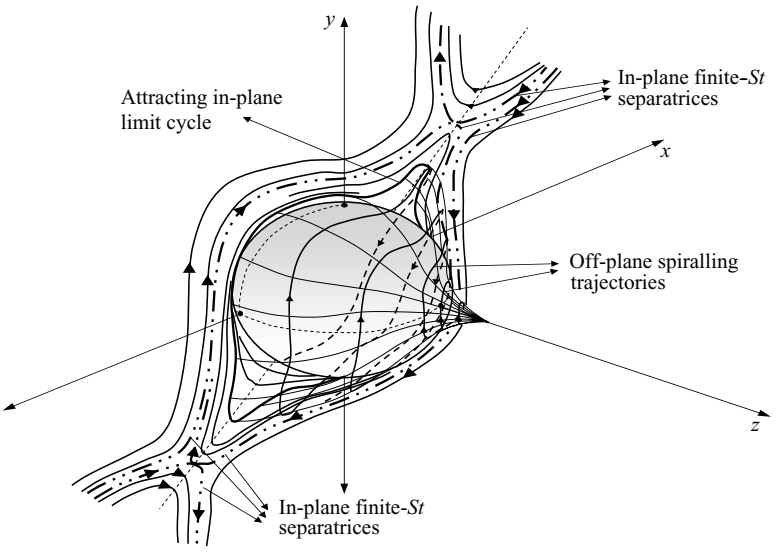

FIGURE 26. The anticipated modifications of off-plane particle pathlines for finite St in a generic two-dimensional linear flow.

the ambient flow streamlines, and find this to result in clustering on sub-Kolmogorov scales. Since the pair-distribution function $g(\boldsymbol{r})$ was only determined in the range $a \ll r \ll \eta_K$, η_K being the Kolmogorov scale, both colloidal and hydrodynamic interactions, important only when $r \sim O(a)$, were neglected. Our results, although of significance, would not directly apply to the turbulent case. This is because DNS investigations have indicated that the total strain, defined as the product of the Kolmogorov shear rate and its correlation time, is order one (Pope 1990; Girimaji & Pope 1990), so any calculation of turbulent coagulation at finite-St must also account for unsteady inertial effects arising from the fact that both the vorticity and rate of strain tensors decorrelate on time scales that are no longer negligible compared to τ_p.

Finally, the inclusion of gravity should not alter the nature of the finite-St relative pair trajectories found here, since sedimentation in the Stokes limit does not allow for any relative motion of a particle pair. Thus, finite-St pair interactions of sedimenting particles in simple shear should, in the centre-of-mass reference frame, conform to the above description. The pair centre-of-mass of a bound pair may undergo a net drift on account of inertia; for instance, in a vertical shear flow it should undergo an $O(St)$ cross-streamline drift owing to the asymmetry in the finite-St orientation distribution.

This work was supported in part by grant NAG3-2166 from NASA.

Appendix A. Equation of motion in one dimension: lubrication effects at finite St

In this Appendix we analyse a simplified one-dimensional form of the particle equation of motion, while accounting for both the acceleration term and the singular hydrodynamic drag at contact, thereby retaining the physics of the full pair problem examined in § 4.

From § 2 (see (2.1)), the equation for relative translational motion for arbitrary St is given by

$$St\frac{\mathrm{d}\boldsymbol{V}}{\mathrm{d}t} = -\left(\boldsymbol{R}_{FU}^{11}-\boldsymbol{R}_{FU}^{12}\right)\cdot(\boldsymbol{V}-\boldsymbol{V}^{\infty})+\left(\boldsymbol{R}_{F\Omega}^{11}+\boldsymbol{R}_{F\Omega}^{12}\right)\cdot(\boldsymbol{\Omega}_1+\boldsymbol{\Omega}_2-2\boldsymbol{\Omega}^{\infty})-2\left(\boldsymbol{R}_{FE}^{11}+\boldsymbol{R}_{FE}^{12}\right):\boldsymbol{E}^{\infty}, \tag{A 1}$$

where $\boldsymbol{V} = (\boldsymbol{V}_2-\boldsymbol{V}_1)$ and $\boldsymbol{\Omega}^{\infty}$ is the angular velocity on account of the vorticity in the ambient linear flow; we have written down the translational, rotational and rate-of-strain contributions separately on the right-hand side. Taking the radial component of the above equation, and using the expressions for the resistance tensors, one obtains

$$St\frac{\mathrm{d}V_i}{\mathrm{d}t}n_i = -\frac{V_r}{r-2}+\lim_{r\to 2}\left(2X^A-\frac{4}{3}X^G\right)E_{rr}, \tag{A 2}$$

for small separations, where X^A and X^G are hydrodynamic functions, defined in Kim & Karrila (1991), that are singular at contact. But the $O(1/(r-2))$ singular terms in X^A and X^G cancel out and $(2X^A-\frac{4}{3}X^G)$ in (A 2) remains $O(1)$ near contact. The solution of the equation is impeded by the fact that $(\mathrm{d}/\mathrm{d}t)(V_in_i) \neq (\mathrm{d}V_i/\mathrm{d}t)n_i$; the curvature of the particle pathlines results in inertial forces proportional to $\mathrm{d}n_i/\mathrm{d}t$. One can, however, retain the essential character of the above problem while considering a simplified form of (A 2) in one dimension, thereby eliminating the effects of curvature. The simplified equation contains the balance of the particle acceleration ($\propto St$), a constant force ($(2X^A-\frac{4}{3}X^G)_{r=2}E_{rr}$) and a singular drag term ($V_r/(r-2)$). Thus,

$$St_1\frac{\mathrm{d}u}{\mathrm{d}t} = 1-\frac{u}{L-x}, \quad u = u_0 \text{ at } t = 0, \quad x = 0 \text{ at } t = 0,$$

where the constant force is scaled to unity, L is chosen as the location of the singularity, and we have used St_1 to denote the magnitude of the acceleration term and to differentiate it from the Stokes number (St) defined in the main text. Rewriting $(\mathrm{d}u/\mathrm{d}t)$ as $(u\,\mathrm{d}u/\mathrm{d}x)$ and using $y = L-x$, $\hat{u} = \mathrm{d}y/\mathrm{d}t$, one obtains

$$\begin{aligned} St_1\,\hat{u}\frac{\mathrm{d}\hat{u}}{\mathrm{d}y} &= -1-\frac{\hat{u}}{y}, \\ \Rightarrow\ St_1\frac{\mathrm{d}\hat{u}}{\mathrm{d}y} &= -\left(\frac{1}{y}+\frac{1}{\hat{u}}\right), \end{aligned} \tag{A 3}$$

with the initial condition $\hat{u} = -u_0$ at $y = L$. We note that the inertialess solution, i.e. the solution for $St_1 = 0$, is simply $\hat{u} = y$. Insight can be gained into the solution for arbitrary St_1 by considering the following two limiting cases:

Case 1: If $u_0 \gg y_0$, which corresponds to an initially highly energetic particle, then the leading-order balance for short times is

$$St_1\frac{\mathrm{d}\hat{u}}{\mathrm{d}y} = -\frac{1}{y},$$

giving

$$\hat{u} = -u_0+\frac{1}{St_1}\ln\left(\frac{y_0}{y}\right). \tag{A 4}$$

Case 2: If $u_0 \ll y_0$, which corresponds to an initially slowly moving particle, then the leading-order balance for short times is

$$St_1\frac{\mathrm{d}\hat{u}}{\mathrm{d}y} = -\frac{1}{\hat{u}},$$

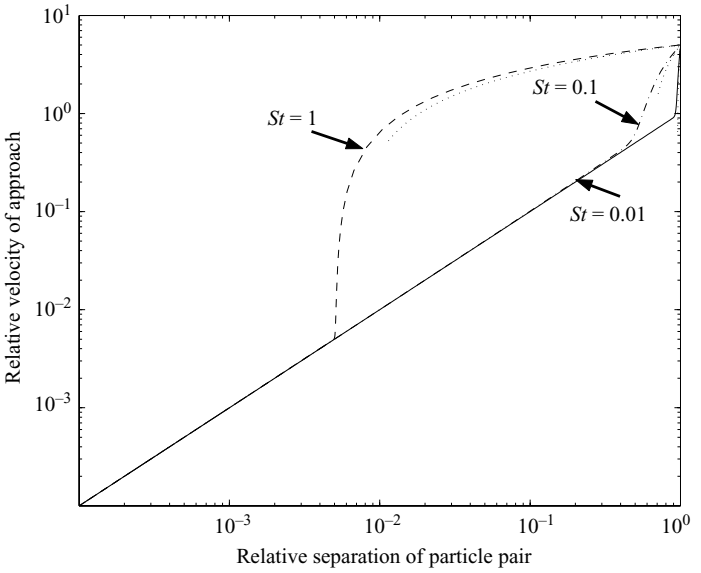

FIGURE 27. Comparison of the theoretical approximation (A 4) (represented by dotted lines in all three cases) and the exact numerical solution for the initial condition $u_0 = 5$, $y_0 = 1$, for three different Stokes numbers. The dashed line denotes the numerical solution for $St_1 = 1$, the dash-dot line for $St_1 = 0.1$, and the solid line for $St_1 = 0.01$.

and the corresponding short time behaviour is

$$\hat{u} = \left[u_0^2 + \frac{2}{St_1}(y_0 - y)\right]^{1/2}. \tag{A 5}$$

Figures 27 and 28 show plots of $|\hat{u}|$ versus y for the two limiting initial conditions considered above for various values of St_1. In figure 27, where $u_0 \gg y_0$, the velocity for short times decreases logarithmically and is described well by (A 4). This solution is, however, not valid for all separations since it predicts a finite separation at which the relative velocity goes to zero. At smaller separations, there is a rapid transition from the steep logarithmic decline to a gradual linear variation, corresponding to the rapidly diminishing magnitude of the acceleration term. This transition becomes increasingly abrupt for large St_1, and shifts to smaller separations with increasing St_1. For the case where $u_0 \ll y_0$, figure 28 shows that the velocity increases for small times in accordance with equation (A 5), and does so untill a point where $|\hat{u}| \gg y$; the dynamics thereafter follow the previous case. Thus, irrespective of the initial condition, the relative velocity $\hat{u}$ asymptotes to a linear variation with y for long times and small separations, in turn implying that interparticle contact does not occur in a finite time similar to the inertialess case.

Appendix B. Estimation of third-particle effects in bound-pair dissociation

Here, we obtain an estimate of the rate of disruption of bound pairs due to distant third-particle interactions. Consider a third particle at a distance $L \gg 1$. A single such particle would cause the centre of mass of the bound pair to be displaced by $O(St/L^3)$. If the pair do not interact hydrodynamically, their relative displacement due to the passing third particle is $O(St/L^4)$. Owing to the close-range lubrication

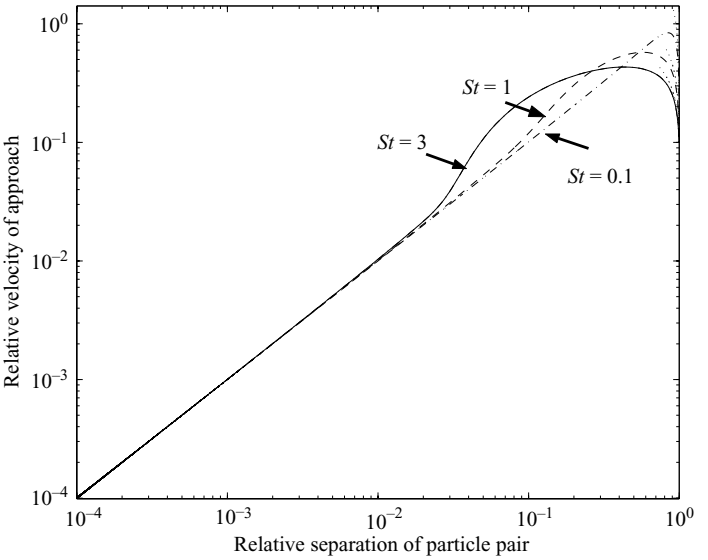

FIGURE 28. Comparison of the theoretical approximation (A 5) (represented by dotted lines in all three cases) and the exact numerical solution for the initial condition $u_0 = 0.1$, $y_0 = 1$, for three different Stokes numbers. The solid line denotes the numerical solution for $St_1 = 3$, the dashed line for $St_1 = 1$, and the dash-dot line for $St_1 = 0.1$.

interactions, however, the effective inertia of each of the particles constituting the bound pair is reduced by a factor r_{sep}, where $r_{sep} \ll 1$ is the non-dimensional separation between the particle surfaces. A single encounter is therefore expected to lead to a relative displacement of $O(St\, r_{sep}/L^4)$ of the particle pair. It must be kept in mind that the bound pair, similar to a dumbbell, rotates in the shear flow; however, the aspect ratio being of order unity, this does not modify the aforementioned scaling. If we denote the dimensionless separation of the finite-St in-plane separatrix at its point of closest approach by $r_{critical}$, then one needs at least $N \sim O(r_{critical}L^4/St\, r_{sep})$ encounters in order to disrupt bound pair. This translates to a dissociation rate of $O(\dot{\gamma} L^3 \phi\phi_d)(r_{sep}St)/(r_{critical}L^4)$. This is, at best, a crude upper estimate since we have neglected the continous process of spiralling-in of the displaced pair that occurs between encounters. In any case, the rate of dissociation may be neglected when compared to that due to approaching particles at $O(St^{1/2})$ gradient offsets.

REFERENCES

ACRIVOS, A., BATCHELOR, G. K., HINCH, E. J., KOCH, D. L. & MAURI, R. 1992 Longitudinal diffusion of spheres in a dilute suspension. *J. Fluid Mech.* **240**, 651.

ARP, P. A. & MASON, S. G. 1997 Kinetics of flowing dispersions:9. Doublets of rigid spheres (experimental). *J. Colloid Interface Sci.* **61**(1), 44.

BAGCHI, P. & BALACHANDAR, S. 2002*a* Steady planar straining flow past a rigid sphere at moderate Reynolds number. *J. Fluid Mech.* **466**, 365.

BAGCHI, P. & BALACHANDAR, S. 2002*b* Effect of free rotation on the motion of a solid sphere in linear shear flow at moderate *Re*. *Phys. Fluids* **14**, 2719.

BAGCHI, P. & BALACHANDAR, S. 2003 Inertial and viscous forces on a rigid sphere in straining flows at moderate Reynolds numbers. *J. Fluid Mech.* **481**, 105.

BATCHELOR, G. K. & GREEN, J. T. 1972*a* The hydrodynamic interaction of two small freely-moving spheres in a linear flow field. *J. Fluid. Mech.* **56**, 375.

Batchelor, G. K. & Green, J. T. 1972*b* The determination of the bulk stress in a suspension of spherical particles to $O(c^2)$. *J. Fluid. Mech.* **56**, 401.

Bidkar, U. R. & Khakhar, D. V. 1990 Collision rates in chaotic flows: Dilute suspensions. *Phys. Rev.* A **42**, 5964.

Brady, J. F. & Bossis, G. 1988 Stokesian dynamics. *Annu. Rev. Fluid Mech.* **20**, 111.

Brunk, B. K., Koch, D. L. & Lion, L. W. 1998 Turbulent coagulation of colloidal particles. *J. Fluid Mech.* **364**, 81.

Chapman, S. & Cowling, T. G. 1970 *The Mathematical Theory of Non-uniform Gases.* Cambridge University Press.

Chun, J., Koch, D. L., Rani, S. L. Ahluwalia, A & Collins, L. R. 2005 Clustering of aerosol particles in isotropic turbulence. *J. Fluid Mech.* **536**, 219.

daCunha, F. R. & Hinch, E. J. 1996 Shear-induced dispersion in a dilute suspension of rough spheres. *J. Fluid Mech.* **309**, 211.

Davis, R. H. 1996 Hydrodynamic diffusion of suspended particles: A symposium. *J. Fluid Mech.* **310**, 325.

Eckstein, E. C., Bailey, D. G. & Shapiro, A. H. 1977 Self-diffusion of particles in shear flow of a suspension. *J. Fluid Mech.* **79**, 191.

Feke, D. L. & Schowalter, W. R. 1983 The effect of Brownian diffusion on binary flow-induced collision rates in colloidal dispersions. *J. Colloid Interface Sci.* **106**, 203.

Feng, J., Hu, H. H. & Joseph, D. D. 1994 Direct simulation of initial-value problems for the motion of solid bodies in a Newtonian fluid. Part 1. Sedimentation. *J. Fluid Mech.* **261**, 95.

Girimaji, S. S. & Pope, S. B. 1990 A diffusion model for velocity gradients in turbulence. *Phys. Fluids* A **2**, 242.

Greene, M. R., Hammer, D. A. & Olbricht, W. L. 1994 The effect of hydrodynamic flow field on colloidal stability. *J. Colloid Interface Sci.* **167**, 232.

Guckenheimer, J. & Holmes, P. 1983 *Nonlinear Oscillations, Dynamical Systems and Bifurcations of Vector Fields.* Springer.

Happel, J. & Brenner, H. 1965 *Low Reynolds Number Hydrodynamics, with Special Applications to Particulate Media.* Prentice-Hall.

Hill, R. J., Koch, D. L. & Ladd, A. J. C. 2001 Moderate Reynolds number flows in ordered and random arrays of spheres. *J. Fluid Mech.* **448**, 213.

Hu, H. H., Joseph, D. D. & Crochet, M. J. 1992 Direct simulation of fluid particle motions. *Theor. Comput. Fluid Dyn.* **3**, 285.

Jeffery, G. B. 1922 The motion of ellipsoidal particles immersed in a viscous fluid. *Proc. R. Soc. Lond.* A **102**, 161.

Jeffrey, D. J. 1992 The calculation of the low Reynolds number resistance functions for two unequal spheres. *Phys. Fluids* A **4**, 16.

Jeffrey, D. J. & Onishi, Y. 1984 Calculation of the resistance and mobility functions for two unequal rigid spheres in low Reynolds number flow. *J. Fluid Mech.* **139**, 261.

Kao, S. V., Cox, R. G., Mason, S. G. 1977 Streamlines around single spheres and trajectories of pairs of spheres in two-dimensional creeping flows. *Chem. Engng. Sci.* **32**, 1505.

Kim, I., Elghobashi, S. & Sirigano, W. A. 1993 Three-dimensional flow over two spheres placed side by side. *J. Fluid Mech.* **246**, 465.

Kim, S. & Karrila, S. J. 1991 *Microhydrodynamics: Principles and Selected Applications*, Chap. 11. Butterworth-Heinemann.

Kim, S. & Mifflin, R. T. 1985 The resistance and mobility functions of two equal spheres in low-Reynolds-number flow. *Phys. Fluids* **28**, 2033.

Koch, D. L. 1990 Kinetic theory for a monodisperse gas-solid suspension. *Phys. Fluids* A **2**, 1711.

Koch, D. L. & Hill, R. J. 2001 Inertial effects in suspension and porous-media flows. *Annu. Rev. Fluid Mech.* **33**, 619.

Koch, D. L. & Ladd, A. J. C. 1997 Moderate Reynolds number flows through periodic and random arrays of aligned cylinders. *J. Fluid Mech.* **349**, 31.

Kumaran, V. & Koch, D. L. 1993*a* Properties of a bidisperse particle-gas suspension. Part 1. collision time small compared with viscous relaxation time. *J. Fluid. Mech.* **247**, 623.

Kumaran, V. & Koch, D. L. 1993*b* Properties of a bidisperse particle-gas suspension. Part 2. viscous relaxation time small compared with collision time. *J. Fluid. Mech.* **247**, 643.

Leal, L. G. 1975 The slow motion of slender rod-like particles in a second order fluid. *J. Fluid Mech.* **69**, 305.

Leal, L. G. 1992 *Laminar Flow and Convective Transport Processes.* Butterworth-Heinmann.

Leighton, D. & Acrivos, A. 1987*a* Measurement of shear-induced self-diffusion in concentrated suspensions. *J. Fluid Mech.* **177**, 109.

Leighton, D. & Acrivos, A. 1987*b* The shear-induced migration of particles in concentrated suspensions. *J. Fluid Mech.* **181**, 415.

Lin, C. J., Peery, J. H. & Schowalter, W. R. 1970 Simple shear flow around a rigid sphere: Inertial effects and suspension rheology. *J. Fluid Mech.* **44**, 1.

Lun, C. K. K., Savage, S. B., Jeffrey, D. J. & Chepurniy, N. 1984 Kinetic theories for granular flow: inelastic particles in Couette flow and slightly inelastic particles in a general flow field. *J. Fluid Mech.* **140**, 223.

Mcquarrie, D. A. 1976 *Statistical mechanics.* Harper & Row.

Ottino, J. M. 1989 *The Kinematics of Mixing: Stretching, Chaos and Transport.* Cambridge University Press.

Pope, S. B. 1990 Lagrangian microscales of turbulence. *Phil. Trans. R. Soc. Lond.* **333**, 309.

Robertson, C. R. & Acrivos, A. 1970 Low Reynolds number shear flow past a rotating cylinder. *J. Fluid. Mech.* **40**, 685.

Ryskin, G. 1980 The extensional viscosity of a dilute suspension of spherical particles at intermediate microscale Reynolds numbers. *J. Fluid. Mech.* **99**, 513.

Sangani, A. S., Mo, G., Tsao, H. K. & Koch, D. L. 1996 Simple shear flow of dense gas-solid suspensions at finite Stokes numbers. *J. Fluid. Mech.* **313**, 309.

Savage, S. B. & Jeffrey, D. J. 1981 The stress tensor in a granular flow at high shear rates. *J. Fluid Mech.* **110**, 255.

Madanshetty, S. I., Nadim, A. & Stone, H. A. 1996 Experimental measurement of shear-induced diffusion in suspensions using long time data. *Phys. Fluids* **8**, 1996.

Subramanian, G. 2002 Inertial effects in suspension dynamics. PhD thesis, California Institute of Technology.

Subramanian, G. & Koch, D. L. 2005 Inertial effects on fibre motion in simple shear flow. *J. Fluid Mech.* **535**, 383.

Subramanian, G. & Koch, D. L. 2006*a* Inertial effects on the transfer of heat or mass from neutrally buoyant spheres in a steady linear velocity field. *Phys. Fluids* (accepted).

Subramanian, G. & Koch, D. L. 2006*b* Centrifugal forces alter streamline topography and greatly enhance the rate of heat and mass transfer from neutrally buoyant particles to a shear flow. *Phys. Rev. Lett.* **96**, 134503.

Sundararajakumar, R. R. & Koch, D. L. 1996 Non-continuum lubrication flows between particles colliding in a gas. *J. Fluid Mech.* **313**, 283.

Tsao, H. K. & Koch, D. L. 1995 Simple shear flows of dilute gas-solid suspensions. *J. Fluid. Mech.* **296**, 211.

Van de Ven, T. G. M. & Mason, S. G. 1976 The microrheology of colloidal dispersions. IV. Pairs of interacting spheres in shear flow. *J. Colloid Inteface Sci.* **57**(3), 505.

Van Dyke, M. 1975 *Perturbation Methods in Fluid Mechanics.* Parabolic Press.

Wylie, J. J., Koch, D. L. & Ladd, A. J. C. 2003 Rheology of suspensions with high particle inertia and moderate fluid inertia. *J. Fluid Mech.* **480**, 95.

Zarraga, I. E. & Leighton, D. T. 2001 Shear-induced diffusivity in a dilute bidisperse suspension of hard spheres. *J. Colloid Interface Sci.* **243**, 503.

Zeichner, G. R. & Schowalter, W. R. 1977 Use of trajectory analysis to study stability of colloidal dispersions in flow fields. *AIChE J.* **23**, 243.